Title
Dynamic state and the receptive field transformation in the lemniscal auditory thalamocortical system

Author
Miller, Lee M.

Publication Date
2001

Peer reviewed|Thesis/dissertation

Dynamic state and the receptive field transformation
in the lemniscal auditory thalamocortical system

by

Lee M. Miller

DISSERTATION

Submitted in partial satisfaction of the requirements for the degree of

DOCTOR OF PHILOSOPHY

in

Bioengineering

in the

GRADUATE DIVISIONS

of the

UNIVERSITY OF CALIFORNIA SAN FRANCISCO

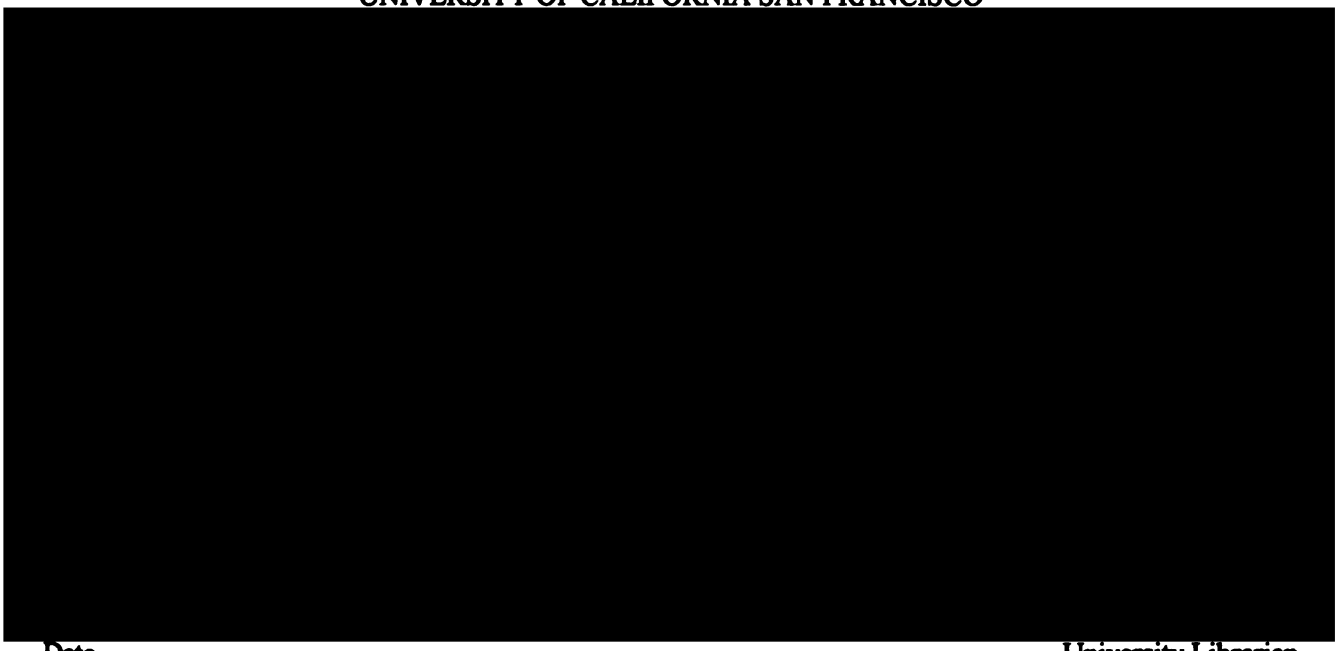

Date University Librarian

Degree Conferred: .....

Dedication

to Lib

Acknowledgments

My deepest appreciation I extend to my colleagues and friends: Monty A. Escabí, Heather L. Read, and my advisor Christoph E. Schreiner. Monty, Heather, and I worked as a team through many long nights in the lab. Their ideas are so interwoven with my own that this dissertation is partly theirs, as well. Christoph was a superb advisor: continually supportive, always willing to engage in discussion, and personally a true gentleman. Above all, I owe him thanks for giving me the freedom to pursue a challenging topic with less-than-certain outcome.

I also owe a great debt to my dissertation committee, who provided crucial guidance: Christoph E. Schreiner, Ted Lewis, Michael P. Stryker, Jeffery A. Winer, and Ken D. Miller. I feel very fortunate to have had such an intellectually creative and demanding group of faculty oversee my work.

The text and figures of Chapter 1 are reprinted from a manuscript submitted to The Journal of Neuroscience. The manuscript was edited by the Journal and published in September 2000 (J Neurosci 20(18): 7011-7016). The co-author listed in the publication (C.E. Schreiner) directed and supervised the research that forms the basis for this dissertation. The Society for Neuroscience is the copyright owner of the publication and has generously given written permission to include this material in the dissertation.

Chapters 2-4 have been prepared for eventual submission to peer-reviewed journals, with the following co-authors listed. Chapters 2 & 3: M.A. Escabí, H.L. Read., C.E. Schreiner; Chapter 4: M.A. Escabí & C.E. Schreiner.

Abstract:

Dynamic state and the receptive field transformation

in the lemniscal auditory thalamocortical system.

Lee M. Miller

In an effort to understand how ecological and communication sounds are processed in the mammalian auditory system, neuroscientists have investigated neural connectivity and response properties in dozens of areas from the cochlea to the auditory cortex. However, little attention has been given to the functional role of connections between different areas. Two central structures, the medial geniculate body of the thalamus (MGB) and the auditory cortex, are considered essential for the processing of complex auditory signals such as vocalizations. Specifically, the substructure of the MGB that sends high-fidelity discriminative auditory information to the cortex is the ventral division (MGBv), which projects heavily to the primary auditory cortex (AI). An understanding of the MGBv-AI interaction, for both its ethological significance and its commonality with other systems, would deepen our understanding of the neurobiological bases of mammalian sensation. We recorded hundreds of single neurons in the MGBv and AI of the anesthetized cat. The focus of this dissertation is the functional role of the MGBv-A1 thalamocortical transformation in the spectral and temporal coding of sounds.

Although each of the four chapters may be read independently, they are arranged in a logically sequential order. The first chapter shows how powerful dynamic state transitions in the thalamocortical network can be controlled with carefully designed, naturalistic stimuli. The second chapter presents a thorough comparison of simultaneously recorded thalamic and cortical cells across spectral, temporal,

spectrotemporal, and aural stimulus domains. While this chapter compares all thalamic versus all cortical cells, it does not consider functional connections between individual neurons. Such monosynaptic connections and the variety of their convergence patterns are taken up in Chapter 3, where we describe how some response properties are faithfully preserved from thalamus to cortex while others are created intracortically. Finally, the last chapter analyzes the functional thalamocortical connections on a more quantitative, spike-by-spike basis. This allows us to address the amount of information a given thalamic cell contributes to its cortical target, and how other inputs cooperate to influence the spectrotemporal character of that information.

Table of Contents

List of Figures

Chapter 4

CHAPTER 1:

STIMULUS-BASED STATE CONTROL IN THE THALAMOCORTICAL SYSTEM

ABSTRACT Neural systems operate in various dynamic states which determine how they process information (Livingstone and Hubel, 1981; Funke and Eysel, 1992; Morrow and Casey, 1992; Guido et al., 1995; Mukherjee and Kaplan, 1995; Abeles et al., 1995; Kenmochi and Eggermont, 1997; Wörgötter et al., 1998; Kisley and Gerstein, 1999). In order to investigate the function of a brain area, it is therefore crucial to determine the state of that system. One grave difficulty is that even under well controlled conditions, the thalamocortical network may undergo random dynamic state fluctuations which alter the most basic spatial and temporal response properties of the neurons. These uncontrolled state changes hinder the evaluation of state-specific properties of neural processing and, consequently, the interpretation of thalamocortical function.

Simultaneous extracellular recordings were made in the auditory thalamus and cortex of the ketamine-anesthetized cat under several stimulus conditions. By considering the cellular and network mechanisms that govern state changes, we develop a complex stimulus that controls the dynamic state of the thalamocortical network. Traditional auditory stimuli have ambivalent effects on thalamocortical state, sometimes eliciting an oscillatory state prevalent in sleeping animals and other times suppressing it. By contrast, our complex stimulus clamps the network in a dynamic state resembling that observed in the alert animal. It thus allows evaluation of neural information processing not confounded by uncontrolled variations. Stimulus-based state control illustrates a general and direct mechanism whereby the functional modes of the brain are influenced by structural features of the external world.

Keywords: dynamic state; thalamocortical; spindles; oscillations; ketamine; alerting stimuli; burst mode; tonic mode

A common dynamic state is characterized by widespread, synchronous neural activity in the thalamus and cerebral cortex. In particular, activity waxes and wanes across both structures at a rate of 7-14 Hz. This state occurs in sensory, motor, and association systems of many mammals including humans during various stimulus-driven and spontaneous epochs, and under diverse behavioral conditions (Moruzzi and Magoun, 1949; Chang, 1950; Andersen and Andersson, 1968; Steriade and Llinás, 1988; Tiihonen et al., 1991; Buzsáki, 1991; Morrow and Casey, 1992; Eggermont, 1992; Pfurtscheller, 1992; Steriade et al., 1993; Contreras and Steriade, 1996; Llinás et al., 1999; Cotillon et al., 2000). The oscillatory activity is imposed upon the neuronal network by the inhibitory thalamic reticular and excitatory thalamocortical cells, which can fire in two distinct modes (Steriade and Llinás, 1988). The rhythmic or 'burst' mode typifies drowsy or sleeping animals; the single-spike or 'tonic' mode is more commonly seen in alert animals. In both awake and unconscious animals, however, random fluctuations between these modes occur (Livingstone and Hubel, 1981; Morrow and Casey, 1992; Mukherjee and Kaplan, 1995; Guido and Weyand, 1995). The fluctuations are, moreover, accompanied by changes in the response patterns and in the spatial and temporal receptive field properties of the neurons (Livingstone and Hubel, 1981; Funke and Eysel, 1992; Morrow and Casey, 1992; Guido et al., 1995; Mukherjee and Kaplan, 1995; Kenmochi and Eggermont, 1997; Wörgötter et al., 1998). Uncontrolled, these changes can severely hinder the evaluation of key aspects of neural processing.

The idea of intentionally altering or arresting such modes, i.e. dynamic state control, has a long history in central neurophysiology. The firing mode of thalamic cells, and therefore the thalamocortical state, is responsive to electrical, chemical, and surgical

manipulation (Moruzzi and Magoun, 1949; Steriade et al., 1985; Steriade and Llinás, 1988; McCormick and von Krosigk, 1992). While these traditional manipulations alter thalamic network properties, they are non-specific and may have widespread and sometimes devastating effects on the brain. Previous studies suggest, however, that such extreme methods are not essential to modulate thalamocortical state, and an external stimulus with the appropriate qualities might suffice (Moruzzi and Magoun, 1949; Pompeiano and Swett, 1962; Tiihonen et al., 1991). A stimulus with these qualities would be defined, with reference to the behavioral correlates of a burst-to-tonic mode change, an 'alerting stimulus' (Tennigkeit et al., 1996).

Clearly, not all stimuli are sufficient to prevent the oscillatory mode, since 7-14 Hz rhythms can be elicited or entrained by traditional clicks and tones, light flashes, mechanical pinches, and synchronous electrical stimulation (Chang, 1950; Pompeiano and Swett, 1962; Andersen and Andersson, 1968; Eggermont, 1992; Pfurtscheller, 1992; Contreras and Steriade, 1996; Dinse et al., 1997). We develop a candidate alerting stimulus for the auditory modality, the 'dynamic ripple', whose spectro-temporal properties are motivated by the cellular and network mechanisms that regulate thalamocortical state changes. We then determine whether the dynamic ripple stimulus affects the oscillatory dynamic state and how its effects differ from traditional stimuli.

MATERIALS AND METHODS

The dynamic ripple stimulus (Escabí et al., 1998) is an elaboration of the static and the moving ripple sounds (Schreiner and Calhoun, 1994; Kowalski et al., 1996). It is a temporally varying broadband sound composed of 230 sinusoidal carriers (500-20,000

Hz) with randomized phase. The magnitude of any carrier at any time is modulated by the spectrotemporal envelope, consisting of sinusoidal amplitude peaks ('ripples') on a logarithmic frequency axis which change through time. Two parameters define the envelope: the number of peaks per octave, or ripple density, and the speed and direction they are sweeping, or temporal frequency modulation (FM). Both ripple density and temporal FM rate were varied randomly and independently during the 20 minute, non-repeating stimulus. Ripple density varied slowly (max. rate of change 1 Hz) between 0 and 4 cycles per octave; the temporal FM parameter varied between 0 and 100 Hz (max. rate of change 3 Hz). Both parameters are statistically independent and unbiased within those ranges. This statistical stimulus quality has relevance for deriving receptive fields with the reverse correlation method (Aertsen and Johannesma, 1980; see also Kowalski et al., 1996). The modulation depth of the spectrotemporal envelope was 45dB. Mean intensity was set appx. 20-30 dB above the neuron's pure-tone threshold. Pure-tone stimuli were used to test the effects of traditional stimuli on the oscillatory dynamic state. Six hundred seventy-five tones were presented at a rate of 2-3 Hz in pseudorandom order at various frequencies and intensities covering the excitatory region of the neuron's receptive field, usually several octaves with a 70 dB intensity range. Each tone was 50 ms in duration, with a 5 ms linear rise/fall envelope.

Young adult cats (N = 4) were anesthetized with Nembutal (15-30 mg/kg) during the surgical procedure, and maintained thereafter in an unreflexive state with a continuous infusion of ketamine/diazepam. All procedures were in strict accordance with the UCSF Committee for Animal Research and the guidelines of the Society for Neuroscience. Simultaneous extracellular recordings (Fig. 1) were made in layers III/IV

of the primary auditory cortex (AI) and in the ventral division of the medial geniculate body (MGBv). All recordings were made with the animal in a sound-shielded anechoic chamber (IAC, Bronx, NY), with stimuli delivered via a closed, binaural speaker system. Electrodes were parylene-coated tungsten (Microprobe Inc., Potomac, MD) with impedances of 1-2 MOhm, or 3-5 MOhm tungsten electrodes plated with platinum black. Localization of thalamic electrodes, placed stereotaxically, was later confirmed with Nissl or neutral red stained sections. Spike trains were recorded on a Cygnus Technology (Delaware Water Gap, PA) CDAT-16 recorder and sorted off-line with a Bayesian spike sorting algorithm (Lewicki, 1994). Dynamic states assessed with single and multi-units were indistinguishable and results from both were therefore combined.

Thalamocortical state was assessed by the degree of synchronous oscillations in the thalamus and cortex in the 7-14 Hz range. This frequency band was chosen because, as described in the introduction, 7-14 Hz spindle-like oscillations are a paradigmatic manifestation of burst mode. Slower oscillations (< 7 Hz), also characteristic of natural sleep, were observed too rarely to afford a comprehensive analysis. The dynamic state was compared across three stimulus conditions: for spontaneous activity (silence), pure-tone stimulation, and dynamic ripple stimulation. All of the data analysis was carried out in MATLAB (Mathworks Inc., Natick, MA). Auto- and cross-spectra were computed using the Welch periodogram method, where the spike trains were binned at 1 ms resolution. The degree of synchronous oscillations was quantified by the coherence among neural spike trains. Coherence is a form of normalized cross-spectrum between unit pairs, giving a measure of the association between the spike trains, as a function of frequency. Coherences, their significance values, and their significant differences among

stimulus conditions were computed (Rosenberg et al., 1989). Only coherences whose contributing spike trains had more than 500 spikes were used. Neuronal pairs whose spontaneous (null) condition showed no evidence of thalamocortical oscillations, as judged by a peak coherence less than 0.05 in the 7-14 Hz range, were discarded. All significance values were set to 95% confidence. Percent change in coherence was computed only for those frequencies within 7-14 Hz which were significantly different across stimulus conditions. Thus, some fraction of valid unit pairs were further analyzed: 392 of 1590 pairs for pure-tone versus spontaneous, 248 of 954 pairs for ripple versus spontaneous, 167 of 565 for ripple versus tuning curve, and 171 of 522 pairs for comparisons across all three conditions. The remaining pairs did not show significant coherence differences, usually because the variability in the data was too high to determine a difference, or because there were no detectable oscillations. The peak coherence criterion, however, was kept at 0.05 to avoid biasing the sample toward units with very strong effects. Only the coherences from intra-thalamic and thalamocortical pairs were included in the analysis, as input-layer (III/IV) corticocortical pairs are probably much less reliable in reflecting dynamic state. This is due to their lack of low-threshold calcium dynamics and their long-lasting depolarization during the thalamic silent phase of the oscillations (Grenier et al., 1998).

RESULTS

The dynamic state of the thalamocortical system was assessed with simultaneous extracellular single- and multi-unit recordings in primary auditory cortex (AI) and the ventral division of the thalamic medial geniculate body (MGBv). Cross-correlation

analysis shows an oscillatory dynamic state under spontaneous (silent) conditions in the anesthetized animal (Fig. 2). Strong oscillatory behavior is expressed as large sidepeaks in the correlograms. The position of the sidepeaks along the delay axis indicates that most of the energy of these oscillations is located ~8 Hz. The widespread and synchronous quality, the frequency range (7-14 Hz), and the thalamic/cortical phase relationship of these oscillations all indicate that the thalamocortical system is in burst mode (Andersen and Andersson, 1968; Steriade and Llinás, 1988; Contreras and Steriade, 1996), the most common mode during quiet sleep.

The dynamic ripple: a candidate alerting stimulus

For a stimulus to effect a state change, namely from an oscillatory to a non-oscillatory mode, it should satisfy certain conditions based on the underlying cellular and network mechanisms. As detailed in the Discussion, such an alerting stimulus could prevent the widespread oscillatory mode through two basic means: depolarization and desynchronization of the thalamocortical cells. Specifically, stimulus features would include a generally persistent excitatory effect on most cells, a relative lack of long silent or hyperpolarizing epochs, and an asynchronous spatiotemporal quality.

The dynamic ripple (Fig. 3), fulfills these conditions for disrupting coherent oscillations. In addition, the formal aspects of its frequency-amplitude statistics permit its use in the reverse correlation method for constructing a neuron's spectro-temporal receptive field (Aertsen and Johannesma, 1980; see also Kowalski et al., 1996). With respect to depolarizing influences, the dynamic ripple stimulus is designed to drive thalamic and cortical neurons very well, as the range of spectral peak densities (Fig. 3,

along the vertical axis) and temporal (along the horizontal) modulations was selected to match the global preferences of these cells. In a system where responses are dominated by phasic onsets, such as the auditory thalamocortical network, a sustained increase in activity is best elicited by repeated excitatory drives within the range of preferred spatiotemporal modulations. As intended, ripple stimulation typically increased the activity of thalamocortical cells above the spontaneous firing rate. This contrasts with constant gaussian white or colored noise, which are poor excitatory stimuli for the lemniscal thalamocortical auditory system; since the rates of spectral and temporal modulations in these noises are much too high, they tend to inhibit many neurons. Additionally, silent or hyperpolarizing influences in the dynamic ripple stimulus, unlike repeated click or tone presentations, tend to be brief (avg. 35 ms.) .

The asynchronous spatiotemporal nature of the dynamic ripple stimulus is also apparent in its spectrogram representation (Fig. 3). Although there is a degree of local correlation across time and frequency, in imitation of many natural and communication sounds (Nelken et al., 1999), large-scale correlations are entirely absent. This is reflected in an impulsive autocorrelation function of the stimulus (not shown). Randomly changing spectral peak spacing and frequency sweeps assure that regions of slightly different receptive field preference will be excited asynchronously. By contrast, traditional stimuli such as bursts of pure tones, white noise, or clicks deliver spectrally limited or temporally highly synchronous excitation. Hence, unlike traditional experimental stimuli, the dynamic ripple coincides well with a principled idea of an alerting stimulus. These features include a generally persistent excitatory effect on most

cells, a relative lack of long silent or hyperpolarizing epochs, and an asynchronous spatiotemporal quality.

Effects of dynamic ripple and traditional stimuli on oscillatory dynamic state

As the dynamic ripple's formal aspects would suggest, its real effects on the auditory thalamocortical dynamic state are dramatic (Fig. 4). Thalamocortical correlograms (Fig. 4*a*) are compared for spontaneous (red) and ripple-driven (blue) conditions. For the spontaneous condition, strong oscillatory behavior in the 7-14 Hz range can again be seen as large sidepeaks in the correlograms. In most cases, ripple stimulation suppressed these synchronous oscillations completely. Coherences for the spike trains (Fig. 4*b*) quantify the degree of association between the two signals, as a function of frequency; it is therefore a highly appropriate assay for the degree to which the thalamocortical network is engaged in the oscillatory (7-14 Hz) dynamic state. Under ripple stimulation, the coherence peak near 8 Hz is markedly suppressed for all pairs shown (Fig. 4*b*), ranging in reduction from 122% to 496%.

To demonstrate the effectiveness of the dynamic ripple stimulus relative to other sounds in suppressing oscillations, we tested the influence of more traditional stimuli on the thalamocortical state. One of the most common experimental stimuli in auditory neurophysiology are sequentially presented bursts of pure tones. Figure 5 shows the population effects on oscillatory state for dynamic ripple and for the traditional pure-tone stimulation, each compared to the spontaneous condition. Pure-tone stimulation (Fig. 5*a*) had ambivalent effects on 7-14 Hz oscillatory synchrony, occasionally suppressing the coherence, occasionally exacerbating it, and on average leaving it virtually unchanged

from the spontaneous case (54% exacerbation). The dynamic ripple, on the other hand (Fig. 5*d*), clearly and consistently suppressed the oscillatory state, by an average of 535%. A direct comparison between pure-tone and dynamic ripple stimulation shows an even greater disparity (Fig. 5*c*), with an average relative suppression of 886%. Finally, the effects on a given unit pair are plotted for both the pure-tone versus spontaneous and the dynamic ripple versus spontaneous conditions (Fig. 5*b*). The distribution is generally unbiased across the horizontal midline but highly skewed to the left of the vertical midline. This ensures that the effects in Figure 5*a* and 5*d* apply to all unit pairs, not just different subpopulations. Therefore, in probing the receptive field properties of neurons, pure tones may drive the thalamocortical network further into *or* out of the oscillatory state, while the dynamic ripple maintains a constant non-oscillatory state resembling the alert animal. That is, unlike traditional stimuli, the dynamic ripple effectively controls the dynamic state of the thalamocortical system.

DISCUSSION

Mechanisms of state control and the design of an alerting stimulus

The specific qualities of an alerting stimulus can be derived with some confidence, since the mechanisms regulating thalamocortical state fall into two closely related categories: depolarizing and desynchronizing influences. Depolarizing influences occur at the cellular level, where a mode change can be elicited by a small fluctuation in resting membrane potential; sustained depolarization induces tonic mode by inactivating the low-threshold Ca^{++} channel, a key element in rhythmic firing (Steriade and Llinás, 1988). Depolarization from high rates of input or simply increased

activity in the circuit itself can drive the system into tonic mode (Andersen and Andersson, 1968; McCormick and Feeser, 1990; McCormick and von Krosigk, 1992). In contrast, a sustained hyperpolarization, either spontaneous or stimulus elicited, can de-inactivate the low-threshold Ca^{++} current and prepare the thalamic network for widespread spindle oscillations (McCormick and Feeser, 1990; Contreras and Steriade, 1995), a paradigmatic feature of burst mode.

In addition to persistent depolarization, an alerting stimulus could also modulate dynamic state by effectively desynchronizing the thalamocortical network. The cellular effects are similar to those described above: asynchronous barrages of afferent EPSPs transiently disrupt rhythmic firing by maintaining the low-threshold Ca^{++} channel in its inactive state (Andersen and Andersson, 1968; McCormick and Feeser, 1990). On a network level, moreover, synchronization mediated by the thalamic reticular nucleus is important for the entrainment of spindles (Steriade et al., 1993), and network desynchronization contributes to their abolition (Andersen and Andersson, 1968).

The functional profile of an alerting stimulus thus includes a persistent excitatory effect, the relative absence of long silent or hyperpolarizing epochs, and an asynchronous spatiotemporal quality. The dynamic ripple stimulus satisfies all these conditions. Its spectral and temporal modulation rates are chosen to persistently excite neurons in the thalamocortical network. Its hyperpolarizing features tend to be brief (avg. 35 ms.) — much too brief to readily enable the de-inactivation of the thalamic low-threshold Ca^{++} current. Finally, it has a broadband, smoothly varying, asynchronous spatiotemporal quality that contributes to network desynchronization. Evidently, these qualities are sufficient to control thalamocortical state.

While sufficient, however, perhaps not all the structural features of the dynamic ripple are necessary to control the state, and some more impoverished stimulus could also consistently alter firing mode. Many other stimuli, however, prove insufficient to suppress the oscillatory activity, including repeated tones presented at the characteristic frequency of the units (Dinse et al, 1997), tones of various frequencies presented for long (4 sec) times (deCharms and Merzenich, 1996), click trains (Eggermont, 1992), and amplitude-modulated (AM) noise (Eggermont, 1994). Both click trains and, especially, AM noise approximate the dynamic ripple as they are broadband and temporally modulated. Yet, they both lack spectral structure or frequency modulations and consist of highly synchronous onsets and offsets, which are virtually absent in the dynamic ripple. It thus appears that in addition to any depolarizing effects, some approximation of the dynamic ripple's asynchronous spectrotemporal modulations are essential for controlling dynamic state.

As mentioned in the introduction, the thalamocortical firing state may be manipulated through many means. Stimulus-based state control, observed with the dynamic ripple but not traditional pure-tone stimuli, differs from electrical, chemical, and surgical methods by acting through primary afferent pathways rather than through direct or indirect mimicry of mesensephalic, hypothalamic, and basal forebrain modulatory systems. Its precise biophysical effects would also differ from the naturally alert state since the typical cast of neuromodulators is presumably not engaged. Several of these modulators drive the thalamocortical system from the oscillatory into the tonic mode by reducing the leak potassium current in thalamic neurons, thereby depolarizing them (Lee and McCormick, 1997). In our case, we surmise that the dynamic ripple stimulus

suppresses burst mode via afferent (colliculo-thalamic) ionotropic excitation that persistently depolarizes thalamic cells and consistently interrupts and desynchronizes the lengthy hyperpolarizations essential for repeated burst firing. Another, mutually compatible possibility is that the stimulus produces state change through massive corticothalamic feedback, which in concert with fast EPSPs could reduce the leak potassium current and depolarize cells via metabotropic glutamate receptors (McCormick and von Krosigk, 1992; Lee and McCormick, 1997).

The interpretive dilemma of variable dynamic state

Thalamocortical dynamic state control is essential to understand how information is processed at this neural juncture so crucial for perception, action, and cognition. Without such control, the processing properties of the thalamocortical neurons are constantly and randomly changing, rendering exceedingly difficult any analysis of state-dependent aspects. The interpretive dilemma presented by a variable dynamic state extends at least to traditional spatial and temporal receptive fields (Livingstone and Hubel, 1981; Morrow and Casey, 1992; Guido et al., 1995; Mukherjee and Kaplan, 1995; Kenmochi and Eggermont, 1997; Wörgötter et al., 1998), to fine temporal correlation properties (Abeles et al., 1995), and perhaps to plasticity (Weinberger, 1995). For instance, fine temporal correlation properties can change with dynamic state, indicating that neurons may be differentially engaged in functional circuits. Similarly, if memory consolidation or topographical map rearrangement occurs preferentially during certain brain states, then to understand changes in neural responses it would be crucial to know which state is manifest. Some mechanism must be invoked to isolate these state-

dependent properties, or to mitigate the effects of unpredictable firing mode fluctuations, and care should be taken to reinterpret previous studies which did not control for dynamic state.

Stimulus-based state control addresses this problem by maintaining a particular dynamic state while probing the system's representational properties. Insofar as it fixes the network in a processing mode, it bears directly on issues of neural coding. Moreover, given the common mechanisms of this state change throughout the thalamocortical system, alerting stimuli could presumably be devised for other modalities as well. It is non-invasive, so it may be used in awake, sleeping, or anesthetized species, including humans under both normal and pathological conditions (Llinás et al., 1999). Indeed, comparative studies in awake, asleep, and comatose humans suggest that suppression of an analogous oscillatory state corresponds to cortical engagement in a task (Pfurtscheller, 1992). Due to the ubiquity of its underlying mechanisms, stimulus-based state control is a phenomenon with direct implications for neural processing in many modalities across the thalamocortical network.

Acknowledgments: This work was supported by the National Institutes of Health (DC02260, NS34835), the National Science Foundation (NSF97203398), and the Whitaker Foundation. We thank Monty A. Escabí for the use of his dynamic ripple stimulus, and both Escabí and Heather L. Read for much help in the conception and execution of the experiments. Mark Kvale developed the spike-sorting software. Jeffery Winer provided helpful comments on the manuscript.

REFERENCES

Abeles M, Bergman H, Gat I, Meilijson I, Seidemann E, Tishby N, Vaadia E (1995) Cortical activity flips among quasi-stationary states. Proc Natl Acad Sci 92: 8616-8620.

Aertsen AMHJ, Johannesma PIM (1980) Spectro-temporal receptive fields of auditory neurons in the grassfrog. Biol Cybern 38: 223-234.

Andersen P, Andersson S (1968) Physiological Basis of the Alpha Rhythm. New York: Appleton-Century-Crofts.

Buzsáki G (1991) The thalamic clock: emergent network properties. Neurosci 41(2/3): 351-364.

Chang H-T (1950) The repetitive discharges of cortico-thalamic reverberating circuit. J Neurophysiol 13: 235-257.

Contreras D, Steriade M (1995) Cellular basis of EEG slow rhythms: a study of dynamic corticothalamic relationships. J Neurosci 15(1): 604-622.

Contreras D, Steriade M (1996) Spindle oscillation in cats: the role of corticothalamic feedback in a thalamically generated rhythm. J Physiol 490: 159-179.

Cotillon N, Nafati M, Edeline J-M (2000) Characteristics of reliable tone-evoked oscillations in the rat thalamo-cortical auditory system. Hear Res 00: 1-18.

deCharms RC, Merzenich MM (1996) Primary cortical representation of sounds by the coordination of action-potential timing. Nature 381: 610-613.

Dinse HR, Krüger K, Akhavan AC, Spengler F, Schöner G, Schreiner CE (1997) Low-frequency oscillations of visual, auditory and somatosensory cortical neurons evoked by sensory stimulation. Int Jo Psychophysiol 26: 205-227.

Eggermont J (1992) Stimulus induced and spontaneous rhythmic firing of single units in cat primary auditory cortex. Hear Res 61: 1-11.

Eggermont JJ (1994) Temporal modulation transfer functions for AM and FM stimuli in cat auditory cortex. Effects of carrier type, modulating waveform and intensity. Hear Res 74: 51-66.

Escabí MA, Schreiner CE, Miller LM (1998) Dynamic time-frequency processing in the cat midbrain, thalamus, and auditory cortex: spectro-temporal receptive fields obtained using dynamic ripple spectra. Soc Neurosci Abs 24: 1879.

Funke K, Eysel UT (1992) EEG-dependent modulation of response dynamics of cat dLGN relay cells and the contribution of corticogeniculate feedback. Brain Res 573: 217-227.

Grenier F, Timofeev I, Steriade M (1998) Leading role of thalamic over cortical neurons during postinhibitory rebound excitation. Proc Natl Acad Sci 95: 13929-13934.

Guido W, Weyand T (1995) Burst responses in thalamic relay cells of the awake behaving cat. J Neurophysiol 74(4): 1782-1786.

Guido W, Lu S-M, Vaughan JW, Godwin DW, Sherman SM (1995) Receiver operating characteristic (ROC) analysis of neurons in the cat's lateral geniculate nucleus during tonic and burst response mode. Visual Neurosci 12: 723-741.

Kenmochi M, Eggermont JJ (1997) Autonomous cortical rhythms affect temporal modulation transfer functions. NeuroReport 8: 1589-1593.

Kisley MA, Gerstein GL (1999) Trial-to-trial variability and state-dependent modulation of auditory-evoked responses in cortex. J Neurosci 19(23):10451-10460.

Kowalski N, Depireux DA, Shamma SA (1996) Analysis of dynamic spectra in ferret primary auditory cortex. I. Characteristics of single-unit responses to moving ripple spectra. J Neurophysiol 76(5): 3503-3523.

Lee KH, McCormick DA (1997) Modulation of spindle oscillations by acetylcholine, cholecystokinin and 1*S*,3*R*-ACPD in the ferret lateral geniculate and perigeniculate nuclei *in vitro*. Neurosci 77(2): 335-350.

Lewicki MS (1994) Bayesian modeling and classification of neural signals. J Neural Comp 6: 1005-1030.

Livingstone MS, Hubel DH (1981) Effects of sleep and arousal on the processing of visual information in the cat. Nature 291: 554-561.

Llinás RR, Ribary U, Jeanmonod D, Kronberg E, Mitra PP (1999) Thalamocortical dysrhythmia: a neurological and neuropsychiatric syndrome characterized by magnetoencephalography. Proc Natl Acad Sci 96(26): 15222-15227.

McCormick DA, Feeser HR (1990) Functional implications of burst firing and single spike activity in lateral geniculate relay neurons. Neurosci 39(1): 103-113.

McCormick DA, von Krosigk M (1992) Corticothalamic activation modulates thalamic firing through glutamate "metabotropic" receptors. Proc Natl Acad Sci 89: 2774-2778.

Morrow TJ, Casey KL (1992) State-related modulation of thalamic somatosensory responses in the awake monkey. J Neurophysiol 67: 305-317.

Moruzzi G, Magoun HW (1949) Brain stem reticular formation and activation of the EEG. Elec Clin Nphys 1: 455-473.

Mukherjee P, Kaplan E (1995) Dynamics of neurons in the cat lateral geniculate nucleus: in vivo electrophysiology and computational modeling. J Neurophysiol 74: 1222-1243.

Nelken I, Rotman Y, Bar Yosef O (1999) Responses of auditory-cortex neurons to structural features of natural sounds. Nature 397: 154-157.

Pfurtscheller G (1992) Event-related synchronization (ERS): an electrophysiological correlate of cortical areas at rest. Elec Clin Neurophys 83: 62-69.

Pompeiano O, Swett JE (1962) EEG and behavioral manifestations of sleep induced by cutaneous nerve stimulation in normal cats. Arch Ital Biol 100: 311-342.

Rosenberg JR, Amjad AM, Breeze P, Brillinger DR, Halliday D M (1989) The Fourier approach to the identification of functional coupling between neuronal spike trains. Prog Biophys Molec Biol 53: 1-31.

Schreiner CE, Calhoun BM (1994) Spectral envelope coding in cat primary auditory cortex: properties of ripple transfer functions. Audit Neurosci 1: 39-61.

Steriade M, Llinás R (1988) The functional states of the thalamus and the associated neuronal interplay. Physiol Rev 68(3): 649-742.

Steriade M, Deschênes M, Domich L, Mulle C (1985) Abolition of spindle oscillations in thalamic neurons disconnected from nucleus reticularis thalami. J Neurophysiol 54: 1473-1497.

Steriade M, McCormick D, Sejnowski T (1993) Thalamocortical oscillations in the sleeping and aroused brain. Science 262: 679-685.

Tennigkeit F, Schwarz DWF, Puil E (1996) Mechanisms for signal transformation in lemniscal auditory thalamus. J Neurophysiol 76(6): 3597-3608.

Tiihonen J, Hari R, Kajola M, Karhu J, Ahlfors S, Tissari S (1991) Magnetoencephalographic 10-Hz rhythm from the human auditory cortex. Neurosci Lett 129: 303-305.

Weinberger NM (1995) Dynamic regulation of receptive fields and maps in the adult sensory cortex. Ann Rev Neurosci 18: 129-158.

Wörgötter F, Suder K, Zhao Y, Kerscher N, Eysel UT, Funke K (1998) State-dependent receptive-field restructuring in the visual cortex. Nature 396: 165-168.

FIGURE LEGENDS

FIG 1. Summary of the experimental procedure. Simultaneous extracellular recordings were made in layers III/IV of primary auditory cortex and in the ventral division of the medial geniculate body. Spike trains were sorted off-line. Thalamocortical temporal relations and dynamic state were assessed with cross-correlograms and coherence measures. (AI, primary auditory cortex; MGB-V, medial geniculate body, ventral division; SSG, suprasylvian gyrus; LGN, lateral geniculate nucleus; HC, hippocampus).

FIG 2. The oscillatory thalamocortical state is apparent in cross-correlograms under spontaneous conditions. On the diagonal are depicted the autocorrelograms for two thalamic and two cortical neurons, recorded simultaneously. Cross-correlograms among the four units are off the diagonal. There is strong oscillatory synchrony within the thalamus, within the cortex, and across the thalamocortical system. The oscillations are manifest as side-peaks with a temporal lag of ~120 ms and thus have a frequency near 8 Hz. They are generally in phase across the entire network, with a typical small (~0-15 ms) thalamic phase lead over cortex. Dashed lines indicate 95% confidence under an independent, Poisson assumption.

FIG 3. The dynamic ripple stimulus satisfies a principled conception of an 'alerting stimulus'. The spectrogram representation of one short segment is shown. Regions of high spectrotemporal energy are represented by red, and regions of low energy by blue. The dynamic ripple is a wideband sound with spectral peaks whose spacing and frequency modulations are varied randomly and independently over ~20 min. The

stimulus mimics many elements of natural sounds, including the temporal modulations and depth or contrast distribution of the modulations. While there is a degree of correlation across the spectral axis of the sound, also in imitation of many natural and communication sounds, the dynamic ripple is devoid of any large-scale correlations or long silent periods. Spectral and temporal modulations are bounded to match the preferred range of thalamic and cortical cells, and acoustic energy moves about rapidly and randomly, assuring a highly asynchronous drive across populations of neurons.

FIG 4. Correlograms and coherences reveal suppression of the oscillatory state with ripple stimulation. Four thalamocortical neural pairs are shown. (*a*) Spontaneous thalamocortical correlograms from Figure 1 are plotted in red. Correlograms under the ripple-driven condition are in blue. The oscillatory activity is markedly suppressed by ripple stimulation. Moreover, evidence for short-time functional thalamocortical correlations (peak lag time ~3 ms) under the ripple condition is either absent or greatly obscured by large-scale oscillations under the spontaneous condition. All correlograms are normalized to the firing rates of the contributing neurons, for comparison across conditions. (*b*) Coherences for the same units. The robust suppression of the oscillatory dynamic state with the ripple stimulus is seen as a clear reduction in the size of the peak (clockwise from upper left, 496%, 474%, 122%, & 135% reduction). Vertical green bars demarcate the 7-14 Hz region of analysis.

FIG 5. For all thalamo-thalamic and thalamocortical pairs, the percent change in 7-14 Hz coherence is shown across the three conditions: pure-tone, dynamic ripple, and

spontaneous. In the histograms, pairs are binned to the left of zero if there is a suppression of 7-14 Hz coherence (oscillatory energy) from the one condition to the other and to the right if there is an exacerbation of the coherence. (*a*) Pure tones tend to have ambivalent effects on spontaneous thalamocortical oscillatory synchrony (mean 54% exacerbation). (*d*) The dynamic ripple sound, in contrast, robustly and consistently suppresses the oscillations (mean -535%). Similar effects are seen (*c*) when comparing dynamic ripple to pure tone stimulation (mean -886% suppression). (In the histograms, striped endbins indicate values beyond that end of the abscissa; the lowest bin in (*c*) is truncated from value 57 for clarity). The scatter plot (*b*) compares, for the same pairs, effects in (*a*) directly to those in (*d*). Circles in quadrant one (upper-right, n=2) indicate that both the ripple sound and pure tones exacerbated the oscillatory synchrony; those above the diagonal line indicate that the pure tone exacerbated the coherence even more than the dynamic ripple. Quadrant two (upper-left, n=77) contains those pairs where the dynamic ripple suppressed but the pure tones exacerbated the coherence. Circles in quadrant three (lower-left, n=92) indicate that both the dynamic ripple and pure tones suppressed the 7-14 Hz coherence; those above the diagonal line (n=80) indicate that the pure tone suppressed the coherence less than the ripple. Finally, quadrant four (lower right, n=0) would contain those pairs where the dynamic ripple exacerbated, but the pure tones suppressed the oscillations.

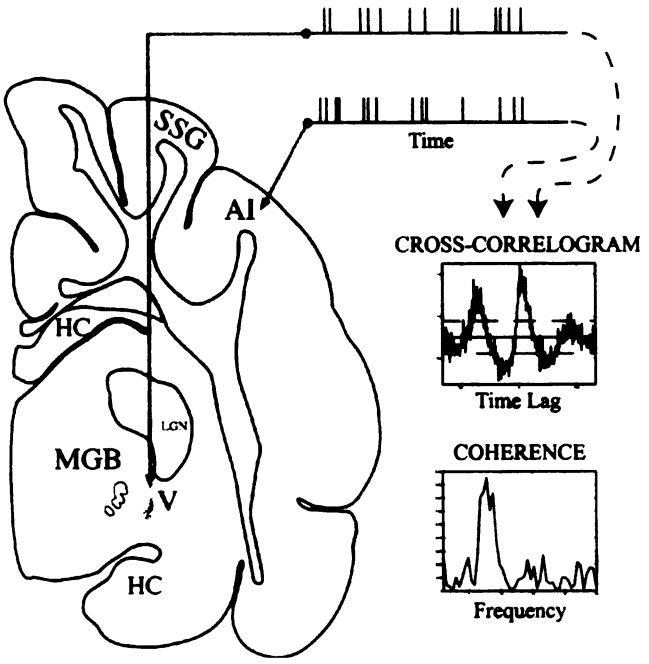
SSG
AI
HC
LGN
MGB
V
HC
Time
CROSS-CORRELOGRAM
Time Lag
COHERENCE
Frequency

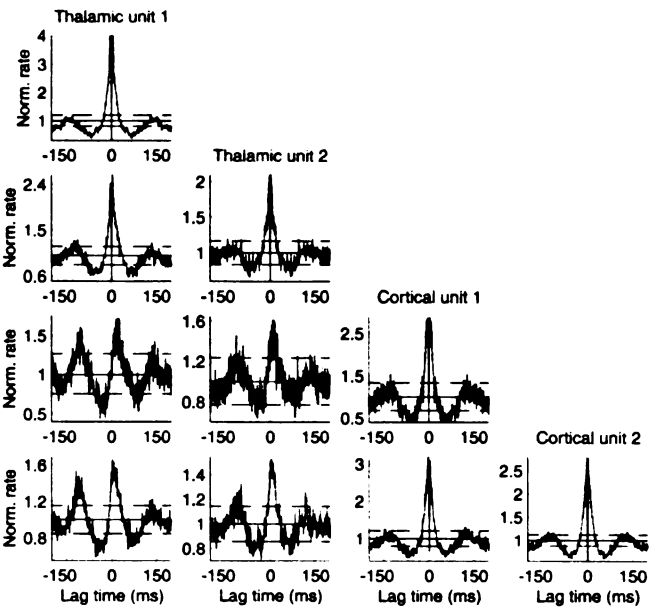
Thalamic unit 1
Thalamic unit 2
Cortical unit 1
Cortical unit 2
Norm. rate
Lag time (ms)
-150
0
150

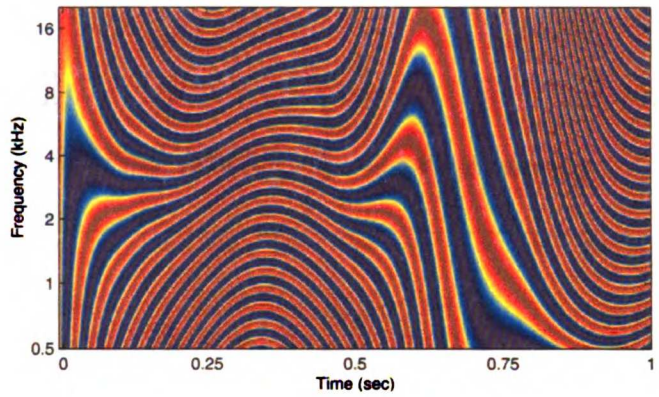
16
8
4
2
1
0.5
Frequency (kHz)
0
0.25
0.5
0.75
1
Time (sec)

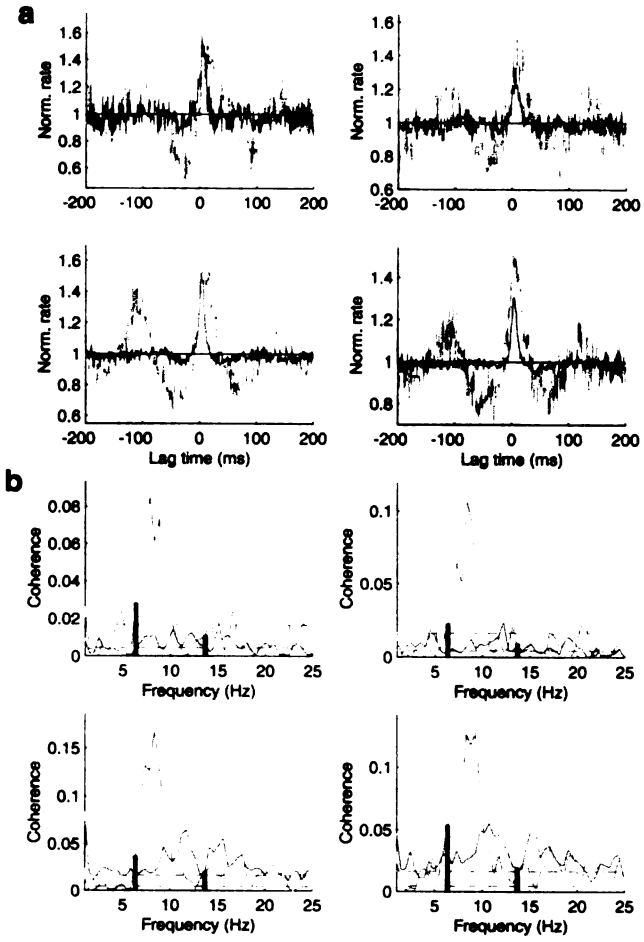
a
Norm. rate
Lag time (ms)
b
Coherence
Frequency (Hz)

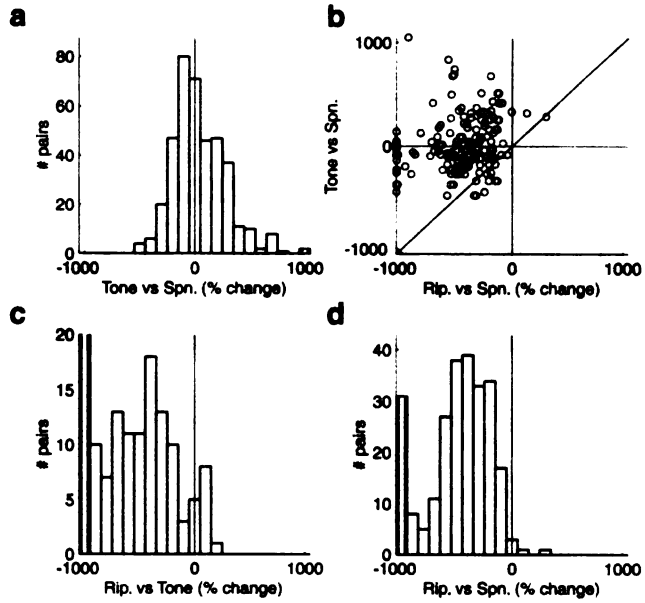
a
pairs
Tone vs Spn. (% change)
b
Tone vs Spn.
Rip. vs Spn. (% change)
c
pairs
Rip. vs Tone (% change)
d
pairs
Rip. vs Spn. (% change)

CHAPTER 2:

SPECTRO-TEMPORAL RECEPTIVE FIELDS IN THE LEMNISCAL AUDITORY THALAMUS AND CORTEX

ABSTRACT: Receptive fields have been characterized independently in the lemniscal auditory thalamus and cortex, usually with spectrotemporally simple sounds tailored to a specific task. No studies have employed naturalistic stimuli to compare the two stations in temporal, spectral, and aural domains simultaneously and under identical conditions. Our understanding of how the thalamocortical system transforms sensory representations thus remains incomplete. We recorded simultaneously in the ventral division of the medial geniculate body (MGBv) and in primary auditory cortex (AI) in the ketamine-anesthetized cat. Spectro-temporal receptive fields of single units (n = 387) were derived by reverse-correlation with a broadband and dynamically varying stimulus, the dynamic ripple. Spectral integration, as measured by excitatory bandwidth and spectral modulation preference, was similar across both stations (mean $Q_{1/e}$ thalamus = 5.8, cortex = 5.4; upper cutoff of spectral modulation transfer function, thalamus = 1.30 cycles/octave, cortex = 1.37 cycles/octave). Temporal modulation rates slowed by a factor of two from thalamus to cortex (mean preferred rate, thalamus = 32.4 Hz, cortex = 16.6 Hz; upper cutoff of temporal modulation transfer function, thalamus = 62.9 Hz, cortex = 37.4 Hz). We found no correlation between spectral and temporal integration properties, suggesting that the excitatory-inhibitory interactions underlying preference in each domain are largely independent. A small number of neurons in each station had highly asymmetric STRFs, evidence of frequency sweep selectivity, but the population showed no directional bias. Binaural preferences differed in their relative proportions, most notably an increased prevalence of excitatory contralateral-only cells in cortex (40%) versus thalamus (23%), indicating a reorganization of this parameter. By comparing simultaneously along multiple stimulus dimensions in both stations, these

observations establish the global characteristics of the thalamocortical receptive field transformation.

INTRODUCTION

The thalamus and cortex are highly interconnected structures whose response properties are intimately related. In the auditory system, many studies have described receptive fields in thalamus or in cortex with a large variety of experimental protocols (for reviews, see Clarey et al. 1994; de Ribaupierre 1997), but very few have characterized both stations simultaneously (Creutzfeldt et al. 1980; Zhang and Suga 1997) or even endeavored to draw thalamocortical comparisons from non-simultaneous recordings (Pelleg-Toiba & Wollberg 1989; Clarey et al. 1995; Barone et al. 1996; Samson et al. 2000). Since differences in animal model, anesthesia, stimuli, and measured response parameters could affect results, the literature cannot support a direct comparison of multiple receptive field dimensions between thalamus and cortex.

The choice of experimental stimulus is of particular importance, since it constrains the sort of knowledge we can gain from a neural system. Traditional, spectrotemporally simple sounds have the advantage of being easily parameterized and manipulated. They suffer, however, from their task-specificity: a given stimulus usually reveals a very limited aspect of neural response preference, whether temporal (e.g. clicks), spectral (e.g. tones of varying frequency), or aural (e.g. best-frequency tones at varying interaural delay/level). Natural sounds such as vocalizations, in contrast, tend to be spectrotemporally complex (Smolders et al 1979; Nelken et al. 1999) and may change along all these dimensions simultaneously. Yet, except for certain highly stereotyped animal vocalizations (Suga and Jen 1976), the complexity of natural sounds resists systematic manipulation along multiple, well-defined parameters. Although numerous studies have revealed how neurons respond to particular aspects of natural sounds

(Symmes et al. 1980; Creutzfeldt et al. 1980; Glass & Wollberg 1983; Müller-Pruess 1986; Doupe and Konishi 1991; Steinschneider et al. 1994; Wang et al. 1995; Rauschecker 1998; Bieser 1998), few have used the sounds to explore the general processing capabilities of thalamic or cortical cells (but see Theunissen & Doupe 1998; Theunissen et al. 2000).

While this variety of investigative methods presents a rich and multifaceted view of thalamic and cortical responses, it thereby renders inaccessible any global characterization of the thalamocortical transformation of sensory representations. We recorded in both stations simultaneously, allowing a direct comparison of thalamic and cortical receptive field properties under identical experimental conditions. Our synthetic and spectrotemporally complex stimulus, the dynamic ripple, was designed to share many properties with natural sounds (Escabí et al. 1999) and to satisfy the formal requirements for deriving receptive fields with reverse correlation. The dynamic ripple therefore enables a unified description of temporal, spectral, spectrotemporal, and aural neural response preferences to well-controlled and naturalistic sensory stimulation.

METHODS

Electrophysiological methods and stimulus design have been described in a previous report (Miller and Schreiner 2000). Essential details are repeated below.

Electrophysiology

Young adult cats (N = 4) were given an initial dose of ketamine (22mg/kg) and acepromazine (0.11mg/kg), then anesthetized with Nembutal (15-30 mg/kg) during the

surgical procedure. The animal's temperature was maintained with a thermostatic heating pad. Bupivicaine was applied to incisions and pressure points. Surgery consisted of a tracheotomy, reflection of the soft tissues of the scalp, craniotomy over AI and the suprasylvian gyrus (for the thalamic approach), and durotomy. After surgery, the animal was maintained in an unreflexive state with a continuous infusion of ketamine/diazepam (10 mg/kg ketamine, 0.5 mg/kg diazepam in lactated ringer's solution). All procedures were in strict accordance with the UCSF Committee for Animal Research and the guidelines of the Society for Neuroscience.

All recordings were made with the animal in a sound-shielded anechoic chamber (IAC, Bronx, NY), with stimuli delivered via a closed, binaural speaker system (diaphragms from Stax, Japan). Simultaneous extracellular recordings were made in the thalamorecipient layers (IIIb/IV) of the primary auditory cortex (AI) and in the ventral division of the medial geniculate body (MGBv). For the purposes of a parallel study we targeted thalamic and cortical neurons with similar best frequency. Except for this constraint, recording locations in thalamus were randomly distributed within the MGBv; and those in AI spanned the central narrowly-tuned and flanking broadly-tuned regions. Electrodes were parylene-coated tungsten (Microprobe Inc., Potomac, MD) with impedances of 1-2 MOhm, or 3-5 MOhm tungsten electrodes plated with platinum black. One or two electrodes were placed in each station with hydraulic microdrives on mechanical manipulators (Narishige, Tokyo, Japan), mounted on a stereotaxic frame (David Kopf Instruments, Tujunga, CA) or on supplementary supports. Localization of thalamic electrodes, which were stereotaxically advanced along the vertical, was confirmed with Nissl stained sections. Spike trains were amplified and bandpass filtered

(500-10,000 Hz), recorded on a Cygnus Technology (Delaware Water Gap, PA) CDAT-16 recorder with 24 kHz sampling rate, and sorted off-line with a Bayesian spike sorting algorithm (Lewicki 1994). Each electrode location yielded an average of 1.9 well-isolated single units. Stimulus-driven neural activity was recorded for approximately 20 minutes at each location.

Stimulus

The dynamic ripple stimulus (Schreiner and Calhoun 1994; Kowalski et al. 1996; Escabí et al. 1998; Miller and Schreiner 2000) is a temporally varying broadband sound composed of 230 sinusoidal carriers (500-20,000 Hz) with randomized phase. The magnitude of any carrier at any time is modulated by the spectrotemporal envelope, consisting of sinusoidal amplitude peaks ('ripples') on a logarithmic frequency axis which change through time. Two parameters define the envelope: a spectral and a temporal modulation parameter. Spectral modulation rate is defined by the number of spectral peaks per octave, or ripple density. Temporal modulations are defined by the speed and direction of the peaks' change. Both the spectral and temporal modulation parameters were varied randomly and independently during the 20-minute, non-repeating stimulus. Spectral modulation rate varied slowly (max. rate of change 1 Hz) between 0 and 4 cycles per octave; the temporal modulation rate varied between –100 Hz (downward sweep) and 100 Hz (upward sweep), with a maximum 3 Hz rate of change. Both parameters were statistically independent and unbiased within those ranges. In one experiment, however, the temporal modulation spectrum decayed slightly; all evidence of this mild bias was readily abolished while thresholding the STRFs (see Analysis). Maximum modulation

depth of the spectrotemporal envelope was 45dB. Mean intensity was set appx. 20-30 dB above the neuron's pure-tone threshold. An independent dynamic ripple sound was presented simultaneously to each ear.

Analysis

Data analysis was carried out in MATLAB (Mathworks Inc., Natick, MA). For each neuron, the reverse correlation method was used to derive the spectrotemporal receptive field (STRF), which is the average spectrotemporal stimulus envelope immediately preceding each spike (Aertsen and Johannesma 1980; Escabí et al. 1998; deCharms et al. 1998; Klein et al. 2000; Theunissen et al. 2000). Positive regions of the STRF indicate that stimulus energy at that frequency and time tends to increase the neuron's firing rate, and negative regions indicate where the stimulus envelope induces a decrease in firing rate (**Fig. 1a**). In all locations, the STRF procedure was performed on the typically dominant, contralateral ear; in 75% of the recordings, we performed an independent STRF calculation for the ipsilateral ear. Only units with robust STRF features from one or both ears were analyzed further. The presence of robust features was determined by the largest contiguous deviation in the significant STRF, where threshold was set at $p < 0.002$. Since spectral and temporal modulations in the stimulus are lowpass (up to 4 cycles/octave and 100 Hz, respectively), the smallest possible STRF feature is as large as the fastest modulation half-cycle. In the absence of noise, the smallest feature would thus be 1/8 octaves x 5 ms. If we require that the peak rise at least twice as high as the noise threshold (a conservative criterion), then the minimum size for a robust STRF feature is 0.095 octaves by 3.8 ms. By this measure, 223 of 240 (93%)

thalamic single units and 164 of 267 (61%) cortical single units were analyzed further. Of the units lacking STRF features, over half occurred at a recording location where another unit had an STRF (65% thalamus, 61% cortex). Thus, 98% of thalamic and 85% of cortical locations yielded at least one well-isolated single unit with an STRF.

Modulation properties were derived by performing a two-dimensional Fourier transform of the significant STRF, smoothed with a 2-D gaussian of standard deviation 2 pixels, to give the ripple transfer function (RTF) (**Fig. 1b**). The RTF is thus a signal in the parameter space of temporal modulation rate versus spectral modulation rate, or ripple density. Preferred temporal and spectral modulation rates are analogous to moving grating speed and spatial frequency, respectively, in the visual system. RTF energy at low (high) ripple densities indicates preference for broadly (narrowly) spaced spectral contours. Energy at large positive (negative) temporal modulations indicates a preference for fast up- (down-) frequency sweeps; energy near zero temporal modulation means the cell has little preference for sweeps. As a Fourier transform is sensitive to periodicities in the STRF envelope, the RTF depends heavily on the relationship of excitatory and inhibitory STRF subfields. For instance, if the sole STRF feature is an excitatory peak, the RTF will tend to be lowpass in both temporal and spectral modulation domains. Strong flanking inhibition in frequency or in time will tend to produce an RTF signal that is bandpass in the spectral or temporal domain, respectively (see **Fig. 1a-l**).

Most response parameters were derived from the feature with maximum deviation in the STRF or RTF. Best frequency (Hz) and peak latency (ms) are the spectral and temporal coordinates of the maximum deviation in the STRF (**Fig. 1a**, gray arrows). The spectrotemporal boundaries of an STRF feature were defined by a contour at 1/e times

the maximum value, which typically circumscribed about 90% of the feature's energy. Bandwidth is the width of this contour in frequency (**Fig. 1a**, black arrows). The sharpness-of-tuning measure $Q_{1/e}$ is defined as the best frequency divided by the bandwidth; thus higher $Q_{1/e}$ is sharper tuning. Best spectral modulation (BSM, in cycles/octave) and best temporal modulation (BTM, in Hz) are the spectral and temporal coordinates of the maximum deviation in the RTF (**Fig. 1b**, arrows). A sharpness-of-tuning measure can also be derived for spectral and temporal modulation preference, identically to that described above for the STRF but from the main RTF feature. The temporal modulation transfer function (tMTF) and spectral modulation transfer function (sMTF) were constructed by first folding the RTF along the temporal modulation = 0 axis, thereby ignoring sweep direction. This RTF was then collapsed or summed along the complementary (spectral/temporal) dimension. For instance, the 2-D RTF was collapsed along the dimension of spectral modulation to yield a 1-D signal in the temporal modulation domain. A composite, or population RTF was constructed by averaging the RTFs from all units in thalamus or cortex, where each unit's RTF was weighted equally. Composite tMTFs and sMTFs were then derived from the composite RTF.

Spectrotemporal asymmetry in the STRF, such as frequency sweep selectivity, was measured in the RTF domain. At each spectral modulation rate, the imbalance of RTF energy to either side of the vertical midline (temporal modulation = 0) was defined as the difference between positive and negative energies divided by the sum of energies. These values were combined by a weighted sum across all spectral modulation rates, with weights equal to the proportion of total RTF energy at each modulation rate, to give an

asymmetry measure. Spectrotemporal asymmetry thus has value –1 for strong down-sweep preference, 0 for no mean asymmetry, and +1 for strong up-sweep preference.

Contralateral and ipsilateral STRFs were compared in two complementary ways. The first was a contra-ipsi peak measure, an ordered pair [contra, ipsi] with the value of greatest contralateral and ipsilateral STRF extremes, in standard deviations above the noise. Excitatory extremes are positive numbers and inhibitory extremes are negative numbers. The second binaural measure was a similarity index (DeAngelis et al. 1999) related to a correlation coefficient. The two significant STRFs were treated as vectors rather than arrays in time and frequency. The binaural similarity index (BSI) is then the inner product of the vectorized contralateral and ipsilateral STRFs, divided by both of their vector norms. A vector norm is the square root of the inner product of a vector with itself. A BSI greater than zero indicates binaural agreement of the STRFs in frequency, time, and sign; a BSI less than zero means binaural inputs are, on average, antagonistic; and a BSI equal to zero indicates no correlation between binaural STRF shapes.

RESULTS

Typical STRFs appear in **Figure 1**. The nearly ubiquitous excitatory peak in the contralateral STRF may be flanked on upper and/or lower frequencies by an inhibitory region (**Fig. 1a**). Also common is an inhibitory region at the best excitatory frequency but at a longer latency; this indicates a preference for energy onsets (i.e. transitions from low to high energy). Since the RTF (**Fig. 1b**) is a Fourier transform of the STRF, it depends heavily on the relationship between excitatory and inhibitory STRF features. Consequently, so do the spectral and temporal modulation transfer functions (sMTF and

tMTF, respectively), which are derived from the RTF. Neighboring excitatory-inhibitory regions impart a bandpass preference for modulations in time or frequency, while a sole excitatory or inhibitory feature indicates lowpass preference for modulations. For instance, if a neuron's STRF has both flanking inhibition in frequency and preceding inhibition in time (**Fig. 1a**), then its RTF tends to be bandpass in both spectral and temporal domains (**Fig. 1b**). The sMTF (**Fig. 1c**) and tMTF (**Fig. 1d**) likewise reflect these preferences. If a neuron's STRF has flanking inhibition in frequency but lacks preceding inhibition in time (**Fig. 1e**), it tends to be bandpass for spectral and lowpass for temporal modulations (**Fig. 1f-h**). If instead the neuron's STRF lacks flanking inhibition but shows strong preceding inhibition in time (**Fig. 1i**), it tends to be lowpass in the spectral and bandpass in the temporal domain (**Fig. 1j-l**).

Examples of less common STRF structures are shown in **Figure 2**. Occasionally, an inhibitory domain forms an uninterrupted swath through time and frequency around the main excitatory peak (**Fig. 2a**). Other neurons have very strong frequency modulation (FM) sweep selectivity (**Fig. 2b**); this cortical neuron prefers a particular speed of upward sweep (upward, since the time axis in an STRF is time-preceding-spike). Very rarely, a well-isolated single unit has multiple excitatory and inhibitory domains in a complex arrangement (**Fig. 2c**) or a single, solely inhibitory STRF (**Fig. 2d**.).

When the ipsilateral ear produces an STRF, the features may vary widely in their binaural spectrotemporal agreement or antagonism. The binaural STRFs in **Figure 3a** have excitatory regions of similar spectrotemporal extent. In contrast, strong binaural overlap of subfields with opposite sign occurs in **Figure 3b**. Although less common, binaural features may show more complex contra-ipsi relationships, such as a single

subfield for one ear aligned with multiple cooperative or antagonistic subfields in the other ear (**Fig. 3c**). Not all cells in thalamus or cortex, however, have an ipsilateral STRF, but most show a contralateral STRF. Therefore, much of the following analysis will describe features for the typically dominant, contralateral ear.

Temporal response preferences

Peak latencies for thalamic and cortical responses are defined by the moment of maximum deviation (usually excitation) in the contralateral STRF. First-spike latencies cannot be unambiguously assessed with a continuous stimulus such as the dynamic ripple. Both thalamus and cortex show a unimodal peak-latency distribution with median 10.5 ms and 13.0 ms (mean 13.2 ms and 17.9 ms), respectively (**Fig. 4**). The distributions are highly overlapping, with most of the thalamic latencies occurring after the earliest cortical ones. That is, the thalamic and cortical populations are simultaneously active for most of their response durations. Nevertheless, the tail of the cortical distribution extends to longer latencies (appx. 45 ms) than the thalamic tail (appx. 30 ms).

The temporal modulation transfer function (tMTF) measures a cell's preference for stimulus energy to fluctuate in time. It is constructed by collapsing the energy in the 2-D ripple transfer function into the temporal modulation domain (see Methods). Since the RTF depends heavily on the relationship of excitatory and inhibitory subfields in the STRF, so do the modulation preferences of the tMTF. Preceding or following the typical excitatory STRF peak, weak or absent STRF inhibition in time tends to produce a

lowpass modulation function. Strong inhibition in time usually results in a bandpass function for temporal selectivity.

Representative tMTFs for thalamus and cortex are shown in **Figures 5a & b**, respectively. Distributions of the absolute value of best temporal modulation rate (BTM) for thalamic and cortical cells are plotted in **Figure 5c**. The histograms from both stations are bimodal, with a small but significant proportion of lowpass units, and most neurons bandpass at higher rates (mean: 32.4 Hz thalamus, 16.6 Hz cortex; median: 27.4 Hz thalamus, 14.4 Hz cortex; 2-sample t-test, $p < 0.001$). While cortical neurons cover a similar range as the thalamic units, most (90%) thalamic best modulation rates fall below 63.6 Hz, whereas 90% of cortical rates fall below 33.5 Hz. Such BTM histograms reveal the single preferred rates for the neurons, but they do not incorporate the overall filter properties of the neural population. By averaging all tMTFs for thalamic and cortical units separately, we approximate the temporal modulation filter of these two stations (**Fig. 5d**). The composite thalamic tMTF has proportionally more energy at higher modulation rates than cortex (peak: 21.9 Hz thalamus, 12.8 Hz cortex; upper 6dB cutoff: 62.9 Hz thalamus, 37.4 Hz cortex). Therefore, whether based on preferred rates alone or the overall filter properties, both stations are effectively bandpass temporal modulation filters with cortical rates about half those in thalamus.

Spectral response preferences

The spectral modulation transfer function (sMTF) measures a neuron's preference for the spacing of spectral contours. Complementary to the tMTF, the sMTF is constructed by collapsing the ripple transfer function into the spectral modulation

domain. It thus depends on the relationship of excitatory and inhibitory STRF subfields across frequency: weak or absent STRF sideband inhibition produces a lowpass modulation function, and strong sideband inhibition results in a sharp bandpass function. Spectral modulation rate or ripple density is expressed as the number of cycles of the ripple stimulus envelope per octave frequency.

Representative examples of thalamic and cortical sMTFs are shown in **Figures 6a & b**, respectively. The distribution of best spectral modulation rates (BSM) for all units shows a heavy bias toward low values, or broad spectral preferences (**Fig. 6c**. mean: 0.58 cyc/oct thalamus, 0.46 cyc/oct cortex; median: 0.42 cyc/oct thalamus, 0.25 cyc/oct cortex). There are proportionally more lowpass cortical cells, which accounts for the significant difference between the means (2-sample t-test, $p = 0.029$), but the distributions are otherwise very similar. As in the temporal domain, the BSM histograms obscure the filter properties of the neural populations. We obtain approximations to the overall spectral transfer functions of thalamus and cortex by summing all the individual unit sMTFs in each station (**Fig. 6d**). Unlike the temporal transfer functions, the composite spectral transfer functions are very similar between thalamus and cortex, with a peak of 0 cyc/oct in both thalamus and cortex, and upper 6dB cutoff values of 1.30 cyc/oct in thalamus and 1.37 cyc/oct in cortex. In general, both thalamic and cortical spectral filters are therefore lowpass and almost perfectly overlapping.

In addition to BSM, we also employ a simpler traditional measure of spectral selectivity, Q. For the main contralateral STRF feature (almost always excitatory), $Q_{1/e}$ is the best frequency divided by the bandwidth at 1/e of the peak magnitude (see **Fig. 1a**). Distributions of $Q_{1/e}$ for thalamus and cortex are highly overlapping (**Fig. 7a**), with a

mean of 5.8 in thalamus and 5.4 in cortex. The thalamus, however, has proportionally more neurons with very sharp tuning (Q>10). Since BSM depends on the relationship between excitatory and inhibitory subfields and $Q_{1/e}$ does not, comparing the BSM and $Q_{1/e}$ for each unit gives a rough measure of how great a role sideband inhibition plays in spectral integration properties (**Fig. 7b,c**). The diagonal line indicates a perfect match between $Q_{1/e}$ and BSM, where sideband inhibition is very strong and of the same spectral envelope periodicity as the main excitatory peak. Units near the bottom of the scatterplot lack strong sideband inhibition and therefore tend toward lowpass transfer functions. In both thalamus and cortex, some neurons have strong sideband inhibition, many have none at all, and most fall somewhere in between. The fact that very few symbols appear above the diagonals indicates that strong sideband inhibition is almost never of higher spatial periodicity than one would infer from the excitatory bandwidth. Whether considering traditional Q values or modulation transfer functions, therefore, thalamus and cortex exhibit very similar spectral response profiles.

Spectro-temporal response preferences

One of the strengths of the STRF is that it describes spectral and temporal response properties under identical stimulus conditions. Overall thalamic and cortical spectrotemporal modulation preferences are summarized in composite RTFs (**Fig. 8a,b**). The joint distribution of BTMs and BSMs (superimposed symbols), moreover, reveals whether spectral and temporal properties are correlated for individual cells. Unlike previous sections where the absolute value of BTM was used, thus ignoring frequency sweep direction preference, this analysis includes the sign of the BTM (see Methods for

details). If modulation properties in time and frequency domains depend on one another, the joint distribution should have an informative structure. For instance, if the same excitatory-inhibitory processes underlie both spectral and temporal modulation preferences, then BSM and BTM will be positively correlated. Or if the cells behave as filters with limited time-frequency resolution, one would expect an anti-correlated limit between temporal and spectral modulation sensitivities. Such a time-frequency tradeoff would require that neurons with high BTMs have low BSMs, and neurons with high BSMs have low BTMs. In fact, neither thalamic nor cortical cells show any correlation between spectral and temporal modulation rates. Except for the biases in both domains described above and reflected in the composite RTFs, BTM-BSM combinations fill the space probed by the stimulus. Nor is there correlation between the sharpness of modulation tuning, or $Q_{1/e}$, in frequency versus time ($p > 0.2$).

An asymmetry in the magnitude of the RTF about the vertical midline (temporal modulation = 0) indicates a spectrotemporal asymmetry or nonseparability of the spectral and temporal aspects in the STRF. Asymmetries in the STRF can take many forms, but the strongest and most paradigmatic example is frequency sweep preference (e.g. **Fig. 2b**), with up-sweep preference resulting in higher RTF energy at positive temporal modulation values, and down-sweep preference resulting in higher energy at negative values. Since the scatterplots overlying Figures 8a & b only give the individual RTF maxima rather than the distributions of energy, and since the underlying composite RTFs obscure the filter properties of the individual cells, they cannot adequately reveal the RTF asymmetries across the population. To directly measure frequency sweep bias for each cell, we compared the RTF energies on either side of the vertical midline (temporal

modulation = 0) at each spectral modulation rate, then combined values from all spectral modulation rates by a weighted sum to derive a spectrotemporal asymmetry measure. The spectrotemporal asymmetry has value –1 for strong down-sweep preference, 0 for no asymmetry, and +1 for strong up-sweep preference. Most cells in both stations have little preference for sweeps in either direction (**Fig. 8c,d**), i.e. their STRFs are spectrotemporally rather symmetric. The STRF in **Figure 4a**, for instance, has an asymmetry measure near zero (-0.07). A small proportion of cells, however, show strong preference for sweeps of the up or down directions, with no clear population bias toward either. The STRF in **Figure 4b**, for example, has a large positive asymmetry of 0.54. The proportion of neurons sensitive to sweep direction, moreover, is similar in MGBv and AI.

Binaural response preferences

The STRF from stimulation of the contralateral ear is typically dominant and thus serves as the basis for most of the preceding analysis. As illustrated in Figure 3, however, many thalamic and cortical cells also show STRFs to independent, simultaneous stimulation of the ipsilateral ear. The STRFs of a given neuron may differ substantially for contra- and ipsilateral stimulation. These differences can be expressed in terms of excitatory or inhibitory dominance as well as in terms of the STRF shapes. Accordingly, we quantify the binaural STRF differences by two means. The first is a contra-ipsi peak measure, where the maximum STRF deviation is measured for each ear in standard deviations above the noise. The values in this numbered pair [contra, ipsi] are positive for excitatory and negative for inhibitory deviations. For instance, the neuron in

Figure 3b has contra-ipsi peak measure [+9, -8]. The contra-ipsi peak measure considers only the single maximum deviation for each STRF, regardless of other weaker features and their binaural spectrotemporal alignment. This measure is reminiscent of the traditional classification of binaural interaction types in terms of excitatory (E) and inhibitory (I) contributions, where our contra-ipsi peak of [+9, -8] might be considered EI_{pk}. However, the STRF-based measure is not categorical but continuous and quantifies the binaural input more than the explicit binaural interaction. Our second assay, the binaural similarity index (BSI), is a correlation coefficient measuring how similar the entire contra and ipsi STRFs are in frequency and time. A BSI of +1 means contra and ipsi STRFs are perfectly matched in frequency, time, and sign. A BSI of –1 occurs when the STRFs are matched in frequency and time, but are of antagonistic sign. Finally, a BSI of zero indicates no correlation between the shapes of the two STRFs. The BSI for the EE_{pk} neuron in Figure 3a, for instance, is 0.75. The EI_{pk} neuron of Figure 3b, on the other hand, has BSI = -0.31. STRFs with competing subregions, some binaurally similar and others opposite, tend to have BSIs closer to zero (e.g. Figure 3c, BSI = 0.14).

Both binaural measures may be plotted on the same figure, where symbol location indicates the contra-ipsi peak value and symbol type and size indicates BSI for each neuron (**Fig. 9**). Considering for now only the contra-ipsi peak values (symbol location), thalamus and cortex show the same response types but different proportions of each. The vast majority of units have an excitatory maximum peak in the contralateral STRF (90% of total in thalamus, 82% cortex). Many of these have no ipsilateral STRF (EO_{pk} = 23% of total in thalamus, 40% cortex). Of those that do, more than twice as many ipsilateral STRFs have an excitatory peak rather than an inhibitory peak (EE_{pk} = 45% thalamus,

30% cortex; EI_{pk} = 21% thalamus, 12% cortex). Binaural similarity indices are indicated in Figure 9 by symbol type and size. Neurons with BSI = 0 are represented by circles. Positive BSIs are plus signs, and negative ones are diamonds; for these non-zero values, symbol size scales with the absolute magnitude of the BSI. BSIs show a bias toward well-matched or unmatched, as opposed to antagonistic, binaural STRFs in both thalamus and cortex (BSI = 0 for 30% thalamus, 58% cortex; BSI > 0 for 56% thalamus, 34% cortex; BSI < 0 for 14% thalamus, 7% cortex; BSI range –0.76 to 0.91 for thalamus, -0.38 to 0.87 cortex). Values for BSI are highly correlated with the contra-ipsi peak measures. The neurons with BSI = 0 necessarily fall mostly along the axes of Figure 9, almost always the horizontal axis indicating a lack of ipsilateral STRF. Most of the neurons with positive BSI are EE_{pk} (upper-right: 78% thalamus, 84% cortex), and most with negative BSI are EI_{pk} (lower-right: 78% thalamus, 89% cortex). Overall, thalamic and cortical cells have similar binaural response types, but they differ in the relative proportions of each.

DISCUSSION

We recorded simultaneously in auditory thalamus and cortex under identical conditions to compare directly the receptive field properties between stations. Our naturalistic and strictly parameterized stimulus characterized spectral, temporal, spectrotemporal, and aural response domains. This multidimensional and internally consistent assay of neural responses enables a unified description of the lemniscal thalamocortical transformation.

Of all parameters measured, temporal response properties differ most systematically between thalamus and cortex. Median peak response latency is 2.5 ms longer in cortex, a reasonable approximation to axonal and synaptic delay. This value agrees with studies of correlated thalamocortical cell pairs in several modalities (Creutzfeldt et al 1980; Tanaka 1983; Reid & Alonso 1995; Swadlow 1995; Johnson & Alloway 1996). While the maximum cortical peak latencies extend to longer values than in thalamus, the distributions are highly overlapping. That is, although thalamus is unsurprisingly activated before cortex, the two stations are simultaneously active for the greater part of their response. Tens of milliseconds of coincident activity would allow ample opportunity for corticothalamic, or even cortico-colliculo-thalamic feedback to shape responses in both stations (Zhang & Suga 1997; Villa et al. 1991; Ghazanfar and Nicolelis 1997; He 1997; Murphy et al. 1999; Zhang and Suga 2000).

A characteristic difference between thalamic and cortical responses is that cortical cells tend to respond to slower temporal modulation rates (Creutzfeldt et al 1980). Unlike previous studies, we quantify the degree of this temporal slowing using strictly parameterized, wideband and dynamic stimuli. The composite temporal MTFs for thalamus and cortex show that the effective filter in cortex is half as fast as thalamus, in both peak and upper cutoff values. While the range of BTMs is similar between the two stations, many more thalamic cells have best responses to higher rates, so that the median value in cortex is also half that in thalamus. Mechanistically, one could imagine that each thalamic input is slowed by the same factor within the cortical network. A study of functionally connected thalamocortical cell pairs in the same system, however, shows no rank correlation between BTMs of thalamic inputs and cortical targets: fast (slow)

thalamic cells do not contribute preferentially to fast (slow) cortical cells (Miller et al. 2000). We should also reiterate, the analyses in this report are sensitive only to neural responses phase-locked to the stimulus envelope. Although periodicities well above our stimulus limit of 100 Hz are important for an animal, phase-locked responses above this rate are very rare in thalamus and cortex, especially in the anesthetized preparation. The question thus remains, how higher periodicities are represented at this level. Some investigators provide evidence that the progressive decrease of phase-locked temporal modulation following rates could be accompanied by a recoding of modulations into a topographic, rate-based response (Pantev et al. 1989; Langner et al. 1997; but see Fishman et al. 1998). Others emphasize instead the perceptual saliency of the lower range of modulations (Arai and Greenberg 1998); such psychophysical observations imply that we might expect to find a preferred representation of lower modulation frequencies in auditory cortex.

While temporal response properties differ significantly between thalamus and cortex, spectral properties are very similar. Although the cortex has somewhat more lowpass cells, the range of best spectral modulations is the same, as is the range of excitatory frequency integration, or $Q_{1/e}$ values. The composite spectral MTFs in both stations are strongly lowpass with similar upper cutoffs. Best spectral modulation rates for cortex are similar to those found with static ripple stimuli (Schreiner & Calhoun 1994), except for a greater percentage of lower values found in this study. Our analysis reveals that many neurons' spectral modulation preferences are strongly determined by strong sideband inhibition, a conclusion reached less directly using static ripples, pure-tone, or multi-tone stimuli (Nelken et al. 1994; Versnel and Shamma 1998; Calhoun &

Schreiner 1998). One related factor not addressed in this report is how stimulus intensity affects spectral bandwidth. Although the dynamic ripple covers a large intensity range of 45 dB, since we always presented it at a mean of 20-30 dB above the pure-tone threshold, we cannot draw firm conclusions about intensity-bandwidth dependence. Our preliminary data agree with previous studies, however, suggesting that changes in excitatory spectral integration with increased stimulus intensity are much less pronounced with wideband stimuli than with pure tones (Ehret & Merzenich 1988; Ehret & Schreiner 1997). Plausibly, active engagement of inhibitory sidebands would tend to limit excitatory spread at high intensities.

Composite RTFs describe the overall spectrotemporal modulation transfer functions for thalamus and for cortex, both of which show the bandpass temporal and lowpass spectral properties described above. Interestingly, the cortical composite RTF bears a striking resemblance to psychophysically derived detection thresholds for moving ripple stimuli (Chi et al. 1999). Individual neuronal preferences are preserved in joint distributions of BSMs and BTMs, which reveal that best modulation rates are uncorrelated between spectral and temporal domains in thalamus and cortex. For instance, a neuron with high spectral modulation preference may have any given temporal preference and vice versa. Not only are best rates uncorrelated, but the sharpness of tuning or Q values for spectral modulations are also uncorrelated with those for temporal modulations. This lack of correlation demonstrates that the excitatory-inhibitory processes underlying modulation preferences are independent for frequency and time. Moreover, the fact that best modulation rates are not constrained by an inverse relationship (e.g. high BSM implying low BTM) indicates an absence of time-frequency

trade-off. This is in contrast to the inferior colliculus, the input station to thalamus, where many neurons appear to respect a maximum time-frequency resolution (Escabí et al. 1998). Another response characteristic not captured by separate temporal and spectral analyses is the asymmetry of the STRF or RTF, in its extreme an indication of frequency sweep selectivity. The proportion of cells showing highly asymmetric RTFs is significant yet low. This suggests that the high proportion of frequency sweep-selective cells found in some previous studies (Mendelson & Cynader 1985; Phillips et al. 1985; Nelken and Versnel 2000) is determined by cells with a relatively symmetrical arrangement of excitatory and inhibitory subfields in frequency and time, not whose STRFs show distinct sweep-like features. Our results agree more closely with early studies that showed only a small proportion of cells in MGB (Whitfield and Purser 1972) and AI (Evans and Whitfield 1964) that respond exclusively to FM tones. Compared to traditional stimuli, the dynamic ripple thus gives a much fuller description of a neuron's joint spectrotemporal response preferences.

Binaural response properties are similar in type but differ in their relative proportions between thalamus and cortex. Using the contra-ipsi peak measure, EE_{pk} cells outnumber EI_{pk} cells by greater than a factor of two. Cortex, however, has proportionally more EO_{pk} cells than thalamus. Similarly with the BSI measure of binaural STRF correlation, most thalamic cells are positively correlated between ears, followed by no correlation and finally binaural antagonism; most cortical cells show no binaural correlation, followed by positive correlation, then antagonism. Although our binaural analysis cannot be cast directly in the traditional categories (EE, EI, etc.) (Aitkin and Webster 1972; Imig & Adrian, 1977; Semple & Aitkin 1979; Calford & Webster 1981;

Phillips & Irvine 1983; Middlebrooks et al. 1980), we have attempted to provide continuity by classifying binaural types in an analogous fashion (an excitatory-excitatory contra-ipsi peak measure is EE_{pk}). The most important difference between our results and traditional measures is that STRFs were derived with simultaneously presented but uncorrelated sounds to each ear, so no explicit binaural interactions were tested. Our contra-ipsi peak measure depends on the dominance of excitation or inhibition in each ear rather than the explicit interaction between them. The combination of the contra-ipsi peak measure with the BSI is nevertheless highly suggestive of the binaural interaction type. The proportions of binaural response types in the present report differ somewhat from previous studies (Aitkin & Webster 1972; Calford & Webster 1981; Middlebrooks et al. 1980; Middlebrooks & Zook 1983), most noticeably in the small percentage of EI_{pk} or binaurally antagonistic (BSI < 0) cells and in the large percentage of EO_{pk} cells, especially in cortex (but see Phillips & Irvine 1983). Proportions differ considerably among many previous studies as well, however, probably due to idiosyncrasies in method. The differences in our study, therefore, may be attributable to our use of a spectrotemporally complex stimulus or to our strict criteria for determining the presence and significance of an STRF (see Methods). By using the same stimulus to evaluate simultaneously many neural response dimensions, we have developed a binaural assay that is internally consistent with monaural spectrotemporal preferences.

There are several promising directions for future studies. Although we recorded over large regions in the MGBv and AI, we made no attempt to systematically map either structure. Many of our response parameters could be spatially organized in both locations (Rodrigues-Dagaeff 1989; Schreiner 1998). Second, many neurons fail to give

STRFs. Surely for some of these, the 20 minute stimulus presentation time was insufficient to overcome low firing rate and/or high response variability. Other neurons without STRFs may respond to the stimulus envelope selectively but in a nonlinear, phase-invariant way, as seen in the inferior colliculus (Escabí et al. 1998) and reminiscent of complex cells in V1. Finally, since anesthesia may affect some of our response parameters (Edeline et al. 1999), especially temporal modulation rates (Kenmochi and Eggermont 1997), it will be important to verify our conclusions in the unanesthetized animal.

In this report, we compare receptive field attributes of thalamic and cortical populations recorded simultaneously in the same preparation. The receptive fields were derived with dynamically changing, spectrotemporally complex stimuli that share many properties with natural sounds (Escabí et al. 1999). These methods enabled a unified description of temporal, spectral, spectrotemporal, and aural response properties under identical stimulus conditions (Miller & Schreiner 2000). Our observations thus lay the groundwork for further study of the thalamocortical transformation of responses to complex auditory stimuli.

ACKNOWLEDGMENTS

Supported by the National Institutes of Health (DC02260, NS34835), the National Science Foundation (NSF97203398), and the Whitaker Foundation.

REFERENCES

Aertsen AMHJ, Johannesma PIM. Spectro-temporal receptive fields of auditory neurons in the grassfrog. *Bio. Cyber* 38: 223-234, 1980.

Aitkin LM, Webster WR. Medial geniculate body of the cat: organization and responses to tonal stimuli of neurons in ventral division. *J Neurophysiol* 35: 365-80, 1972.

Arai, T., Greenberg, S. Speech intelligibility in the presence of cross-channel spectral asynchrony. In: *Proceedings of the 1998 IEEE International Conference on Acoustics, Speech and Signal Processing. Vol. 2.* New York: IEEE, 1998, p.933-6.

Barone P, Clarey JC, Irons WA, Imig TJ. Cortical synthesis of azimuth-sensitive single-unit responses with nonmonotonic level tuning: a thalamocortical comparison in the cat. *J Neurophysiol* 75: 1206-20, 1996.

Bieser A. Processing of twitter-call fundamental frequencies in insula and auditory cortex of squirrel monkeys. *Exp Br Res* 122: 139-48, 1998.

Calford MB, Webster WR. Auditory representation within principal division of cat medial geniculate body: an electrophysiology study. *J Neurophysiol* 45: 1013-28, 1981.

Calhoun BM, Schreiner CE. Spectral envelope coding in cat primary auditory cortex: linear and non-linear effects of stimulus characteristics. *Eur J Neurosci* 10: 926-40, 1998.

Chi T, Gao Y, Guyton MC, Ru P, Shamma S. Spectro-temporal modulation transfer functions and speech intelligibility. *J Acoust Soc Am* 106: 2719-32, 1999.

Clarey JC, Barone P, Imig TJ. in *The Mammalian Auditory Pathway: Neurophysiology,* (eds. Popper AN, Fay RR). New York: Springer-Verlag, 1994, p. 232-334.

Clarey JC, Barone P, Irons WA, Samson FK, Imig TJ. Comparison of noise and tone azimuth tuning of neurons in cat primary auditory cortex and medical geniculate body. *J Neurophysiol* 74: 961-80, 1995.

Creutzfeldt O, Hellweg FC, Schreiner CE. Thalamocortical transformation of responses to complex auditory stimuli. *Exp Br Res* 39:87-104, 1980.

DeAngelis GC, Ghose GM, Ohzawa I, Freeman RD. Functional micro-organization of primary visual cortex: receptive field analysis of nearby neurons. *J Neurosci* 19:4046-64, 1999.

deCharms RC, Blake DT, Merzenich MM. Optimizing sound features for cortical neurons. *Science* 280: 1439-43, 1998.

de Ribaupierre F. in *The Central Auditory System*, (eds. Ehret G, Romand R). New York: Oxford, 1997, p. 317-397.

Doupe AJ, Konishi M. Song-selective auditory circuits in the vocal control system of the zebra finch. *Proc Natl Acad Sci* 88(24): 11339-43, 1991.

Ehret G, Merzenich MM. Complex sound analysis (frequency resolution, filtering and spectral integration) by single units of the inferior colliculus of the cat. *Br Res* 472(2):139-63, 1988.

Ehret G, Schreiner CE. Frequency resolution and spectral integration (critical band analysis) in single units of the cat primary auditory cortex. *J Comp Physiol A: Sens Neur Behav Physiol* 181(6):635-50, 1997.

Edeline JM, Manunta Y, Nodal FR, Bajo VM. Do auditory responses recorded from awake animals reflect the anatomical parcellation of the auditory thalamus? *Hear Res* 131(1-2):135-52, 1999.

Escabí MA, Schreiner CE, Miller LM. Dynamic time-frequency processing in the cat midbrain, thalamus, and auditory cortex: spectrotemporal receptive fields obtained using dynamic ripple spectra. (Abstract) *Soc Neurosci Abs* 24:1879, 1998.

Escabí MA, Miller LM, Read HL, Schreiner CE. Naturalistic stimuli reveal contrast tuning in the cat auditory midbrain. (Abstract) *Soc Neurosci Abs* 25:397, 1999.

Evans EF, Whitfield IC. Classification of unit responses in the auditory cortex of the unanesthetized and unrestrained cat. *J Physiol* 171: 476-493, 1964.

Fishman YI, Reser DH, Arezzo JC, Steinschneider M. Pitch vs. spectral encoding of harmonic complex tones in primary auditory cortex of the awake monkey. *Br Res* 786(1-2):18-30, 1998.

Ghazanfar AA, Nicolelis MA. Nonlinear processing of tactile information in the thalamocortical loop. *J Neurophysiol* 78(1):506-10, 1997.

Glass I, Wollberg Z. Responses of cells in the auditory cortex of awake squirrel monkeys to normal and reversed species-specific vocalizations. *Hear Res* 9(1):27-33, 1983.

He J. Modulatory effects of regional cortical activation on the onset responses of the cat medial geniculate neurons. *J Neurophysiol* 77(2):896-908, 1997.

Imig TJ, Adrián HO. Binaural columns in the primary field (A1) of cat auditory cortex. *Br Res* 138(2):241-57, 1977.

Johnson MJ, Alloway KD. Cross-correlation analysis reveals laminar differences in thalamocortical interactions in the somatosensory system. *J Neurophysiol* 75:1444-57, 1996.

Kenmochi M, Eggermont JJ. Autonomous cortical rhythms affect temporal modulation transfer functions. *Neuroreport* 8(7):1589-93, 1997.

Klein DJ, Depireux DA, Simon JZ, Shamma SA. Robust spectrotemporal reverse correlation for the auditory system: optimizing stimulus design. *J Comp Neurosci* 9:85-111, 2000.

Kowalski N, Depireux DA, Shamma SA. Analysis of dynamic spectra in ferret primary auditory cortex. I. Characteristics of single-unit responses to moving ripple spectra. *J Neurophysiol* 76:3503-23, 1996.

Langner G, Sams M, Heil P, Schulze H. Frequency and periodicity are represented in orthogonal maps in the human auditory cortex: evidence from magnetoencephalography. *J Comp Physiol A: Sens Neur Behav Physiol* 181(6):665-76, 1997.

Lewicki MS. Bayesian modeling and classification of neural signals. *J Neur Comp* 6:1005-1030, 1994.

Mendelson JR, Cynader MS. Sensitivity of cat primary auditory cortex (AI) neurons to the direction and rate of frequency modulation. *Br Res* 327(1-2):331-5, 1985.

Middlebrooks JC, Dykes RW, Merzenich MM. Binaural response-specific bands in primary auditory cortex (AI) of the cat: topographical organization orthogonal to isofrequency contours. *Br Res* 181(1):31-48, 1980.

Middlebrooks JC, Zook JM. Intrinsic organization of the cat's medial geniculate body identified by projections to binaural response-specific bands in the primary auditory cortex. *J Neurosci* 3:203-24, 1983.

Miller LM, Schreiner CE. Stimulus-based state control in the thalamocortical system. *J Neurosci* 20:7011-6, 2000.

Miller LM, Escabí MA, Read HL, Schreiner CE. Functional convergence and divergence in the auditory thalamocortical system. (Abstract) *Soc Neurosci Abs* 26: 358.3, 2000.

Müller-Preuss P. On the mechanisms of call coding through auditory neurons in the squirrel monkey. *Eur Arch Psych Neurol Sci* 236(1):50-5, 1986.

Murphy PC, Duckett SG, Sillito AM. Feedback connections to the lateral geniculate nucleus and cortical response properties. *Science* 286(5444):1552-4, 1999.

Nelken I, Prut Y, Vaadia E, Abeles M. Population responses to multifrequency sounds in the cat auditory cortex: four-tone complexes. *Hear Res* 72(1-2):223-36, 1994.

Nelken I, Rotman Y, Bar Yosef O. Responses of auditory-cortex neurons to structural features of natural sounds. *Nature* 397(6715):154-7, 1999.

Nelken I, Versnel H. Responses to linear and logarithmic frequency-modulated sweeps in ferret primary auditory cortex. *Eur J Neurosci* 12(2):549-62, 2000.

Pantev C, Hoke M, Lütkenhöner B, Lehnertz K. Tonotopic organization of the auditory cortex: pitch versus frequency representation. *Science* 246(4929):486-8, 1989.

Pelleg-Toiba R, Wollberg Z. Tuning properties of auditory cortex cells in the awake squirrel monkey. *Exp Br Res* 74(2):353-64, 1989.

Phillips DP, Irvine DR. Some features of binaural input to single neurons in physiologically defined area AI of cat cerebral cortex. *J Neurophysiol* 49(2):383-95, 1983.

Phillips DP, Mendelson JR, Cynader MS, Douglas RM. Responses of single neurones in cat auditory cortex to time-varying stimuli: frequency-modulated tones of narrow excursion. *Exp Br Res* 58(3):443-54, 1985.

Rauschecker JP. Parallel processing in the auditory cortex of primates. *Audiol Neuro-Otol* 3(2-3):86-103, 1998.

Reid RC, Alonso JM. Specificity of monosynaptic connections from thalamus to visual cortex. *Nature* 378:281-4, 1995.

Rodrigues-Dagaeff C, Simm G, De Ribaupierre Y, Villa A, De Ribaupierre F, Rouiller EM. Functional organization of the ventral division of the medial geniculate body of the cat: evidence for a rostro-caudal gradient of response properties and cortical projections. *Hear Res* 39(1-2):103-25, 1989.

Samson FK, Barone P, Irons WA, Clarey JC, Poirier P, Imig TJ. Directionality derived from differential sensitivity to monaural and binaural cues in the cat's medial geniculate body. *J Neurophysiol* 84(3):1330-45, 2000.

Schreiner CE. Spatial distribution of responses to simple and complex sounds in the primary auditory cortex. *Audiol Neuro-Otol* 3(2-3):104-22, 1998.

Schreiner CE, Calhoun BM. Spectral envelope coding in cat primary auditory cortex: properties of ripple transfer functions. *Aud Neurosci* 1:39-61, 1994.

Semple MN, Aitkin LM. Representation of sound frequency and laterality by units in central nucleus of cat inferior colliculus. *J Neurophysiol* 42(6):1626-39, 1979.

Smolders JW, Aertsen AM, Johannesma PI. Neural representation of the acoustic biotope. A comparison of the response of auditory neurons to tonal and natural stimuli in the cat. *Biol Cyb* 35(1):11-20, 1979.

Steinschneider M, Schroeder CE, Arezzo JC, Vaughan HG Jr. Speech-evoked activity in primary auditory cortex: effects of voice onset time. *Electroenceph Clin Neurophysiol* 92(1):30-43, 1994.

Suga N, Jen PH. Disproportionate tonotopic representation for processing CF-FM sonar signals in the mustache bat auditory cortex. *Science* 194(4264):542-4, 1976.

Swadlow HA. Influence of VPM afferents on putative inhibitory interneurons in S1 of the awake rabbit: evidence from cross-correlation, microstimulation, and latencies to peripheral sensory stimulation. *J Neurophysiol* 73:1584-99, 1995.

Symmes D, Alexander GE, Newman JD. Neural processing of vocalizations and artificial stimuli in the medial geniculate body of squirrel monkey. *Hear Res* 3(2):133-46, 1980.

Tanaka K. Cross-correlation analysis of geniculostriate neuronal relationships in cats. *J Neurophysiol* 49:1303-18, 1983.

Theunissen FE, Doupe AJ. Temporal and spectral sensitivity of complex auditory neurons in the nucleus HVc of male zebra finches. *J Neurosci* 18(10):3786-802, 1998.

Theunissen FE, Sen K, Doupe AJ. Spectral-temporal receptive fields of nonlinear auditory neurons obtained using natural sounds. *J Neurosci* 20(6):2315-31, 2000.

Versnel H, Shamma SA. Spectral-ripple representation of steady-state vowels in primary auditory cortex. *J Acoust Soc Am* 103(5 Pt 1):2502-14, 1998.

Villa AE, Rouiller EM, Simm GM, Zurita P, de Ribaupierre Y, de Ribaupierre F. Corticofugal modulation of the information processing in the auditory thalamus of the cat. *Exp Br Res* 86(3):506-17, 1991.

Wang X, Merzenich MM, Beitel R, Schreiner CE. Representation of a species-specific vocalization in the primary auditory cortex of the common marmoset: temporal and spectral characteristics. *J Neurophysiol* 74(6):2685-706, 1995.

Whitfield IC, Purser D. Microelectrode study of the medial geniculate body in unanesthetized free-moving cats. *Br Behav Evol* 6: 311-322, 1972.

Zhang Y, Suga N. Corticofugal amplification of subcortical responses to single tone stimuli in the mustached bat. *J Neurophysiol* 78(6):3489-92, 1997.

Zhang Y, Suga N. Modulation of responses and frequency tuning of thalamic and collicular neurons by cortical activation in mustached bats. *J Neurophysiol* 84(1):325-33, 2000.

FIGURE LEGENDS

Fig. 1 Typical STRFs, with their spectrotemporal, spectral, and temporal transfer functions. (**a**) STRFs are expressed in differential rates, where red regions indicate an increase and blue regions a decrease in firing rate relative to the mean, in response to stimulus energy at that time and frequency. In this thalamic STRF, gray arrows designate the neuron's latency (Lat, appx. 15 ms) and best frequency (BF, appx. 9 kHz). A black contour circumscribes the main excitatory peak of the STRF at 1/e times its maximum value; this typically captures around 90% of the peak energy. The cell's bandwidth (black arrows, BW) is the width of this contour in frequency. Relative to the main excitatory peak, this neuron has inhibitory regions flanking in frequency and preceding in time. Consequently its RTF (**b**), a Fourier transform of the STRF, is bandpass in both temporal and spectral modulation domains. The best modulation rates in time and frequency are denoted by arrows (BTM = 22 Hz, BSM = 0.75 cycles/octave). Bandpass filter properties are also evident in the sMTF (**c**) and tMTF (**d**). Since the tMTF is derived by folding the RTF about its vertical axis then collapsing across all spectral modulations, the sign or direction of temporal modulations is ignored, giving a signal in absolute value of temporal modulation rate. (**e**) This cortical STRF shows flanking inhibition in frequency but lacks preceding inhibition in time, so its RTF (**f**) is bandpass for spectral and lowpass for temporal modulations, properties shared by the separate sMTF (**g**) and tMTF (**h**). (**i**) If instead an STRF lacks flanking inhibition in frequency but has preceding inhibition in time, as does this thalamic cell, its RTF (**j**) tends to be lowpass for spectral and bandpass for temporal modulations. Again, these filter characteristics are shared by sMTF (**k**) and tMTF (**l**).

Fig. 2 Atypical STRFs. (**a**) Surround inhibition forms a continuous band through time and frequency around the main excitatory peak of a cortical neuron's STRF. (**b**) This cortical cell shows strong specificity for a certain speed (appx. 30 octaves/sec) and direction (up) of frequency-modulated sweeps. Rarely, a well-isolated single unit shows (**c**) multiple excitatory and inhibitory regions in a complex arrangement, or (**d**) a solely inhibitory STRF (**c** & **d** both thalamic).

Fig. 3 Binaural STRFs. (**a**) This thalamic neuron shows strong excitatory-excitatory alignment between its contralateral and ipsilateral STRFs. (**b**) This cortical cell shows equally strong overlap, but between subregions of opposite sign: excitatory contralateral and inhibitory ipsilateral. (**c**) Contra- and ipsilateral STRF features do not always match in shape. For this thalamic cell, the main contralateral excitatory peak aligns with both excitatory and inhibitory subregions in the ipsilateral STRF.

Fig. 4 Latency distributions for thalamic and cortical populations, as measured by the peak of the STRF. While the distributions for thalamic (gray bars) and cortical (black bars) cells are highly overlapping, thalamic latencies tend to be shorter than cortical ones by 2.5 ms (median 10.5 ms and 13.0 ms, respectively). Thalamic cells are much more likely than cortical cells to have latencies of 7-10 ms, and proportionally more cortical cells have latencies greater than about 30 ms.

Fig. 5 Temporal response properties for thalamus and cortex. Temporal preferences are expressed as tMTFs for representative thalamic (**a**) and cortical (**b**) cells. (**c**) Across the populations, the absolute value of the BTM for thalamic cells (gray bars) tends toward higher values than cortical cells (black bars) (mean thalamus 32.4 Hz, cortex 16.6 Hz). (**d**) The composite tMTFs for thalamus (dashed line --) and cortex (solid line −) give the overall temporal transfer functions for the two stations. Both are temporally bandpass, with a peak of 21.9 Hz in thalamus and 12.8 Hz in cortex. Dotted lines indicate the upper 6dB cutoff for thalamus (62.9 Hz) and cortex (37.4 Hz).

Fig. 6 Spectral response properties for thalamus and cortex. Spectral preferences are expressed as sMTFs for representative thalamic (**a**) and cortical (**b**) cells, in cycles per octave. (**c**) Across the populations, BSMs for thalamic cells (gray bars) and cortical cells (black bars) tend to cluster around low values (mean thalamus 0.58 cyc/oct, cortex 0.46 cyc/oct). There are proportionally more strictly lowpass (BSM = 0) cells in cortex than in thalamus, but the distributions are otherwise very similar. (**d**) The composite sMTFs for thalamus (dashed line --) and cortex (solid line −) give the overall spectral transfer functions for the two stations. Both are spectrally lowpass, with a peak of 0 cyc/oct. Dotted lines indicate the upper 6dB cutoff for thalamus (1.30 cyc/oct) and cortex (1.37 cyc/oct).

Fig. 7 Excitatory sharpness-of-tuning and best spectral modulation preference. (**a**) Distributions of $Q_{1/e}$, or excitatory sharpness of tuning, are very similar in thalamus (gray bars) and cortex (black bars). The thalamus, however, has a slightly greater number of

the most sharply tuned cells (Q>10). (**b,c**) Since BSM depends upon the relationship between excitatory and inhibitory subfields and $Q_{1/e}$ does not, comparing $Q_{1/e}$ and BSM for all cells suggests how great a role sideband inhibition plays in determining spectral integration preferences. Symbols near the bottom of the plots represent neurons with weak or absent flanking inhibition. Symbols on the diagonal line are neurons with strong flanking inhibition of exactly the same spectral periodicity as the excitatory peak. (**b**) For the thalamic population, symbols fill the space under the diagonal line, demonstrating that for each $Q_{1/e}$ an entire range of spectral modulation preferences is possible. (**c**) The cortical population is very similar. For both thalamus and cortex, very few symbols lie above the diagonal line, indicating that strong flanking inhibition is almost never of higher spectral periodicity than one would surmise from the excitatory bandwidth alone.

Fig. 8 Joint spectrotemporal response properties. Composite RTFs for the entire thalamic (**a**) and cortical (**b**) populations are shown in color. Overlying the RTFs are black circles denoting the individual neurons' BTM-BSM combinations. Except for the biases already evident in the composite RTFs, the BTM-BSM joint distributions lack informative structure. Spectral and temporal modulation preferences, therefore, are relatively independent of one another. (**c,d**) An asymmetry in RTF energy about the vertical midline (temporal modulation = 0) results from an asymmetry or nonseparability of features in the STRF. A neuron whose STRF is perfectly symmetric has a spectrotemporal asymmetry value of zero. Although asymmetries take many forms, an illustrative case of large asymmetry is a neuron with strong frequency modulation sweep selectivity. In that case, the sign of the spectrotemporal asymmetry is positive for

upsweep and negative for downsweep preferences. (**c**) The distribution of asymmetries for all thalamic cells shows that most cells are rather symmetric, with only a small proportion having asymmetry larger than magnitude 0.5. (**d**) Cortical cells show a similar distribution. Neither thalamic nor cortical populations have a strong bias toward positive or negative asymmetries.

Fig. 9 Binaural STRF properties in (**a**) thalamus and (**b**) cortex. Symbol location represents the contra-ipsi peak measure, in standard deviations above the STRF noise. Positive peak values mean the dominant STRF feature for stimulation of that ear is excitatory, and negative peak values mean the dominant feature is inhibitory. For instance, symbols in the upper right quadrant have dominant excitation from both ears (EE_{pk}). Those in the lower right have dominant excitation from the contralateral ear and inhibition from the ipsilateral ear (EI_{pk}). Neurons with an STRF for only one ear are represented by symbols along the axes (e.g. EO_{pk}). Axes are truncated for clarity: therefore, 18 thalamic points (11%) lie beyond the plot, all but one of which are in the upper right quadrant (mean contra-ipsi peak = [58.8, 15.6]), and one cortical point lies beyond the axes in the upper right quadrant (contra-ipsi peak = [21.0, 33.4]). Symbols lying on the diagonal, dashed lines are neurons with equal peak strength in both contra- and ipsi-STRFs. The prevalence of symbols to the right of both diagonals in each plot reflects the contralateral and excitatory dominance in both thalamus and cortex. The similarity of contra- and ipsilateral STRFs is assessed with the BSI and represented by symbol type and size. Neurons with BSI = 0 are shown as circles (O), those that are binaurally similar with BSI > 0 are shown as plus signs (+), and those that are binaurally

antagonistic with BSI < 0 are shown as diamonds (◊). Relative size of the + or ◊ indicates the magnitude of the BSI. Symbol location and type are highly correlated: most neurons with positive BSI are EE_{pk} (upper-right: 78% thalamus, 84% cortex) and most with negative BSI are EI_{pk} (lower-right: 78% thalamus, 89% cortex). Overall proportions of binaural properties are as follows. Thalamus: 45% EE_{pk}, 23% EO_{pk}, 21% EI_{pk}, 1% OE_{pk}, 1% OI_{pk}, 2% IE_{pk}, 3% IO_{pk}, 3% II_{pk}. Cortex: 30% EE_{pk}, 40% EO_{pk}, 12 % EI_{pk}, 2% OE_{pk}, 3% OI_{pk}, 3% IE_{pk}, 10% IO_{pk}, 1% II_{pk}. Thalamic BSI: 56% > 0, 30% = 0, 14% < 0. Cortical BSI: 34% > 0, 58% = 0, 7% < 0. In general, relative numbers of EE_{pk} versus EI_{pk} and relative numbers of BSI>0 versus BSI<0 are similar in thalamus and cortex, but the cortex has proportionally more cells with EO_{pk} and, consequently, BSI = 0.

Chp. 2, Figure 1

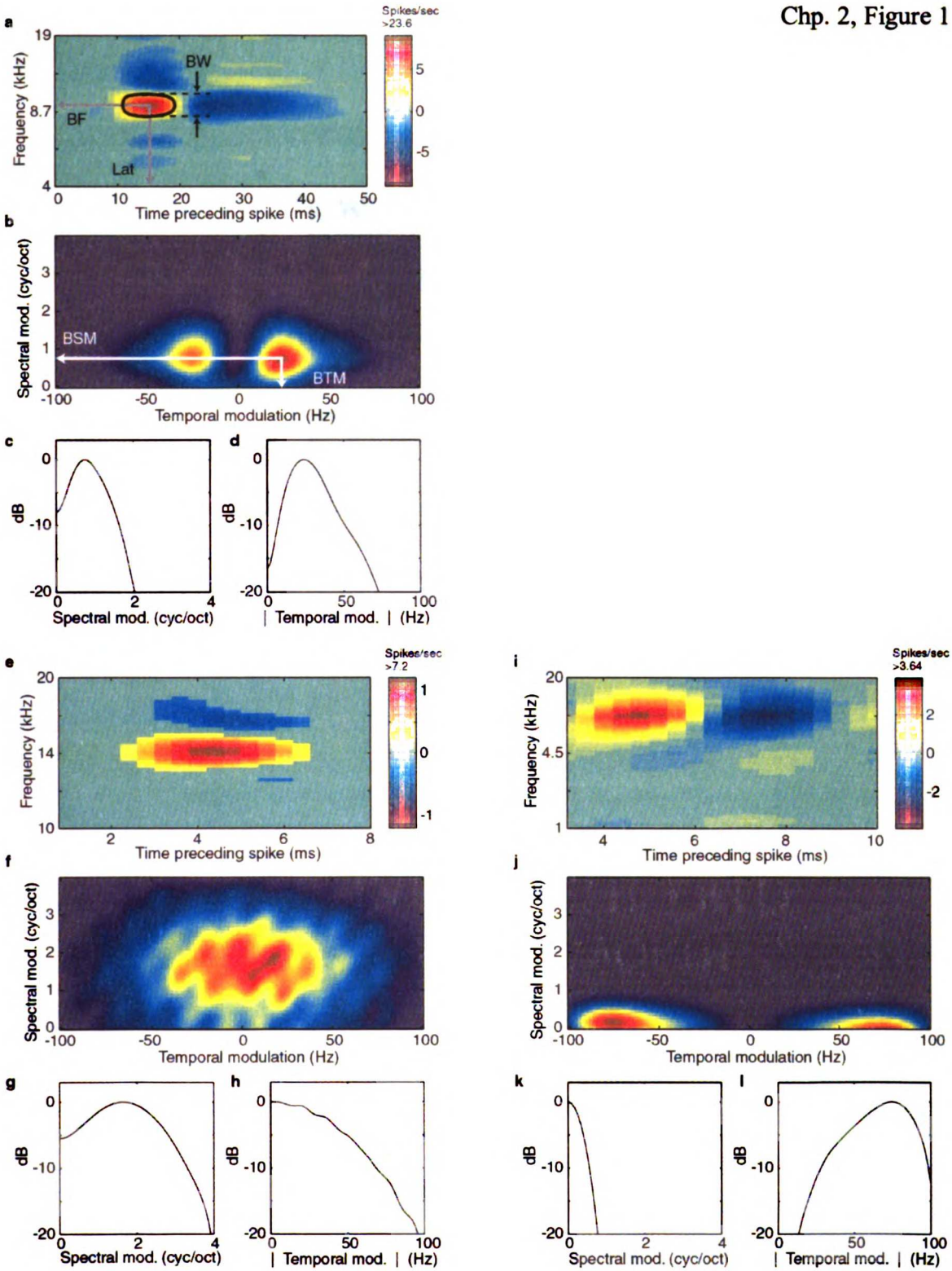

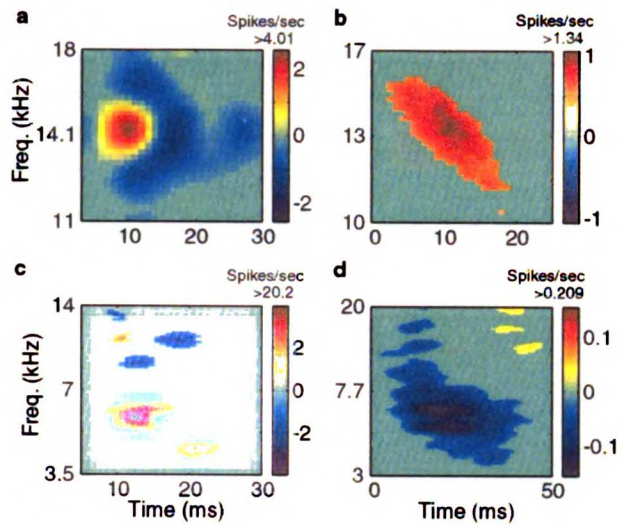
a
Spikes/sec
>4.01
18
14.1
11
Freq. (kHz)
10
20
30
2
0
-2
b
Spikes/sec
>1.34
17
13
10
0
10
20
1
0
-1
c
Spikes/sec
>20.2
14
7
3.5
Freq. (kHz)
10
20
30
Time (ms)
2
0
-2
d
Spikes/sec
>0.209
20
7.7
3
0
50
Time (ms)
0.1
0
-0.1

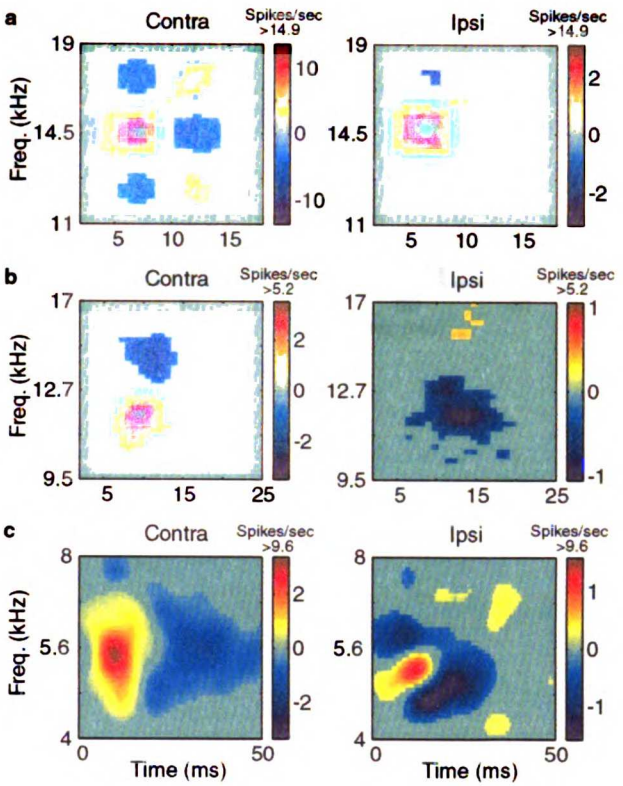
a
Contra
Spikes/sec
>14.9
Ipsi
Spikes/sec
>14.9
Freq. (kHz)
19
14.5
11
5
10
15
10
0
-10
2
0
-2
b
Contra
Spikes/sec
>5.2
Ipsi
Spikes/sec
>5.2
Freq. (kHz)
17
12.7
9.5
5
15
25
2
0
-2
1
0
-1
c
Contra
Spikes/sec
>9.6
Ipsi
Spikes/sec
>9.6
Freq. (kHz)
8
5.6
4
0
50
Time (ms)
2
0
-2
1
0
-1

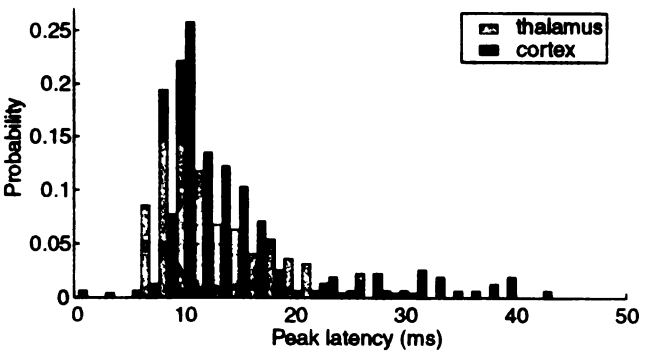
thalamus
cortex
Probability
0.25
0.2
0.15
0.1
0.05
0
0
10
20
30
40
50
Peak latency (ms)

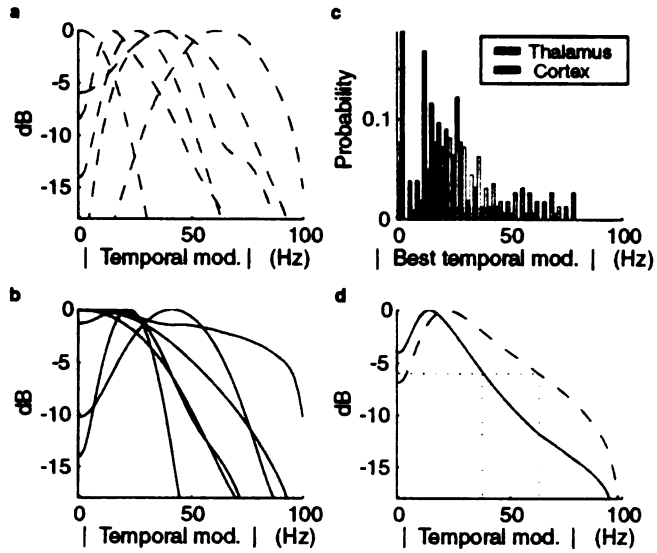
a
0
-5
-10
-15
dB
0
50
100
| Temporal mod. | (Hz)
c
Thalamus
Cortex
Probability
0.1
0
0
50
100
| Best temporal mod. | (Hz)
b
0
-5
-10
-15
dB
0
50
100
| Temporal mod. | (Hz)
d
0
-5
-10
-15
dB
0
50
100
| Temporal mod. | (Hz)

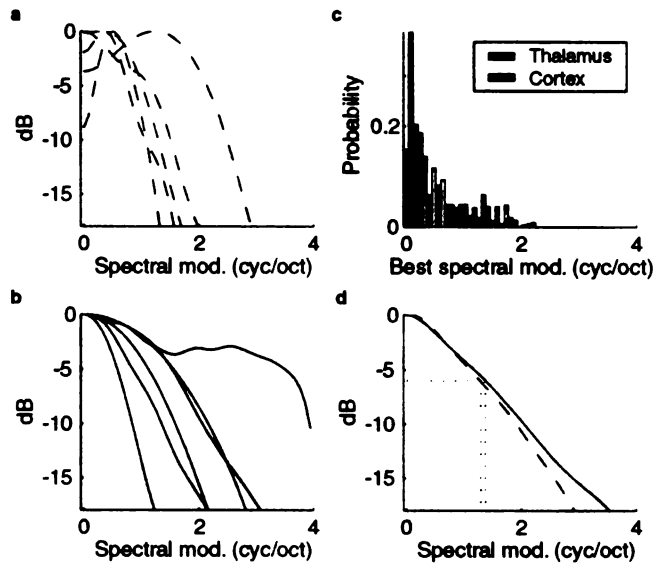
a
0
-5
-10
-15
dB
0
2
4
Spectral mod. (cyc/oct)
c
Thalamus
Cortex
Probability
0.2
0
0
2
4
Best spectral mod. (cyc/oct)
b
0
-5
-10
-15
dB
0
2
4
Spectral mod. (cyc/oct)
d
0
-5
-10
-15
dB
0
2
4
Spectral mod. (cyc/oct)

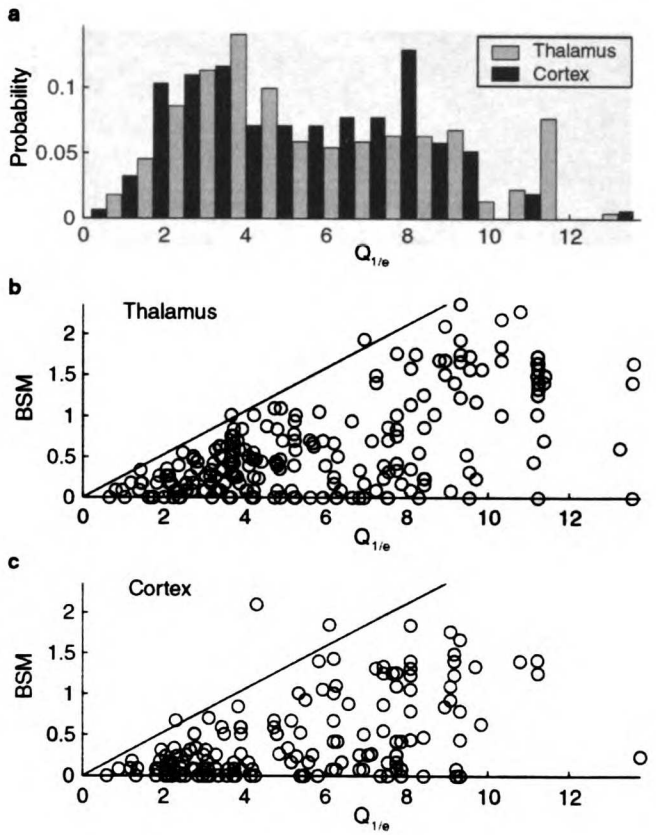
a
Probability
0.1
0.05
0
Thalamus
Cortex
0
2
4
6
8
10
12
$Q_{1/e}$
b
Thalamus
BSM
2
1.5
1
0.5
0
0
2
4
6
8
10
12
$Q_{1/e}$
c
Cortex
BSM
2
1.5
1
0.5
0
0
2
4
6
8
10
12
$Q_{1/e}$

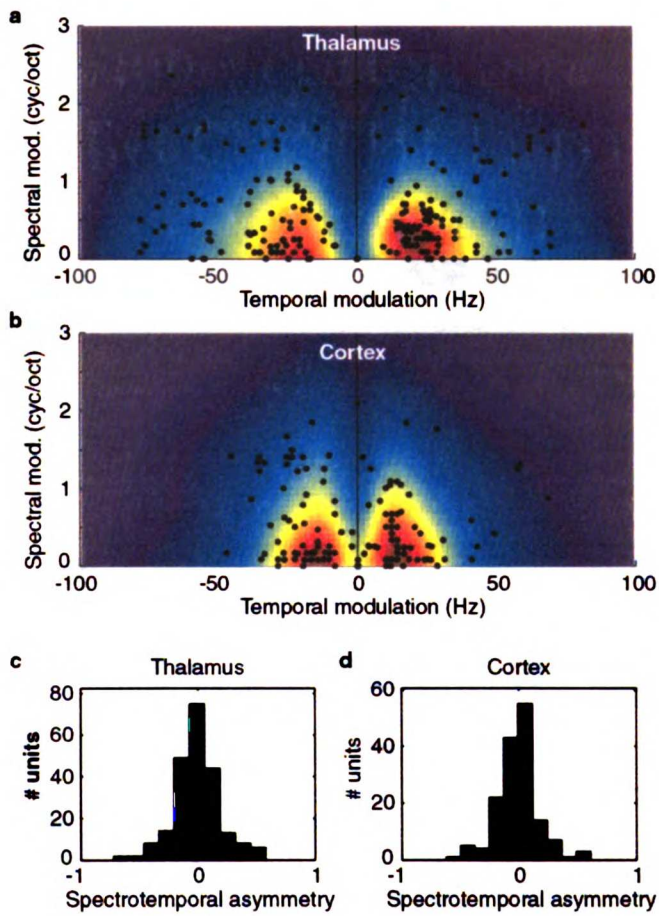
a
Thalamus
Spectral mod. (cyc/oct)
3
2
1
0
-100
-50
0
50
100
Temporal modulation (Hz)
b
Cortex
Spectral mod. (cyc/oct)
3
2
1
0
-100
-50
0
50
100
Temporal modulation (Hz)
c
Thalamus
units
80
60
40
20
0
-1
0
1
Spectrotemporal asymmetry
d
Cortex
units
60
40
20
0
-1
0
1
Spectrotemporal asymmetry

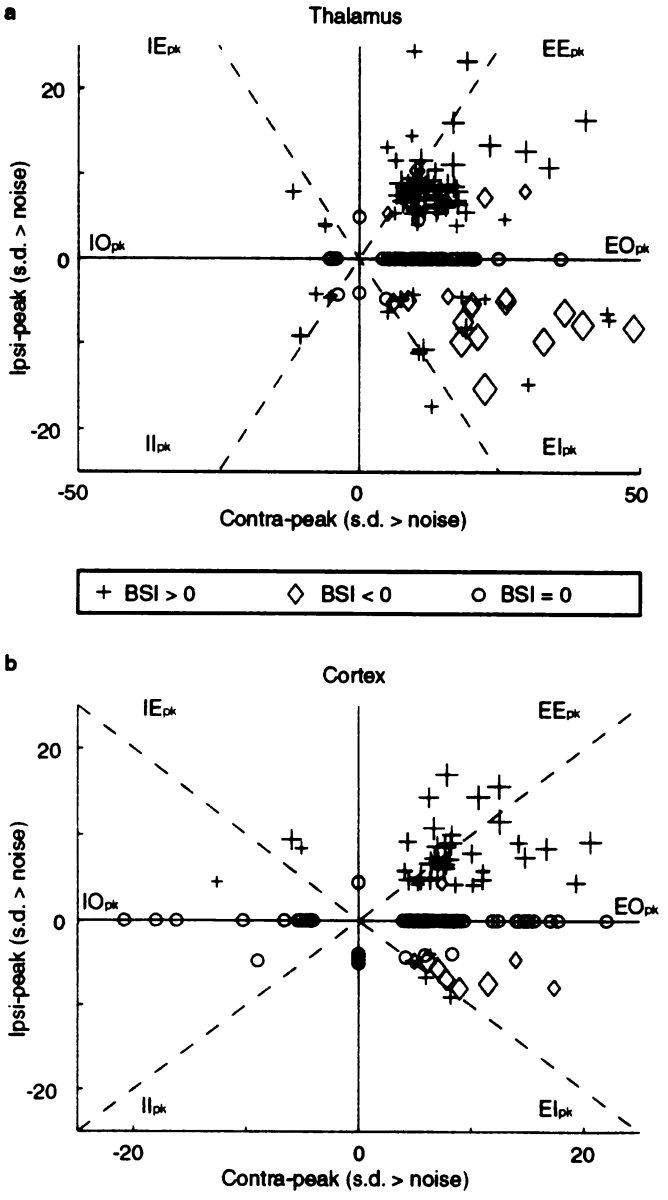
a
Thalamus
IEpk
EEpk
IOpk
EOpk
IIpk
EIpk
20
0
-20
-50
0
50
Ipsi-peak (s.d. > noise)
Contra-peak (s.d. > noise)
+ BSI > 0
◇ BSI < 0
o BSI = 0
b
Cortex
IEpk
EEpk
IOpk
EOpk
IIpk
EIpk
20
0
-20
-20
0
20
Ipsi-peak (s.d. > noise)
Contra-peak (s.d. > noise)

CHAPTER 3:

FUNCTIONAL CONVERGENCE OF RESPONSE PROPERTIES IN THE AUDITORY THALAMOCORTICAL SYSTEM

Summary

One of the brain's fundamental tasks is to construct and transform representations of an animal's environment, yet few studies describe how individual neurons accomplish this. Our results from correlated pairs in the auditory thalamocortical system show that cortical excitatory receptive field regions can be inherited, constructed from smaller inputs, and assembled by the cooperative activity of neuronal ensembles. The prevalence of functional thalamocortical connectivity is strictly governed by tonotopy, but connection strength is not. Finally, spectral and temporal modulation preferences in cortex are not strongly determined by thalamic input. These observations reveal a radical reconstruction of response properties from thalamus to cortex, and illustrate how some properties are propagated with great fidelity while others are significantly transformed or generated intracortically.

Introduction

Sensory processing in the thalamocortical system has endured continual investigation since the earliest days of single-cell neurophysiology (Adrian, 1941). The most straightforward studies of thalamocortical function develop mechanistic models by comparing receptive fields from these anatomically subsequent stations (Hubel and Wiesel, 1962; Kyriazi and Simons, 1993). Others use more sophisticated methods, such as removing cortical influence to reveal only the thalamic contribution to cortical receptive fields (Chapman et al., 1991; Chung and Ferster, 1998). How the neurons construct and modify these response properties, however, has remained largely a matter of inference. Only a few studies have directly addressed the transformation of response properties between individual cells in the thalamus and cerebral cortex (Creutzfeldt et al., 1980; Tanaka, 1983; Swadlow, 1995; Reid and Alonso, 1995; Johnson and Alloway, 1996).

The auditory system presents a unique challenge. In contrast to the visual thalamocortical system, which shows the marked transformation from center-surround to simple cell, auditory thalamic and cortical receptive fields are remarkably similar. Except for the well-known temporal slowing (Creutzfeldt et al., 1980), no fundamental response properties have been demonstrated to differ across the lemniscal auditory thalamocortical synapse (Clarey et al., 1994). Nevertheless, thalamocortical anatomy would allow for massive functional convergence and divergence. Individual thalamic axons can ramify to span up to 7 mm of cortical space (de Venecia and McMullen, 1994; Cetas et al., 1999), and a single cortical locus can receive thalamic input from large regions in thalamus (Andersen et al., 1980; Middlebrooks and Zook, 1983; Brandner and

Redies, 1990; Read H. L. et al., *Abs. Assoc. Res. Otolaryngol.* **22**:49 (1999); Huang and Winer, 2000). It thus remains unclear what functional properties are being transformed across the thalamocortical synapse. This study addresses the basic rules whereby auditory cortical receptive fields are constructed from their thalamic inputs.

We propose a heuristic framework of functional thalamocortical convergence types then investigate several detailed aspects of the transformation, such as: the spectral and temporal specificity of inputs to cortical cells, the complementary roles of excitatory and inhibitory receptive field subregions, and the thalamocortical transfer of spectral and temporal modulation properties. Recordings were made simultaneously from pairs of single units in the ventral medial geniculate body (MGBv) and its target layers in primary auditory cortex (AI) in the ketamine-anesthetized cat. Spectro-temporal receptive fields (STRFs) and spike train cross-correlations enabled us to evaluate the quality, strength, and specificity of functional thalamocortical convergence.

Results

Action potential trains from all thalamocortical pairs were cross-correlated. Functionally connected pairs (n=29, from a total 741) of single units were chosen by the monosynaptic-like peaks in their correlograms, using strict criteria under both spontaneous and stimulus-driven conditions (see Experimental Procedures). Spectrotemporal receptive field properties were derived for each unit with reverse-correlation of a noise-like stimulus. An STRF is the average spectrotemporal stimulus

envelope immediately preceding an action potential. It shows positive regions in time and frequency where stimulus energy tends to increase firing rate, and negative regions where it decreases firing rate, relative to the mean.

Functional convergence types

The theoretically possible range of functional convergence can be heuristically characterized with three extremes: inheritance, constructive convergence, and ensemble convergence (**Fig. 1**). These extremes are not intended to be categorical: a given thalamocortical connection need not fall neatly into any one of these types. Nor do we expect a cortical receptive field is made up of only one extreme convergence type. In all likelihood, each cortical cell receives a composite of many types of input. The three types illustrated simply delimit the possible range of functional convergence. For instance, inheritance (**Fig. 1a**), the simplest case, occurs if a cortical cell's receptive field is completely determined by functionally identical thalamic inputs. Constructive convergence (**Fig. 1b**) builds the cortical receptive field by integrating a number of thalamic inputs with smaller receptive fields, in frequency and/or time. This convergence-by-union is a variant of the Hubel-Wiesel model (Hubel and Wiesel, 1962; Tanaka, 1983; Reid and Alonso, 1995). Conversely, in ensemble convergence (**Fig. 1c**), the thalamic inputs extend beyond the spectrotemporal borders of the resultant cortical receptive field. This convergence-by-intersection logically requires the participation of an ensemble of cells, cooperating either to amplify the receptive field regions that are ultimately represented in cortex, or to suppress regions that are not.

Representative functionally connected thalamocortical pairs are shown in Figure 2. In **Fig. 2a-c**, the excitatory peak in the thalamic STRF is in almost perfect register with that of the cortical cell. For assessing overlap (Fig. 2c, contours), the thalamic STRF has been shifted in time by the peak correlogram delay, i.e. the expected travel and synaptic delay between the cells. The high similarity of STRFs suggests that a cortical unit could theoretically inherit its main excitatory region from functionally identical thalamic cells. Mixed constructive/ensemble convergence is shown in **Fig. 2d-f**, where a smaller thalamic receptive field is integrated into a larger, composite cortical receptive field. This emphasizes that convergence types in Fig. 1 are not strictly categorical: the thalamic input not only participates in construction but also in ensemble convergence insofar as its excitatory region extends to frequencies beyond those of the cortical cell. Full ensemble convergence appears in **Fig. 2g-i**, where a thalamic unit with large receptive field converges onto a cortical cell whose receptive field composes only a subset of the thalamic input. Other functionally diverse inputs must cooperate to strengthen the region of overlap, elevating it above some threshold, or to suppress the non-overlapping region. There is also an area of mismatch in this example, where strong thalamic excitation coincides with strong cortical inhibition. Evidently a large overlap of opposing features, at least with the further excitatory-excitatory match, need not preclude significant functional connectivity.

Rather than force each thalamocortical pair into one of the three functional convergence types, **Fig. 3** parses each pair along two continua: cortical coverage and thalamic overlap. Cortical coverage is the proportion of the cortical receptive field peak covered by that of the thalamus, where peaks are circumscribed by contours as in Figs.

2c, f, and i (1/e of maximum amplitude). Thalamic overlap is the proportion of the thalamic receptive field peak that overlaps that of the cortex. High cortical coverage and high thalamic overlap occur when the thalamic and cortical receptive fields are nearly identical, as for inheritance. Low cortical coverage but high thalamic overlap occurs when a small thalamic receptive field is completely subsumed by the cortical one, as in constructive convergence. Finally, low thalamic overlap with varying degrees of cortical coverage indicates ensemble convergence, when the thalamic input possesses receptive field regions that are not ultimately shared by the cortical cell. The paradigmatic receptive field relationships for these general ranges are indicated in Fig. 3 (schematic insets). Functional thalamocortical pairs fill the domain of thalamic overlap and cortical coverage, demonstrating that the transformation of receptive fields utilizes all possible types of convergence.

Spectrotemporal specificity

The spectrotemporal specificity of thalamocortical connections is addressed only indirectly by the metrics of Figure 3. To compare the pairwise specificity directly, the thalamic inputs were normalized relative to their cortical targets. For **Fig. 4**, the excitatory peak of each cortical target has been stretched in frequency and in time to match an arbitrary standard, which is plotted as a light gray circle (**Fig. 4a**) with bandwidth and duration equal to one. Each thalamic input is then stretched by the same amount as its target, shifted by the correlogram peak delay, and plotted as a contour on the standardized axes. Such normalization maintains the relative thalamocortical overlap in frequency and time, allowing direct comparison across all pairs. Nearly all thalamic

inputs show significant overlap with their cortical targets. The STRF energies within the contours, moreover, may be summed across time to give the distribution in relative frequency of the thalamic inputs (**Fig. 4b**). Most (72%) of the energy falls within one normalized cortical bandwidth. Likewise, when the energies are summed across frequency, giving the distribution in relative timing of the thalamic inputs (**Fig. 4c**), most (80%) of the input energy falls within one normalized cortical duration. Although our cross-correlation criteria favor cell pairs that tend to fire in close temporal proximity, that does not require that all or most thalamic STRF energy should fall within a single cortical duration. Thus, thalamic input is highly specific in both relative frequency and relative time. On average, the inputs contribute very little excitatory energy outside the spectrotemporal extent of their cortical targets.

Another measure of frequency convergence is the best frequency difference between members of a functional pair. **Fig. 5a** compares the differences of the thalamic best frequencies to those of their cortical targets (mean difference 0.077 octaves). If the best frequency difference exceeds about one quarter of an octave, functional thalamocortical connections disappear. **Figure 5b** shows the difference in the margins of the receptive field peaks (i.e. the edges on the frequency side farthest from the cortical best frequency) in octaves relative to the cortical best frequency. While this measure necessarily spans a larger frequency range, functional connections are still limited to about 1/3 octave.

By considering the STRF differences between all recorded thalamocortical pairs, including the uncorrelated ones, we can determine how the prevalence of functionally connected pairs depends on receptive field similarity. The best frequency differences for

all thalamocortical pairs reveals a sampling bias toward small differences (**Fig. 6a**). On the basis of previous work (Creutzfeldt et al., 1980), we deliberately targeted pairs with small best frequency difference as they are most likely to be functionally connected. Although biased, our sample is continuous to differences greater than one octave. The proportion of recorded pairs that are functionally connected varies strongly with best frequency difference (**Fig. 6b**), with the highest proportion of correlated pairs having the smallest best frequency difference. Interestingly, while the prevalence of functional correlation depends on frequency difference, the strength of the correlation does not (mean strength 0.045, median 0.026) (**Fig. 6c**). A similar result emerges when we compare not simply best frequencies but rather the overall thalamic and cortical STRFs, with a correlation coefficient called the similarity index. Similarity index is thus a broader comparison of receptive fields, though it tends to be associated with the simpler measure of best frequency difference (corr. coef. = -0.69, $p<0.001$ for functionally connected pairs; -0.39, $p<0.001$ for all pairs). The population of all recorded pairs is biased toward low similarity indices (**Fig. 6d**), and the prevalence of functionally connected pairs increases systematically with greater overall STRF similarity (**Fig. 6e**). Nonetheless, as with best frequency alone the strength of correlation does not depend on similarity index (**Fig. 6f**).

Modulation and inhibitory properties

The spectrotemporal convergence described in Figs. 3-5 is determined by a characteristic and ubiquitous lemniscal auditory receptive field feature, a main excitatory peak. Many response properties, however, depend not only on the excitatory region but on its relation

to neighboring inhibitory regions. Two such response properties that are important for processing complex sounds are temporal and spectral modulation preferences. Best temporal modulation measures a neuron's preferred rate for energy in the stimulus to fluctuate in time. It is analogous to the speed of moving visual gratings. Best spectral modulation is a neuron's preferred size for spectral envelope contours. It is analogous to the spatial frequency of visual gratings.

With the dynamic ripple stimulus, modulation preferences are derived through a two-dimensional Fourier transform of the STRF. This yields a preferred value for temporal (in Hz) and spectral (in cycles per octave) modulations. In **Fig. 7a**, the preferred temporal modulations for each pair are connected by lines. Temporal modulation preferences in cortex are slower than in thalamus (mean thalamus 44.3 Hz, cortex 27.5 Hz; median thalamus 48.2 Hz, cortex 21.5 Hz; paired-sample t-test, $p=0.0067$). While such slowing may be expected, it is notable that temporal modulation preferences in thalamus and cortex are not correlated by rank (Spearman rank correlation, $p>0.2$): thalamic cells preferring the fastest modulations do not project preferentially to the cortical cells preferring the fastest modulations, nor do slow thalamic cells project only to slow cortical cells. Many pairs including the examples from Figure 2 are evidently rank-correlated, but given our entire sample one is unable to predict cortical temporal preference from its thalamic input. Spectral modulation preferences (**Fig. 7b**) show similar trends. Cortical neurons prefer significantly lower (broader) spectral modulation preferences than thalamic cells (mean thalamus 1.27 cyc/oct, cortex 0.49 cyc/oct; median thalamus 1.47 cyc/oct, cortex 0.18 cyc/oct; paired-sample t-test $p<0.001$). As with temporal modulations, spectral modulation preferences lack a ranked

order (Spearman rank correlation, $p>0.2$): thalamic cells preferring broad spectral envelopes have no privileged influence on cortical cells preferring broad envelopes, and narrow-preferring thalamic cells are not necessarily linked to similar cortical cells. Thus, in contrast to the construction of brute spectral and temporal preferences for excitatory stimuli, modulation preferences in both time and frequency are not transmitted faithfully between thalamus and cortex.

Modulation properties depend essentially on the relationship between excitatory and inhibitory receptive field regions. The virtual absence of their propagation from thalamus to cortex, coupled with excitatory-inhibitory thalamic-cortical mismatches (Fig. 2i), suggests that inhibitory receptive field features are far less important in the thalamocortical transformation. As a test of this hypothesis, similarity indices were calculated for each STRF pair. One index was computed only for excitatory thalamic features and another only for inhibitory thalamic features, relative to the cortical receptive field. The average similarity indices for excitatory input features (0.328 +/- 0.18, mean +/- s.d.) and inhibitory input features (0.123 +/- 0.13, mean +/- s.d.) differ significantly (paired-sample t-test, $p<0.001$). Excitatory receptive field features thus play a larger role than inhibitory features in functional thalamocortical connectivity.

Discussion

Functional convergence types

Our observations on the specificity and complexity of functional thalamocortical convergence have several implications for neural processing. Convergence types fill the possible space delimited by the three extremes of inheritance, construction, and ensemble convergence. While a given cortical cell's receptive field may arise through any combination of functional convergence types, the extremes are nevertheless illustrative since each supports an operation the brain must perform upon sensory representations. Inheritance, where the cortical cell's receptive field is largely determined by functionally identical thalamic input, would preserve information for downstream processing. Constructive convergence would create selectivity for composite features, such as visual oriented lines or auditory formant combinations. Ensemble convergence, by requiring cooperative inputs to amplify some parts of the input and/or suppress others, would support feature selectivity of a more exacting nature than at the previous processing station. Admittedly, since no thalamocortical connections are of a one-to-one nature, all convergence is some type of 'ensemble' convergence. Our analysis, however, explores the constraints on and distribution of conceptually distinct convergence types.

Spectrotemporal specificity

Thalamocortical specificity is highly focal in both spectral and temporal domains, with most of the excitatory input energy falling within the cortical receptive field. This strong concentration of energy occurs despite the prevalence of ensemble convergence, which would tend to smear the input energy across a wider spectrotemporal domain. Such highly specific coupling occurs between the lateral geniculate and primary visual cortex

(Tanaka, 1983; Reid and Alonso, 1995), suggesting that functional convergence in any thalamocortical modality is highly accurate.

Given the comparably large range of convergence that thalamocortical anatomy would allow, this high degree of functional specificity raises the possibility that many non-functional or subthreshold synapses exist outside the bounds of physiological convergence (Schroeder et al., 1995; Moore and Nelson, 1998; Feldman et al., 1999; Bringuier et al., 1999; Carandini and Ferster, 2000). Such a network could selectively integrate inputs with certain parameters, and thus may establish the basis of functional zones in primary auditory cortex (Schreiner et al., 2000). It would also constitute a coding system capable of great plasticity. If an otherwise uncommitted pool of neighboring, non-functional connections were subject to recruitment, then the network could support significant changes in response to neural damage or behaviorally relevant stimuli (Recanzone et al., 1993; Weinberger, 1995; Rajan and Irvine, 1998; Kilgard and Merzenich, 1998; Nicolelis et al., 1998; Jones and Pons, 1998). This plasticity, moreover, would be uncorrelated for spectrotemporal excitatory versus modulation properties (Kilgard and Merzenich, 1998), since the thalamocortical transformation treats these factors independently.

The prevalence of functional connectivity is strictly determined by tonotopy and overall thalamocortical receptive field similarity. Remarkably, up to thirty percent of recorded pairs with virtually the same best frequency (within 0.05 octaves) are functionally connected. Likewise, if the thalamic and cortical receptive fields have an extremely high similarity index, a large proportion are connected. Our sampling biases reveal, however, that it is experimentally very difficult to find such pairs.

Although the prevalence of functional connectivity depends on receptive field similarity, the strength of connectivity does not. Strong functional connections occur not only between cells with well-matched receptive fields, as with the inheritance type of convergence. Equally powerful connections occur between cells with little receptive field features in common, as with ensemble convergence. Average connection strength is a rough guide to the number of thalamic inputs that drive a typical cortical target. Our strength estimates suggest that 20-40 thalamic inputs are required to fully activate a cortical cell. Since our analysis does not consider cooperation among inputs, however, this value may underestimate the actual numerical convergence (Reid and Alonso, 1995; Alonso et al., 1996).

Modulation and inhibitory properties

Modulation preferences are not well-preserved from thalamus to cortex, even in a lower-valued but ranked order. This reflects the fact that although excitatory receptive field properties are decisive in functional correlation, inhibitory features are not transmitted with great fidelity. The dichotomy implies that excitatory receptive field subregions of input-layer cortical cells are driven by direct thalamic input, while the inhibitory subregions, and thus modulation properties, are constructed or at least strengthened intracortically. That is, inhibitory subregions of cortical cells do not appear to come about through withdrawal of the solely excitatory thalamic input; rather, they likely come about through active inhibition from cortical interneurons. Evidence of such active excitatory/inhibitory ("push/pull") circuitry has been observed in the visual and

somatosensory systems (Ferster, 1988; Hirsch et al., 1998; Swadlow and Gusev, 2000; Ferster and Miller, 2000).

Concluding remarks

This investigation has considered only the robust, feed-forward convergence of those neural response properties that are phase-locked to the stimulus envelope. Our selection criteria under both spontaneous and stimulus-driven conditions ensures that only robust functional correlations are allowed. Since cross-correlation is a noisy measure, our dataset naturally favors the strongest connections. Weaker or labile functional connections may embody different convergence properties. Especially in the awake animal, dynamic state and corticofugal feedback may have powerful effects on the strength and quality of thalamic input to cortical receptive fields (Zhang and Suga, 1997; Fanselow and Nicolelis, 1999; Wörgötter and Eysel, 2000). Moreover, parallel non-lemniscal pathways may perform different operations than the primary lemniscal network (Ahissar et al., 2000). Finally, the STRFs used here are linear descriptors with respect to, and are necessarily phase-locked with, the spectrotemporal envelope. The high degree of functional specificity for excitatory receptive field features, however, makes it unlikely that independent, nonlinear response parameters significantly affect the transformation between these cell pairs.

This report describes what information is and, importantly, what information is not preserved in the auditory thalamocortical transformation. It illustrates how the brain realizes the varieties of functional convergence, whether by direct inheritance or with

cooperative ensembles of inputs. Above all, it shows how a remarkable specificity of connections coexists with a fundamental re-construction of receptive fields in cortex.

Experimental Procedures

Electrophysiology

Some of the experimental methods have been reported previously (Miller and Schreiner, 2000). Young adult cats (N = 4) were given an initial dose of ketamine (22mg/kg) and acepromazine (0.11mg/kg), then anesthetized with Nembutal (15-30 mg/kg) during the surgical procedure. The animal's temperature was maintained with a thermostatic heating pad. Bupivicaine was applied to incisions and pressure points. Surgery consisted of a tracheotomy, reflection of the soft tissues of the scalp, craniotomy over AI and the suprasylvian gyrus (for the thalamic approach), and durotomy. After surgery, the animal was maintained in an unreflexive state with a continuous infusion of ketamine/diazepam (10 mg/kg ketamine, 0.5 mg/kg diazepam in lactated ringer's solution). All procedures were in strict accordance with the UCSF Committee for Animal Research and the guidelines of the Society for Neuroscience.

All recordings were made with the animal in a sound-shielded anechoic chamber (IAC, Bronx, NY), with stimuli delivered via a closed, binaural speaker system (diaphragms from Stax, Japan). Simultaneous extracellular recordings were made in the thalamorecipient layers (IIIb/IV) of the primary auditory cortex (AI) and in the ventral division of the medial geniculate body (MGBv). Electrodes were parylene-coated

tungsten (Microprobe Inc., Potomac, MD) with impedances of 1-2 MOhm, or 3-5 MOhm tungsten electrodes plated with platinum black. One or two electrodes were placed in each station with hydraulic microdrives on mechanical manipulators (Narishige, Tokyo, Japan), mounted on a stereotaxic frame (David Kopf Instruments, Tujunga, CA) or on supplementary supports. Localization of thalamic electrodes, which were stereotaxically advanced along the vertical, was confirmed with Nissl stained sections. Spike trains were amplified and bandpass filtered (500-10,000 Hz), recorded on a Cygnus Technology (Delaware Water Gap, PA) CDAT-16 recorder with 24 kHz sampling rate, and sorted off-line with a Bayesian spike sorting algorithm (Lewicki, 1994). Each electrode location yielded an average of 1.9 well-isolated single units. Spontaneous neural activity (in silence) was recorded for about 35 minutes, and stimulus-driven activity for approximately 20 minutes.

Stimulus

The dynamic ripple stimulus (Schreiner and Calhoun, 1994; Kowalski et al., 1996; Escabí M. A., Schreiner C. E., Miller L. M. *Soc. Neurosci. Abs.* **24**:1879 (1998); Miller and Schreiner, 2000) is a temporally varying broadband sound composed of 230 sinusoidal carriers (500-20,000 Hz) with randomized phase. The magnitude of any carrier at any time is modulated by the spectrotemporal envelope, consisting of sinusoidal amplitude peaks ('ripples') on a logarithmic frequency axis which change through time. Two parameters define the envelope: the number of spectral peaks per octave, or ripple density, and the speed and direction of the peaks' change, or temporal frequency modulation. Both ripple density and temporal frequency modulation rate were varied

randomly and independently during the 20-minute, non-repeating stimulus. Ripple density varied slowly (max. rate of change 1 Hz) between 0 and 4 cycles per octave; the temporal frequency modulation parameter varied between 0 and 100 Hz (max. rate of change 3 Hz). Both parameters were statistically independent and unbiased within those ranges. In one experiment, however, the temporal modulation spectrum decayed slightly; all evidence of this mild bias was readily abolished while thresholding the STRFs (see Analysis). Maximum modulation depth of the spectrotemporal envelope was 45dB. Mean intensity was set appx. 20-30 dB above the neuron's pure-tone threshold.

Analysis

Data analysis was carried out in MATLAB (Mathworks Inc., Natick, MA). Spike trains were cross-correlated (Perkel et al., 1967) with 1 ms bin width, and significant bins ($p<0.01$) were determined with respect to an independent, Poisson assumption. Functionally connected pairs of neurons (n=29, from a total 741) were chosen by a strict set of criteria. Most pairs, including those in Fig. 2, showed a maximum and significant correlogram peak within 1-5 ms lag time, thalamus leading cortex, under both spontaneous and stimulus-driven conditions. It is important to use spontaneous activity when possible, as it indicates functional connectivity when the auditory system is at rest, in terms of representing stimuli. Thus, by requiring monosynaptic-like peaks under both spontaneous and driven conditions, we select particularly stable functional connections. There are, however, two potential difficulties with using spontaneous activity. The first is that a widespread, oscillatory state in the 7-14 Hz range may obscure fast correlation features (Eggermont, 1992; Cotillon et al., 2000; Miller and Schreiner, 2000). Therefore,

if thalamocortical oscillations were present under the spontaneous condition, as indicated by a significant peak in the power spectrum between 7-14 Hz, the correlogram was high-pass filtered above 25 Hz. This eliminates broad, unspecific correlation peaks and leaves intact the narrow, specific peaks that reflect direct functional connectivity. The significance level was then adjusted accordingly, and the 1-5 ms peak criterion applied. The second challenge in using spontaneous activity is that some neurons' spike rates are so low in silence that their correlograms are too noisy to show significant features. To avoid biasing our sample toward neurons with high spontaneous rates, we applied an additional, more conservative criterion. We looked more closely at recording locations where some pairs showed the significant, maximum 1-5 ms peak in both conditions, and considered thalamocortical pairs whose spontaneous correlograms' coefficient of variation exceeded one. If those pairs also had a very fast (3 ms width at half-height), short-latency (1-5 ms lag) peak under the driven condition, they were included in the analysis (n=6). Given intrinsic response variability to the dynamic ripple stimulus in thalamus and cortex, this criterion is strict enough that pairs with solely stimulus-driven correlations are rejected; with typical quasi-linear responses, the peak width is so brief that our maximum driving rate of 100 Hz is too slow to account for it. Thus in finding functionally connected pairs, we usually used both spontaneous and driven activity, and otherwise applied an even more stringent criterion to the driven activity to rule out solely stimulus-driven correlogram features. Two pairs were excluded from the analysis because either the cortical unit (n=1) or the thalamic unit (n=1) had an STRF too weak to characterize. Finally, three pairs were excluded because the receptive field features extended beyond our frequency sampling range (500-20,000 Hz).

Strength of correlation was computed under driven conditions with the traditional measure of contribution (Levick et al., 1972). Contribution is the percentage of cortical spikes immediately preceded by a thalamic spike (1-10ms lag), above that expected by chance. Intuitively, the contribution gives the proportion of the cortical cell's activity that is presumed to be caused by the thalamic unit.

For each neuron, the reverse correlation method was used to derive the spectrotemporal receptive field, or STRF, which is the average spectrotemporal stimulus envelope immediately preceding each spike (Aertsen and Johannesma, 1980; Escabí M. A., Schreiner C. E., Miller L. M. *Soc. Neurosci. Abs.* 24, 1879 (1998); Klein et al., 2000). Positive regions of the STRF indicate that stimulus energy at that frequency and time tends to increase the neuron's firing rate, and negative regions indicate where the stimulus envelope induces a decrease in firing rate. In this report, only STRFs derived from the typically dominant, contralateral ear were used. For display, the STRFs were thresholded to show significant regions ($p<0.002$). High-energy peaks in the STRF were defined by contours at 1/e times the maximum value, which typically circumscribed approximately 90% of the peak energy. Modulation properties were derived by performing a two-dimensional Fourier transform of the STRF, giving a signal in the parameter space of temporal modulation rate versus spectral modulation rate, or ripple density. Preferred temporal and spectral modulation rates are analogous to moving grating speed and spatial frequency, respectively, in the visual system.

Thalamic and cortical STRFs were compared with a similarity index (deAngelis et al., 1999) related to a correlation coefficient. For functionally connected pairs, the thalamic STRF was shifted by the peak correlogram delay. For non-connected pairs, the

thalamic STRF was shifted by the mean delay for all connected pairs of 2.6 ms. The two significant STRFs were then treated as vectors rather than arrays in time and frequency. The similarity index is the inner product of the vectorized thalamic and cortical STRFs, divided by both of their vector norms. A vector norm is the square root of the inner product of a vector with itself. Therefore, STRFs that are similar in shape and sign have a similarity index near 1, those of similar shape but opposite sign have an index near –1, and those that are orthogonal have an index of 0. Thalamocortical similarity indices were calculated with the entire thalamic STRF and with excitatory and inhibitory thalamic subregions separately.

Acknowledgments

Supported by the National Institutes of Health (DC02260, NS34835), the National Science Foundation (NSF97203398), and the Whitaker Foundation. Thanks to M. Kvale for writing the spike-sorting software.

References

Adrian E. D. (1941). Afferent discharges to the cerebral cortex from peripheral sense organs. J. Physiol. *100*, 159-91.

Aertsen A. M. H. J., Johannesma P. I. M. (1980). Spectro-temporal receptive fields of auditory neurons in the grassfrog. Biol. Cyber. *38*, 223-234.

Ahissar E., Sosnik R., Haidarliu S. (2000). Transformation from temporal to rate coding in a somatosensory thalamocortical pathway. Nature *406*, 302-6.

Alonso J. M., Usrey W. M., Reid R. C. (1996) Precisely correlated firing in cells of the lateral geniculate nucleus. Nature *383*:815-9.

Andersen R. A., Knight P. L., Merzenich M. M. (1980). The thalamocortical and corticothalamic connections of AI, AII, and the anterior auditory field (AAF) in the cat: evidence for two largely segregated systems of connections. J. Comp. Neurol. *194*, 663-701.

Brandner S., Redies H. (1990). The projection from medial geniculate to field AI in cat: organization in the isofrequency dimension. J. Neurosci. *10*, 50-61.

Bringuier V., Chavane F., Glaeser L., Frégnac Y. (1999). Horizontal propagation of visual activity in the synaptic integration field of area 17 neurons. Science *283*:695-9.

Carandini M., Ferster D. (2000) Membrane potential and firing rate in cat primary visual cortex. J. Neurosci. *20*:470-84.

Cetas J. S., de Venecia R. K., McMullen N. T. (1999). Thalamocortical afferents of Lorente de Nó: medial geniculate axons that project to primary auditory cortex have collateral branches to layer I. Brain. Res. *830*, 203-208.

Chapman B. Zahs K. R., Stryker M. P. (1991). Relation of cortical cell orientation selectivity to alignment of receptive fields of the geniculocortical afferents that arborize within a single orientation column in ferret visual cortex. J. Neurosci. *11*, 1347-58.

Chung S., Ferster D. (1998). Strength and orientation tuning of the thalamic input to simple cells revealed by electrically evoked cortical suppression. Neuron *20*, 1177-89.

Clarey J. C., Barone, P., Imig T. J. (1994). Physiology of thalamus and cortex. In The Mammalian Auditory Pathway: Neurophysiology, A. N. Popper and R. R. Fay, eds. (New York: Springer-Verlag), pp. 232-334.

Cotillon N., Nafati M., Edeline J.M. (2000). Characteristics of reliable tone-evoked oscillations in the rat thalamo-cortical auditory system. Hear. Res. *142*, 113-30.

Creutzfeldt O., Hellweg F. C., Schreiner C. E. (1980). Thalamocortical transformation of responses to complex auditory stimuli. Exp. Br. Res. *39*, 87-104.

DeAngelis G. C., Ghose G. M., Ohzawa I., Freeman R. D. (1999). Functional micro-organization of primary visual cortex: receptive field analysis of nearby neurons. J. Neurosci. *19*, 4046-64.

de Venecia R. K., McMullen N. T. (1994). Single thalamocortical axons diverge to multiple patches in neonatal auditory cortex. Br. Res., Dev. Br. Res. *81*, 135-42.

Eggermont J. J. (1992). Stimulus induced and spontaneous rhythmic firing of single units in cat primary auditory cortex. Hear. Res. *61*, 1-11.

Fanselow E. E., Nicolelis M. A. (1999) Behavioral modulation of tactile responses in the rat somatosensory system. J. Neurosci. *19*: 7603-16.

Feldman D. E., Nicoll R. A., Malenka R. C. (1999). Synaptic plasticity at thalamocortical synapses in developing rat somatosensory cortex: LTP, LTD, and silent synapses. J. Neurobiol. *41*, 92-101.

Ferster D. (1988). Spatially opponent excitation and inhibition in simple cells of the cat visual cortex. J. Neurosci. *8*, 1172-80.

Ferster D., Miller K. D. (2000) Neural mechanisms of orientation selectivity in the visual cortex. Ann. Rev. Neurosci. *23*: 441-71.

Hirsch J. A., Alonso J-M., Reid R. C., Martinez L. M. (1998). Synaptic integration in striate cortical simple cells. J. Neurosci. *18*, 9517-28.

Huang C. L., Winer J. A. (2000). Auditory thalamocortical projections in the cat: laminar and areal patterns of input. J. Comp. Neurol. *427*, 302-331.

Hubel D. H., Wiesel T. N. (1962). Receptive fields, binocular interaction and functional architecture in the cat's visual cortex. J. Physiol. (Lond) *160*, 106-154.

Johnson M. J., Alloway K. D. (1996). Cross-correlation analysis reveals laminar differences in thalamocortical interactions in the somatosensory system. J. Neurophysiol. *75*, 1444-57.

Jones E. G., Pons T. P. (1998). Thalamic and brainstem contributions to large-scale plasticity of primate somatosensory cortex. Science *282*, 1121-5.

Kilgard M. P., Merzenich M. M. (1998). Plasticity of temporal information processing in the primary auditory cortex. Nature Neurosci. *1*, 727-31.

Klein D. J., Depireux D. A., Simon J.Z., Shamma S. A. (2000). Robust spectrotemporal reverse correlation for the auditory system: optimizing stimulus design. J. Comp. Neurosci. *9*, 85-111.

Kowalski N., Depireux D. A., Shamma S. A. (1996). Analysis of dynamic spectra in ferret primary auditory cortex. I. Characteristics of single-unit responses to moving ripple spectra. J. Neurophysiol. *76*, 3503-23.

Kyriazi H. T., Simons D. J. (1993). Thalamocortical response transformations in simulated whisker barrels. J. Neuroscience *13*, 1601-15.

Levick W. R., Cleland B. G., Dubin M. W. (1972). Lateral geniculate neurons of cat: retinal inputs and physiology. Investigative Ophthalmology *11*, 302-11.

Lewicki M. S. (1994). Bayesian modeling and classification of neural signals. J. Neural Comp. *6*, 1005-1030.

Middlebrooks J. C., Zook J. M. (1983). Intrinsic organization of the cat's medial geniculate body identified by projections to binaural response-specific bands in the primary auditory cortex. J. Neurosci. *3*, 203-24.

Miller L. M., Schreiner C. E. (2000). Stimulus-based state control in the thalamocortical system. J. Neurosci. *20*, 7011-6.

Moore C. I., Nelson S. B. (1998). Spatio-temporal subthreshold receptive fields in the vibrissa representation of rat primary somatosensory cortex. J. Neurophysiol. *80*, 2882-92.

Nicolelis M. A., Katz D., Krupa D. J. (1998). Potential circuit mechanisms underlying concurrent thalamic and cortical plasticity. Rev. Neurosci. *9*, 213-24.

Perkel D. H., Gerstein G. L., Moore G. P. (1967). Neuronal spike trains and stochastic point processes. II. Simultaneous spike trains. Biophys. J. *7*, 419-40.

Rajan R., Irvine D. R. (1998). Neuronal responses across cortical field A1 in plasticity induced by peripheral auditory organ damage. Audiol. Neuro-Otol. *3*, 123-44.

Recanzone G. H., Schreiner C. E., Merzenich M. M. (1993). Plasticity in the frequency representation of primary auditory cortex following discrimination training in adult owl monkeys. J. Neurosci. *13*, 87-103.

Reid R. C., Alonso J-M. (1995). Specificity of monosynaptic connections from thalamus to visual cortex. Nature *378*, 281-4.

Schreiner C. E., Calhoun B. M. (1994). Spectral envelope coding in cat primary auditory cortex: properties of ripple transfer functions. Aud. Neurosci. *1*, 39-61.

Schreiner C. E., Read H. L., Sutter M. L. (2000). Modular organization of frequency integration in primary auditory cortex. Ann. Rev. Neurosci. *23*, 501-29.

Schroeder C.E., Seto S., Arezzo J. C., Garraghty P. E. (1995) Electrophysiological evidence for overlapping dominant and latent inputs to somatosensory cortex in squirrel monkeys. J. Neurophysiol. *74*: 722-32.

Swadlow H. A. (1995). Influence of VPM afferents on putative inhibitory interneurons in S1 of the awake rabbit: evidence from cross-correlation, microstimulation, and latencies to peripheral sensory stimulation. J. Neurophysiol. *73*, 1584-99.

Swadlow H. A., Gusev A. G. (2000) The influence of single VB thalamocortical impulses on barrel columns of rabbit somatosensory cortex. J. Neurophysiol. *83*: 2802-13.

Tanaka K. (1983). Cross-correlation analysis of geniculostriate neuronal relationships in cats. J. Neurophysiol. *49*, 1303-18.

Weinberger N. M. (1995). Dynamic regulation of receptive fields and maps in the adult sensory cortex. Ann. Rev. Neurosci. *18*, 129-58.

Wörgötter F., Eysel U. T. (2000) Context, state and the receptive fields of striatal cortex cells. TINS *23*: 497-503.

Zhang Y., Suga N. (1997) Corticofugal amplification of subcortical responses to single tone stimuli in the mustached bat. J. Neurophysiol. *78*: 3489-92.

Figure legends

Fig. 1. Heuristic illustration of the possible extremes of functional thalamocortical convergence. Shapes within the ellipses represent different spectrotemporal receptive field features. (**a**) The simplest case is inheritance, where a cortical cell's receptive field is determined by functionally identical thalamic inputs. (**b**) In constructive convergence, a cortical cell's receptive field is a composite of many smaller (in spatiotemporal extent) thalamic inputs. (**c**) In ensemble convergence, the thalamic inputs have some receptive field properties that are not shared by the cortical target cell. This requires an ensemble of other inputs either to amplify the features that are ultimately represented by the cortical cell, or to suppress the features that are not. This figure is not intended to suggest that a given thalamocortical connection must categorically be one of these types, or that a given cortical cell must receive only one type from all its thalamic inputs.

Fig. 2. Representative examples of functionally connected thalamocortical pairs. (**a-c**) Inheritance. (**a**) Spectrotemporal receptive fields (STRFs) for the thalamic and cortical cell. The STRFs are depicted with time-preceding-spike on the abscissa, and frequency on the ordinate. Warm and cool colors indicate an excitatory or inhibitory effect, respectively, that the stimulus induced in a particular spectrotemporal region. The values on the colorbar are thus differential rates, in spikes/sec, relative to the mean rate. (**b**) Cross-correlograms between the two units, normalized to firing rate. The bar plot is the cross-correlogram under the ripple-driven condition, and the line plot (truncated for clarity) is under the spontaneous condition. The brief, short-latency peak, with cortical spike lagging thalamic (2 ms), is indicative of a monosynaptic-like functional connection

(correlation strength = .082). The cyan line is the mean, and the red lines are the 99% confidence intervals for the stimulus-driven correlogram, under an assumption of independent, Poisson spike trains. (**c**) Expanded views of the excitatory peaks of the STRFs in (a). Superimposed on the cortical STRF are contours circumscribing the high-energy region of the cortical (green) and thalamic (black) STRFs (see Methods). The thalamic contour has been shifted in time by the peak correlogram delay. In this case, the cortical cell appears to inherit its excitatory features from the thalamic input.

(d-f) Mixed constructive/ensemble convergence. (**d**) STRFs for the thalamic and cortical cells. (**e**) Thalamocortical cross-correlograms, rate-normalized, with a bar plot depicting the stimulus-driven and a line plot depicting the spontaneous correlogram. As in Fig. 2a, the brief, short-latency peak (2 ms) indicates monosynaptic-like functional connectivity (correlation strength = .029). (**f**) Expanded views of the excitatory peaks of the STRFs above. In this case, a thalamic cell with smaller receptive field helps construct a larger, composite cortical STRF. This example emphasizes that the convergence types schematized in Fig. 1 are not, in fact, categorical. Notice, this thalamic cell also participates in ensemble convergence, as a portion of its peak lies outside that of the cortex.

(g-i) Ensemble convergence. (**g**) STRFs for the thalamic and cortical cells. (**h**) Thalamocortical cross-correlograms (3 ms peak lag), rate-normalized, with a bar plot depicting the stimulus-driven and a line plot depicting the spontaneous correlogram (driven correlation strength = .037). (**i**) Expanded views of the excitatory peaks of the STRFs above. In this case, a thalamic cell with much larger excitatory receptive field is pared down to contribute to a smaller cortical STRF. This logically demands the

participation of an ensemble of other inputs, acting in concert. Moreover, the higher frequency excitatory region of the thalamic STRF overlaps a strong inhibitory region in cortex, a mismatch that evidently does not preclude the presence of functional connectivity.

Fig. 3. Distribution of thalamocortical convergence types. Types of functional convergence for the main excitatory peak are parsed along two dimensions: cortical coverage and thalamic overlap. Cortical coverage is the proportion of the cortical receptive field peak that is covered by that of the thalamic input. Thalamic overlap is the proportion of the thalamic receptive field peak that overlaps that of the cortex. Thus, high cortical coverage and thalamic overlap indicate inheritance; low cortical coverage but high thalamic overlap indicates constructive convergence; and low thalamic overlap with varying degrees of cortical coverage characterizes ensemble convergence. The cartoon insets represent paradigmatic receptive field relationships for a given region of the plot, where dotted lines (--) represent the cortical, and solid lines (—) the thalamic receptive fields. The thalamocortical pairs from Fig. 2 are represented by stars (*).

Fig. 4. Summary of normalized thalamic receptive field inputs. (**a**) An idealized cortical excitatory peak is depicted as a light grey circle. Contours outline the thalamic inputs, each normalized to its own cortical target. Contour color indicates thalamocortical correlation strength under the stimulus-driven condition (mean .045), with cool colors low and warm colors high values. (**b**) Peak energies of the thalamic inputs, summed across time. Most (72%) of the energy falls within one normalized cortical bandwidth.

(c) Peak energies of the thalamic inputs, summed across frequency. Most (80%) of the energy falls within one normalized cortical duration.

Fig. 5. Degree of thalamocortical convergence in octaves. **(a)** The difference in thalamic vs. cortical best frequencies (absolute value) is summarized in a histogram (mean difference 0.077 octaves). Black bars are thalamocortical pairs from Fig. 2. If the difference in best frequencies is greater than about 1/4 octave, functional connections are not observed. **(b)** For each thalamocortical pair, the frequencies at the far edges of the excitatory receptive fields, relative to cortical best frequency, are connected by a line. Very little convergence is observed for edges greater than 1/3 octave from the cortical best frequency. Due to the frequency sampling (~40/octave), several values from different pairs are so similar as to be indistinguishable. Thick lines are pairs from Fig. 2.

Fig. 6. Prevalence but not strength of functional connectivity depends on best frequency difference (**a-c**) and similarity index (**d-f**). (**a**) A histogram of all recorded thalamocortical pairs reveals a sampling bias toward pairs with small best frequency difference but extends well beyond one-octave separation. (**b**) The proportion of recorded pairs that are functionally correlated depends strongly on the best frequency difference, with the greatest proportion having the least difference. (**c**) The strength of correlation for functionally connected thalamocortical pairs does not depend on best frequency difference. (**d**) Our population of all recorded thalamocortical pairs is biased toward low, positive similarity indices. Similarity index is less than 0.2 in 78% of pairs. (**e**) The proportion of recorded pairs that are functionally correlated depends strongly on

the overall STRF similarity. (**f**) The strength of correlation for functionally connected thalamocortical pairs does not depend on STRF similarity.

Fig. 7. Convergence of temporal and spectral modulation preferences. (**a**) Temporal modulation preferences for each thalamocortical pair, in Hz, are connected by lines. Cortical cells tend to prefer slower modulations (mean thalamus 44.3 Hz, cortex 27.5 Hz; median thalamus 48.2 Hz, cortex 21.5 Hz; paired-sample t-test, $p=0.0067$). There is no rank correlation among the pairs; that is, slow (fast) thalamic cells do not tend to project to slow (fast) cortical cells (Spearman rank correlation, $p>0.2$). (**b**) Spectral modulation preferences for each thalamocortical pair, in ripple cycles per octave, are connected by lines. There is a significant trend toward broader, or wider-band preferences in cortex (mean thalamus 1.27 Hz, cortex 0.49 Hz; median thalamus 1.47 Hz, cortex 0.18 Hz; paired-sample t-test $p<0.001$). As with temporal modulations, there is no rank correlation among the pairs: broad (narrow) thalamic cells do not project preferentially to broad (narrow) cortical cells (Spearman rank correlation, $p>0.2$). Thick lines are pairs from Fig. 2

Types of functional convergence

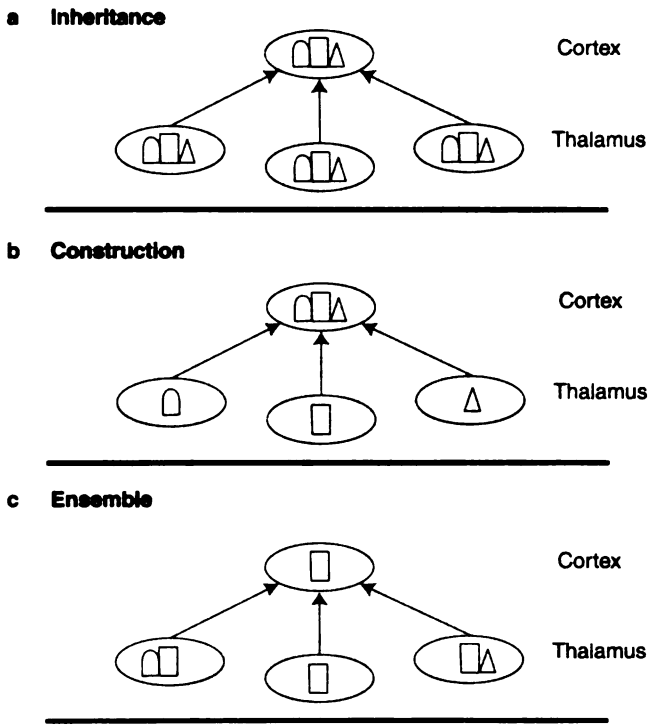

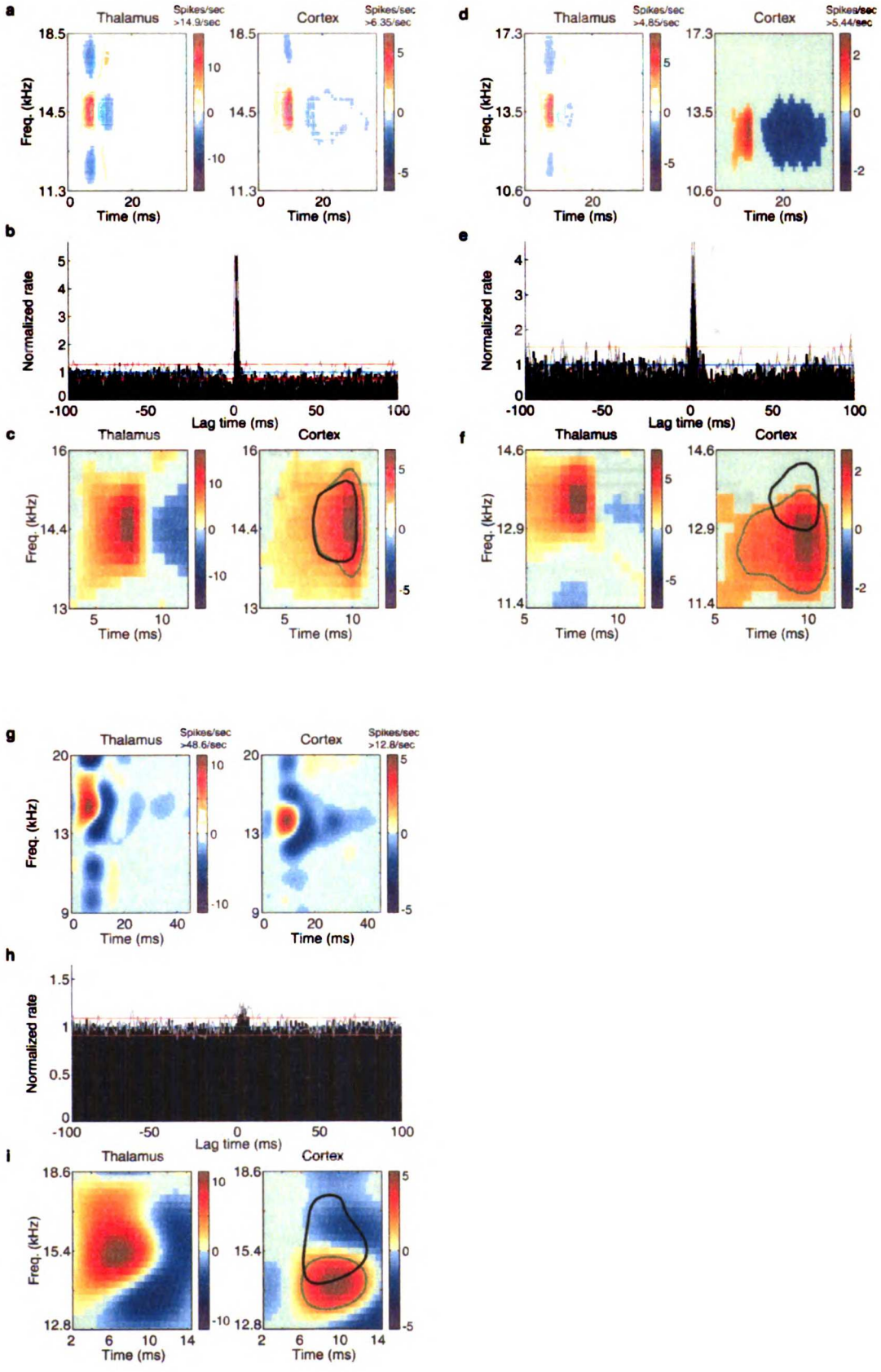
a
Thalamus
Spikes/sec
>14.9/sec
Cortex
Spikes/sec
>6.35/sec
Freq. (kHz)
Time (ms)
b
Normalized rate
Lag time (ms)
c
Thalamus
Cortex
Freq. (kHz)
Time (ms)
d
Thalamus
Spikes/sec
>4.85/sec
Cortex
Spikes/sec
>5.44/sec
Freq. (kHz)
Time (ms)
e
Normalized rate
Lag time (ms)
f
Thalamus
Cortex
Freq. (kHz)
Time (ms)
g
Thalamus
Spikes/sec
>48.6/sec
Cortex
Spikes/sec
>12.8/sec
Freq. (kHz)
Time (ms)
h
Normalized rate
Lag time (ms)
i
Thalamus
Cortex
Freq. (kHz)
Time (ms)

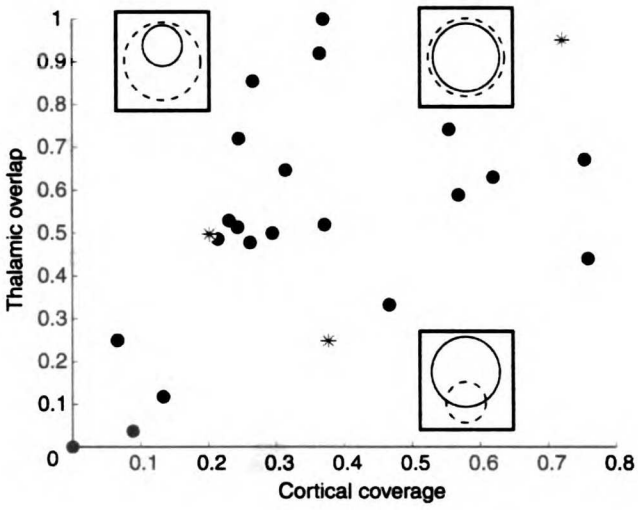
Thalamic overlap
Cortical coverage
0
0.1
0.2
0.3
0.4
0.5
0.6
0.7
0.8
0.9
1

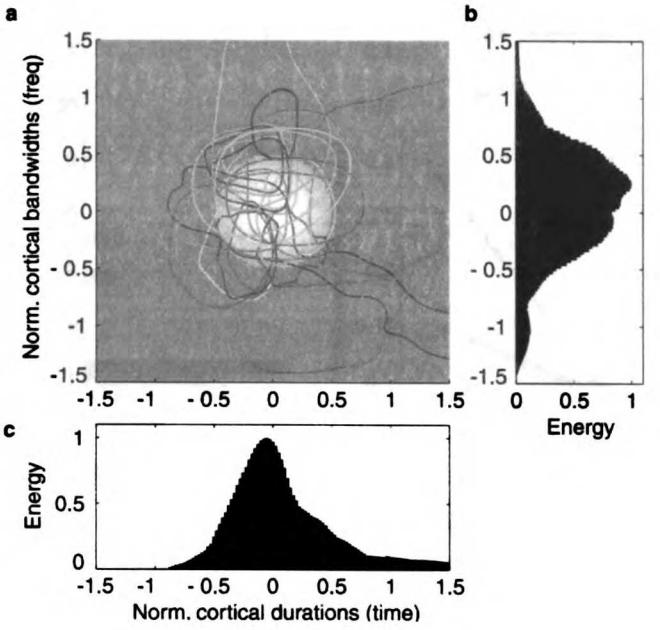
a
b
c
Norm. cortical bandwidths (freq)
Energy
Energy
Norm. cortical durations (time)
1.5
1
0.5
0
- 0.5
-1
-1.5
-1.5 -1 - 0.5 0 0.5 1 1.5
0 0.5 1

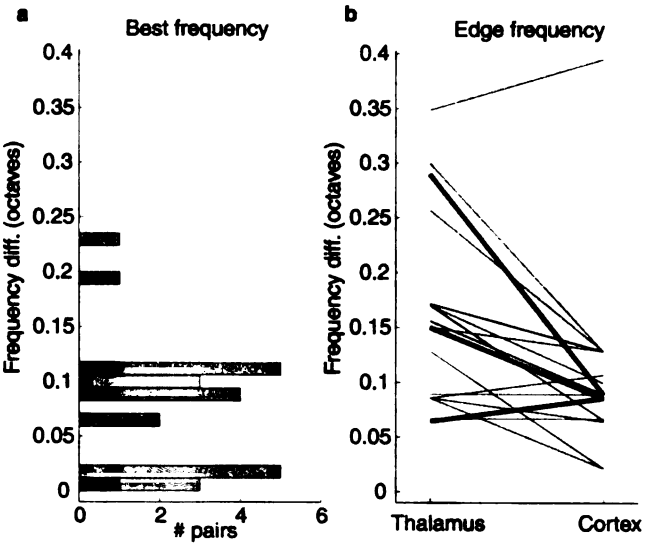
a
Best frequency
Frequency diff. (octaves)
0.4
0.35
0.3
0.25
0.2
0.15
0.1
0.05
0
0
2
4
6
pairs
b
Edge frequency
Frequency diff. (octaves)
0.4
0.35
0.3
0.25
0.2
0.15
0.1
0.05
0
Thalamus
Cortex

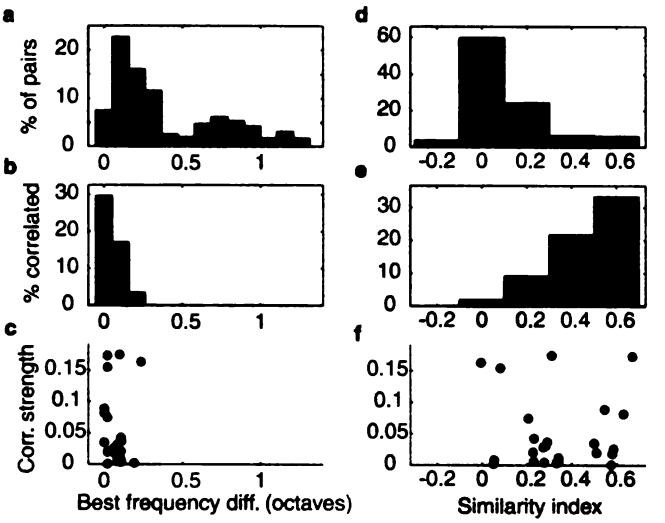
a
% of pairs
20
10
0
0
0.5
1
b
% correlated
30
20
10
0
0
0.5
1
c
Corr. strength
0.15
0.1
0.05
0
0
0.5
1
Best frequency diff. (octaves)
d
60
40
20
0
-0.2
0
0.2
0.4
0.6
e
30
20
10
0
-0.2
0
0.2
0.4
0.6
f
0.15
0.1
0.05
0
-0.2
0
0.2
0.4
0.6
Similarity index

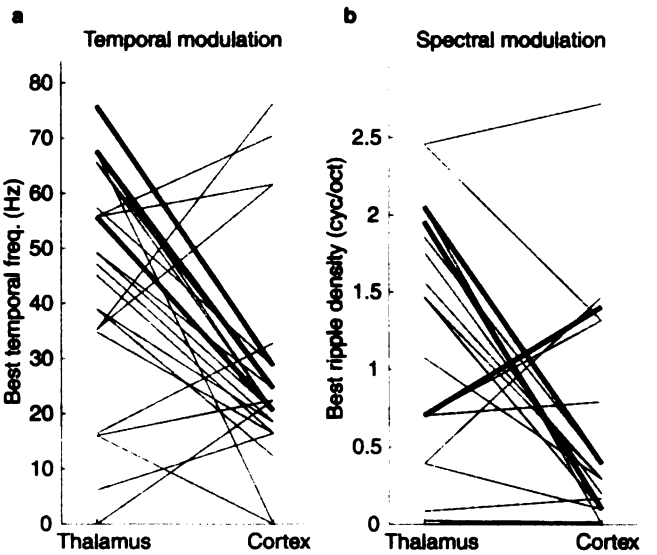
a
Temporal modulation
Best temporal freq. (Hz)
80
70
60
50
40
30
20
10
0
Thalamus
Cortex
b
Spectral modulation
Best ripple density (cyc/oct)
2.5
2
1.5
1
0.5
0
Thalamus
Cortex

CHAPTER 4:

FEATURE SELECTIVITY AND INTERNEURONAL COOPERATION IN THE THALAMOCORTICAL SYSTEM

ABSTRACT: Action potentials are a universal currency for fast information transfer in the nervous system, yet few studies address how some spikes carry more information than others. We focused on the transformation of sensory representations in the lemniscal (high-fidelity) auditory thalamocortical network. While stimulating with a complex sound, we recorded simultaneously from functionally connected cell pairs in the ventral medial geniculate body (MGBv) and primary auditory cortex (AI). Thalamic action potentials that immediately preceded, or potentially caused a cortical spike were more selective than the average thalamic spike for spectrotemporal stimulus features. This net improvement of thalamic signaling indicates that for some thalamic cells, spikes are not propagated through cortex independently but interact with other inputs onto the same target cell. We then developed a method to identify the spectrotemporal nature of these interactions, and found they could be cooperative or antagonistic to the thalamic cell's average receptive field. The degree of cooperativity with the thalamic cell determined the increase in feature selectivity for potentially causal thalamic spikes. We therefore show how some thalamic spikes carry more receptive field information than average, and how other inputs cooperate to constrain the information communicated through a cortical cell.

Keywords: convergence; information; receptive field; feature selectivity

INTRODUCTION

Despite decades of research on receptive fields in anatomically connected regions, we have only a rudimentary understanding of how neurons transform information between stations and how cooperation influences the transformation. A detailed comparison of receptive fields between functionally connected thalamic inputs and their cortical targets illustrates the remarkable specificity of the thalamocortical transformation (Creutzfeldt et al., 1980; Tanaka, 1983; Reid and Alonso, 1995; Miller et al., 2000; Roy and Alloway, 2001). While such comparisons provide essential constraints on the degree of functional convergence, they reveal only how all the spikes of an input cell relate to all those of its target. The next goal, therefore, has been to identify whether some spikes might be more important than others. For instance, action potentials from two thalamic cells that occur in tight synchrony can drive a cortical target much more effectively than non-synchronous spikes (Alonso et al., 1996; Usrey et al., 2000; Roy and Alloway, 2001). Yet these latter studies did not characterize the functional role that synchronous or otherwise temporally unique spikes play in transmitting receptive field information to cortex.

The explicit relationship between timing among action potentials and the receptive field information carried by a neuron has been investigated within thalamus (Dan et al., 1998) and within cortex (Ghose et al., 1994; Reich et al., 2000), but not explicitly across the thalamocortical synapse. A crucial element of the thalamocortical transformation, therefore, has not been addressed: whether thalamic spikes that potentially cause cortical spikes carry more or less receptive field information than expected. The answer to this question is illustrative, since it suggests whether influences

external to a given thalamic cell affect the information transmitted through cortex. Of all the thalamic spikes that impinge upon a cortical cell, only a small proportion are transmitted. If potentially causal thalamic spikes tend to carry the same receptive field information as the average, then they are being propagated independently or at random with respect to the stimulus. No external influence is necessary to explain their success or failure at the thalamocortical synapse. But if on the other hand they carry different receptive field information than average, then their propagation through cortex is not random. Other inputs must affect which input spikes are successful and which fail. We would like to describe, then, what functional, stimulus-specific role other inputs play to modulate the character of a thalamic cell's contribution to cortex.

We introduce a novel approach to these questions, relying on simultaneous recordings of functionally connected neurons in the thalamus and cortex. Spectrotemporal receptive fields describe the neural responses to dynamic, wideband sounds. A neuron's selectivity to stimulus features quantifies whether thalamic spikes that potentially cause a cortical cell to fire carry more or less information than expected. We then estimate the spectrotemporal, stimulus-dependent conditioning influence of other cells on a given thalamic input. Finally we show how the degree of cooperation between conditioning influence and thalamic input relates to the differences in feature selectivity between potentially causal and average thalamic spikes.

METHODS

Electrophysiology. A detailed account of our experimental methods has been reported previously (Miller and Schreiner, 2000). Young adult cats (N = 4) were given

an initial dose of ketamine (22mg/kg) and acepromazine (0.11mg/kg), then anesthetized with Nembutal (15-30 mg/kg) during the surgical procedure. The animal's temperature was maintained with a thermostatic heating pad. Bupivicaine was applied to incisions and pressure points. Surgery consisted of a tracheotomy, reflection of the soft tissues of the scalp, craniotomy over AI and the suprasylvian gyrus (for the thalamic approach), and durotomy. After surgery, the animal was maintained in an unreflexive state with a continuous infusion of ketamine/diazepam (10 mg/kg ketamine, 0.5 mg/kg diazepam in lactated ringer's solution). All procedures were in strict accordance with the UCSF Committee for Animal Research and the guidelines of the Society for Neuroscience.

All recordings were made with the animal in a sound-shielded anechoic chamber (IAC, Bronx, NY), with stimuli delivered via a closed, binaural speaker system (diaphragms from Stax, Japan). Simultaneous extracellular recordings were made in the thalamorecipient layers (IIIb/IV) of the primary auditory cortex (AI) and in the ventral division of the medial geniculate body (MGBv). Electrodes were parylene-coated tungsten (Microprobe Inc., Potomac, MD) with impedances of 1-2 MOhm, or 3-5 MOhm tungsten electrodes plated with platinum black. One or two electrodes were placed in each station with hydraulic microdrives on mechanical manipulators (Narishige, Tokyo, Japan), mounted on a stereotaxic frame (David Kopf Instruments, Tujunga, CA) or on supplementary supports. Localization of thalamic electrodes, which were stereotaxically advanced along the vertical, was confirmed with Nissl stained sections. Spike trains were amplified and bandpass filtered (500-10,000 Hz), recorded on a Cygnus Technology (Delaware Water Gap, PA) CDAT-16 recorder with 24 kHz sampling rate, and sorted off-line with a Bayesian spike sorting algorithm (Lewicki, 1994). Each electrode location

yielded an average of 1.9 well-isolated single units. Spontaneous neural activity (in silence) was recorded for about 35 minutes, and stimulus-driven activity for approximately 20 minutes.

Stimulus. The dynamic ripple stimulus (Schreiner and Calhoun, 1994; Kowalski et al., 1996; Escabí et al., 1998; Miller and Schreiner, 2000) is a temporally varying broadband sound composed of 230 sinusoidal carriers (500-20,000 Hz) with randomized phase. The magnitude of any carrier at any time is modulated by the spectrotemporal envelope, consisting of sinusoidal amplitude peaks ('ripples') on a logarithmic frequency axis which change through time. Two parameters define the envelope: the number of spectral peaks per octave, or ripple density, and the speed and direction of the peaks' change, or temporal frequency modulation. Both ripple density and temporal frequency modulation rate were varied randomly and independently during the 20-minute, non-repeating stimulus. Ripple density varied slowly (max. rate of change 1 Hz) between 0 and 4 cycles per octave; the temporal frequency modulation parameter varied between 0 and 100 Hz (max. rate of change 3 Hz). Both parameters were statistically independent and unbiased within those ranges. In one experiment, however, the temporal modulation spectrum decayed slightly; all evidence of this mild bias was readily abolished while thresholding the STRFs (see below). Maximum modulation depth of the spectrotemporal envelope was 45dB. Mean intensity was set appx. 20-30 dB above the neuron's pure-tone threshold.

Cross-correlation. Data analysis was carried out in MATLAB (Mathworks Inc., Natick, MA). Spike trains were cross-correlated (Perkel et al., 1967) with 1 ms bin width, and significant bins ($p<0.01$) were determined with respect to an independent,

Poisson assumption. Functionally connected pairs of neurons (n=29, from a total 741) were chosen by a strict set of criteria. Most pairs, including those in Figs. 4-6, showed a maximum and significant correlogram peak within 1-5 ms lag time, thalamus leading cortex, under both spontaneous and stimulus-driven conditions. It is important to use spontaneous activity when possible, as it indicates functional connectivity when the auditory system is at rest, in terms of representing stimuli. Thus, by requiring monosynaptic-like peaks under both spontaneous and driven conditions, we select particularly stable functional connections. There are, however, two potential difficulties with using spontaneous activity. The first is that a widespread, oscillatory state in the 7-14 Hz range may obscure fast correlation features (Eggermont 1992; Cotillon et al.2000; Miller and Schreiner, 2000). Therefore, if thalamocortical oscillations were present under the spontaneous condition, as indicated by a significant peak in the power spectrum between 7-14 Hz, the correlogram was high-pass filtered above 25 Hz. This eliminates broad, unspecific correlation peaks and leaves intact the narrow, specific peaks that reflect direct functional connectivity. The significance level was then adjusted accordingly, and the 1-5 ms peak criterion applied. The second challenge in using spontaneous activity is that some neurons' spike rates are so low in silence that their correlograms are too noisy to show significant features. To avoid biasing our sample toward neurons with high spontaneous rates, we applied an additional, more conservative criterion. We looked more closely at recording locations where some pairs showed the significant, maximum 1-5 ms peak in both conditions, and considered thalamocortical pairs whose spontaneous correlograms' coefficient of variation exceeded one for the presumably featureless regions of ± 300-3000 ms lag time. If those pairs also had a very

fast (3 ms width at half-height), short-latency (1-5 ms lag) peak under the driven condition, they were included in the analysis (n=6). Given intrinsic response variability to the dynamic ripple stimulus in thalamus and cortex, this criterion is strict enough that pairs with solely stimulus-driven correlations are rejected; with typical quasi-linear responses, the peak width is so brief that our maximum driving rate of 100 Hz is too slow to account for it. Thus in finding functionally connected pairs, we usually used both spontaneous and driven activity, and otherwise applied an even more stringent criterion to the driven activity to rule out solely stimulus-driven correlogram features. Two pairs were excluded from the analysis because either the cortical unit (n=1) or the thalamic unit (n=1) had an STRF too weak to characterize. Finally, one pair was removed because a cell was so bursty as to preclude our analysis, and three pairs were excluded because the receptive field features extended beyond our frequency sampling range (500-20,000 Hz).

Spectrotemporal receptive fields. For each neuron, the reverse correlation method was used to derive the spectrotemporal receptive field, or STRF, which is the average spectrotemporal stimulus envelope immediately preceding each spike (Aertsen et al., 1980; Escabí et al., 1998; Klein et al., 2000). Positive regions of the STRF indicate that stimulus energy at that frequency and time tends to increase the neuron's firing rate, and negative regions indicate where the stimulus envelope induces a decrease in firing rate. In this report, only STRFs derived from the typically dominant, contralateral ear were used. For display, the STRFs were thresholded to show significant regions ($p<0.002$). For visual reference in some figures, the high energy peak of an STRF is indicated by a contour at 1/e times its maximum magnitude; such a contour typically circumscribes approximately 90% of the energy in the STRF feature. In all figures, plots are bounded

to show details of the main excitatory peak and any areas that show a peak or conditioning influence. The entire STRFs will be covered in another report (L.M., in preparation).

Similarity index. STRFs were compared to each other with a similarity index (DeAngelis et al., 1999; Reich et al., 2000) related to a correlation coefficient. The two significant STRFs were treated as vectors rather than arrays in time and frequency. The similarity index is then the inner product of the vectorized STRFs, divided by both of their vector norms. A vector norm is the square root of the inner product of a vector with itself. Therefore, STRFs that are similar in shape and sign have a similarity index near 1, those of similar shape but opposite sign have an index near –1, and those that are orthogonal have an index of 0.

Feature Selectivity Index. The relative amount of information a neuron transmits reflects the degree to which it fires selectively to certain stimulus features. The features most relevant to a neuron, on average, are those embodied in its STRF. We can therefore calculate how selectively a neuron responds by comparing its STRF with all the stimuli that preceded action potentials. If a neuron is highly selective, it fires only when the features in the stimulus exactly match the STRF. If a neuron has low selectivity, it fires to stimuli bearing little overall resemblance to the STRF.

Just as a similarity index (see *Similarity index* above) quantifies the resemblance between two STRFs, it can be used to compare an STRF and a pre-spike spectrotemporal stimulus envelope. Each spike, then, has a similarity index associated with it. In this context, a similarity index near 1 means the spike was very selective and a similarity index near zero means the spike was random with respect to the stimulus. The typically

thousands of spikes from a given cell yield a range of similarity indices, distributed from approximately zero to one. The more the distribution is biased toward one, the more selective the cell is for stimulus features. The feature selectivity index (FSI) measures this bias: an ideal feature selector has FSI of one and a random neuron has FSI of zero.

Details of the FSI procedure have been reported previously (Escabí et al., 2000). Briefly, the FSI is computed from the cumulative distribution function (CDF) of the STRF-vs.-stimulus similarity index distribution. The area under a neuron's CDF is compared to that of an ideal feature selector and that from a theoretically random neuron. Since all the similarity indices from an ideal feature selector are equal to one, its CDF has value zero everywhere except one. The area under the feature-selective cell's CDF is thus zero. The CDF for a theoretically random neuron is constructed from the similarity indices of the actual STRF versus the stimulus preceding 12,000 random, fabricated spikes; this accounts for variability solely from STRF idiosyncrasies. Since the similarity indices for a random neuron are clustered near zero, its CDF rises near zero and reaches its maximum at a low similarity index. The area under the random CDF is thus large and roughly equal to one. The area under the actual CDF lies somewhere between the extremes of large (random neuron) and zero (ideal feature selector). The FSI is therefore the difference in area between the random CDF versus the actual CDF, divided by the area under the random CDF: $FSI = (A_{rand} - A_{actual}) / A_{rand}$. An FSI of zero means the neuron fires randomly with respect to the stimulus, and an FSI of one means the neuron is perfectly selective.

Correlation-dependent STRFs. Typically, STRFs are derived using all of a cell's spikes. We were interested in the STRF from only those thalamic spikes that caused a

cortical spike. The following procedure is described in the Results and graphically in **Figure 3**. The first step was to isolate the subset of thalamic spikes that potentially caused cortical spikes. These thalamic spikes that precede a cortical spike by 1-10 ms are labeled time-locked. The time-locked STRF was derived from these spikes alone.

In the description below, it is helpful to use different notation for conventionally valued STRFs and for spike-normalized STRFs. Conventional STRFs (in units spikes/sec) are denoted only with a subscript identifying the set of contributing spikes, e.g. $STRF_{time\text{-}locked}$. A conventional STRF can be normalized by the number of contributing spikes, e.g. $n_{time\text{-}locked}$, to give a per-spike STRF distinguished with a superscript N, as in $STRF^{N}_{time\text{-}locked}$. Therefore, the conventional STRF is equal to the number of contributing spikes times the normalized STRF: $STRF_{time\text{-}locked} = n_{time\text{-}locked} \cdot STRF^{N}_{time\text{-}locked}$.

Time-locked spikes are conceptually of two types: those that actually caused a cortical spike and those that would have occurred anyway, in the absence of any functional connection. In reference to the correlogram features with which they are associated (**Fig. 3a**), the former are termed peak spikes and the latter baseline spikes. While we had no independent means of identifying which time-locked spikes were peak and which were baseline, we knew however how many of each there were (n_{peak}, $n_{baseline}$) and we could estimate their STRFs. Since STRF derivation is a linear operation, the time-locked STRF minus an estimate of the baseline STRF yields the peak STRF.

An estimate for the baseline STRF must reflect the properties of such time-locked but non-causal spikes. First, baseline spikes are very similar to the average thalamic spikes. Therefore, one contribution to the baseline STRF is simply the average thalamic

STRF. But baseline spikes have additional properties by virtue of their temporal proximity to cortical spikes, and may consequently represent the cortical STRF to varying degrees. To approximate these characteristics, a control STRF was constructed from fabricated thalamic spikes, timed to precede actual non-time-locked cortical spikes by the same interspike intervals as actual time-locked thalamic spikes. The control STRF thus takes into account relative response variability, temporal modulation preference, and other firing properties of both cells that can affect how much of the cortical STRF is parasitically represented by time-locked thalamic spikes. To estimate the baseline STRF, we added a spike-normalized average thalamic STRF to a spike-normalized control STRF: $STRF^{N}_{baseline} = STRF^{N}_{thalamus} \cdot STRF^{N}_{control}$. This yields a spike-normalized baseline STRF, which when multiplied by the number of baseline spikes gives an estimate for the total baseline STRF: $STRF_{baseline} = n_{baseline} \cdot STRF^{N}_{baseline}$. When we tested this procedure in several functionally unconnected pairs which have no peak, the baseline estimate tended to match the time-locked STRF extremely well, thereby corroborating the method.

The peak STRF is simply the time-locked STRF minus the baseline STRF: $STRF_{thal.peak} = STRF_{time\text{-}locked} - STRF_{baseline}$. It describes the response properties of those thalamic spikes that presumably caused cortical spikes, and it may or may not be the same as the average thalamic STRF. The difference between the two, on a spike-normalized basis, is the conditioning influence STRF: $STRF^{N}_{conditioning} = STRF^{N}_{thal.peak} - STRF^{N}_{thalamus}$.

Cortical peak STRFs were computed for STRF-based contribution (see *Contribution* below) in exactly the same manner as thalamic peak STRFs, except with cortical rather than thalamic spikes.

Contribution. Intuitively, contribution approximates the proportion of a cortical cell's activity that is caused by a thalamic input. Traditional contribution (Levick et al., 1972) was computed under driven conditions as the percentage of cortical spikes immediately preceded by a thalamic spike (1-10ms lag, for consistency with the analysis above), greater than expected by chance. Receptive-field-based contribution is the proportion of cortical STRF ($STRF_{cortex}$) energy provided by the cortical peak STRF ($STRF_{ctx.peak}$), i.e. presumably caused by the thalamic cell (*see Correlation-dependent STRFs* above). Only the significant and non-spike-normalized STRFs were used for this procedure. Moreover, all sums are over the absolute magnitude of the pixels, whether they are excitatory or inhibitory; this captures STRF energy regardless of sign. To derive STRF-based contribution, we summed all pixels in $STRF_{ctx.peak}$ with the same sign as the corresponding pixels in $STRF_{cortex}$ (a sum abbreviated here as Σ_{same}). We then summed all pixels in $STRF_{ctx.peak}$ with the opposite sign as those in $STRF_{cortex}$. (Σ_{opp}). Finally, subtracting the opposite-sign sum from the same-sign sum, and dividing by the total pixel sum of $STRF_{cortex}$ (Σ_{all}) gives the STRF-based contribution:

$$Contribution_{STRF} = (\Sigma_{same} | STRF_{ctx.peak} | - \Sigma_{opp} | STRF_{ctx.peak} |) / \Sigma_{all} | STRF_{cortex} |.$$

Thus, we essentially add all positive input, subtract all negative input, and divide by the total output to give the proportion of cortical STRF presumably caused by the thalamic cell. STRF-based contribution could therefore be negative if strong overlap of opposite sign occurs.

Unlike the traditional measure, we can also evaluate the specific contribution of those STRF regions where both $STRF_{ctx.peak}$ and $STRF_{cortex}$ are excitatory, or where they are both inhibitory. Again, the sums are over the absolute magnitude of pixels, whether they are excitatory or inhibitory. This isolates the amount of contribution only where the input has matching sign and matching spectrotemporal extent as the output (a sum denoted by Σ_{same+} for excitatory subfields). Thus, STRF-based excitatory-only contribution for this restricted spectrotemporal range is

$Contribution_{STRF+} = \Sigma_{same+} | STRF_{ctx.peak} | / \Sigma_{same+} | STRF_{cortex} |$.

The inhibitory contribution is evaluated in the same way, with the corresponding range of inhibitory overlap.

RESULTS

Functionally connected thalamocortical cell pairs are characterized by a sharp, short-latency peak in the cross-correlogram of their action potentials (**Fig. 1a**). Their spectrotemporal receptive fields (STRFs) always show some degree of overlap in frequency and time (**Fig. 1b,c**). The correlogram expresses thalamic firing rate as a function of its temporal relationship to a cortical spike. For instance, the sharp peak at -2 ms (**Fig. 1a**) means that the thalamic cell fires 2 ms before a cortical spike much more often than expected. Or conversely, whenever the thalamic cell fires the cortical cell is more likely to fire 2 ms later. From the correlogram, we can identify the subset of thalamic spikes that could have caused a cortical spike. Considering axonal delays and synaptic integration (Usrey et al., 2000), the potentially causal thalamic spikes are those

preceding a cortical spike by approximately 1-10 ms (**Fig. 1a**, yellow box), labeled time-locked spikes.

Feature selectivity

Conceivably the time-locked, potentially causal thalamic spikes could represent stimuli in an average way. Alternately, they may carry more or less information than the average spikes. One way to establish how much information a set of spikes transmits is to determine how selective the spikes are for stimulus features. Therefore, to quantify the relative difference in information carried by time-locked versus average thalamic spikes, we computed a feature selectivity index (FSI) for each set. A randomly firing neuron would have an FSI equal to zero; a neuron that is perfectly selective for a particular stimulus feature would have an FSI of one. FSIs for real neurons fall somewhere between these extremes. Overall, time-locked thalamic spikes have a higher FSI than the average spikes (0.37 vs. 0.28, paired t-test p=0.011). The relative difference in FSI can be expressed as percent change and the distribution shown as a histogram (**Fig. 2**). Many cells are grouped near zero, indicating no difference in feature selectivity; a few show a decreased FSI; and many more show increased selectivity, up to fourfold in magnitude. Time-locked spikes have a 65% greater mean feature selectivity than average spikes (paired t-test p=0.013). Potentially causal thalamic spikes tend to be significantly more selective than average spikes for spectrotemporal stimulus features.

Conditioning influence

The increase in feature selectivity for time-locked spikes suggests that other inputs influence whether a thalamic cell's spikes are propagated by the cortical cell. Although all the thalamic spikes impinge upon the cortical cell, only some are propagated. If thalamic spikes were passed through cortex randomly with respect to the stimulus, there would be no difference in FSI for the time-locked subset. Evidently for many cells, though, spikes are not propagated at random. Rather, they are passed through cortex in a unique, stimulus-dependent manner. Other inputs must interact with those thalamic cells to set stimulus-dependent conditions on whether spikes are propagated.

We can determine the spectrotemporal nature of these net conditioning inputs by comparing the estimated STRFs for thalamic spikes that cause a cortical spike to the average thalamic STRF (**Fig. 3**). Time-locked, potentially causal thalamic spikes are conceptually of two types: those that caused a cortical cell to fire and those that occurred at random. The causal spikes would be found in the peak of the cross-correlogram, and the random or baseline spikes would be found below the peak (**Fig. 3a**). Baseline spikes would have occurred in temporal proximity to cortical spikes even in the absence of a functional connection. While we cannot determine which particular spikes belong in the peak and which belong in the baseline, we can estimate net STRFs for each subset. By subtracting a weighted estimate of the baseline STRF (**Fig. 3c**) (see Methods) from the time-locked STRF (**Fig. 3b**), we obtain an estimate of the peak, or causal STRF. The degree to which the peak STRF (**Fig. 3e**) differs from the average thalamic STRF (**Fig. 3f**) shows the stimulus-dependent conditions that must be satisfied for a thalamic spike to be propagated by the cortical cell. That is, it shows the net spectrotemporal conditioning influence of other inputs on whether this thalamic cell's spikes cause a cortical spike

(**Fig. 3g**). A positive region in the conditioning STRF indicates that in order for a thalamic spike to be propagated by cortex, there must be more energy at that spectrotemporal location than would, on average, cause the thalamic cell to fire. Negative energy in the conditioning STRF means that in order for a thalamic spike to be propagated, there must be less stimulus energy than would normally cause the thalamic cell to fire.

The conditioning influence is derived for a functionally connected thalamocortical pair in **Figure 4**. This thalamic cell appears to contribute to the upper frequency region of the cortical STRF (**Fig. 4b,c**). To aid interpretation, only the significant ($p < 0.002$) STRFs are plotted. In deriving the peak and conditioning STRFs, however, all operations were performed on the raw, non-thresholded signals. In this case the peak, or causal STRF (**Fig. 4d**) is of similar magnitude and spectrotemporal location as the rate-normalized, average thalamic STRF (**Fig. 4e**). The two are similar enough that when the average STRF is subtracted from the peak, only noise remains, so no significant features result in the conditioning STRF (**Fig. 4f**). For this thalamic cell, there is no conditioning influence, i.e. the thalamic spikes are causing cortical spikes at random with respect to the stimulus. No stimulus-related conditions affect whether the thalamic spikes are propagated.

When conditioning influence is present, it may be specifically cooperative (**Fig. 5**). For this cell, the peak STRF (**Fig. 5d**) is considerably stronger, but of the same sign as the average thalamic STRF (**Fig. 5e**). Therefore the conditioning influence (**Fig. 5f**) potentiates what the thalamic cell represents on average. The conditioning is not perfectly matched, since its influence increases the thalamic input in the lower range of

its excitatory frequencies, at the expense of higher frequencies. Nevertheless, in order for this thalamic cell's spikes to cause a spike in the cortex, both excitatory and inhibitory stimulus features must be increased in magnitude. In other words, not only do conditioning inputs demand a narrower range of excitatory stimulus frequencies, but they require an increased stimulus contrast to propagate thalamic spikes through cortex.

The conditioning influence need not cooperate with the thalamic unit's average receptive field. Sometimes the conditioning is thoroughly antagonistic (**Fig. 6**). In this case, the peak STRF (**Fig. 6d**) is much more limited in spectrotemporal extent than the average thalamic STRF (**Fig. 6e**), and the conditioning influence (**Fig. 6f**) has a negative, or opposite-signed influence on the thalamic input. This net inhibitory influence on the thalamic STRF pares it down to a more restricted spectrotemporal range. The negative region of the conditioning does not mean that there must be a lack of energy in the stimulus in order for thalamic spikes to be propagated. It is a relative measure: in order for spikes to pass through cortex there must be less energy at that spectrotemporal location than the average stimulus that causes the thalamic cell to fire. The conditioning works against or antagonizes what the thalamic cell is doing independently.

Conditioning influence versus feature selectivity

If conditioning influences, as hypothesized, affect the feature selectivity of time-locked spikes, then there may be a systematic relationship between the cooperativity of conditioning and change in FSI. For example, cooperation might tend to smear thalamic spectrotemporal inputs, thereby degrading their FSI, while antagonism may increase FSI

through selective culling. Or perhaps cooperative and antagonistic conditioning both increase FSI.

To quantify the net conditioning effect on the thalamic input, we computed a correlation coefficient, the similarity index (deAngelis et al., 1999), between the conditioning STRF and the original thalamic STRF. The similarity index only compares the shapes of the STRFs, not their absolute magnitudes. STRFs with identical shapes and sign have similarity index of one, those with identical shape but opposite sign have similarity index equal to -1, and STRFs that are uncorrelated have similarity index of zero. In terms of conditioning influence, then, positive similarity indices indicate cooperation and negative indices indicate antagonism. For each cell, we compared the similarity index to the difference in FSI between time-locked and average thalamic spikes (**Fig. 7**). Most cells show little net conditioning influence. Some of these had no conditioning STRF, and others had a non-zero conditioning STRF uncorrelated with that of the thalamic cell. Approximately 1/3-1/4 of cells show conspicuous (appx. 0.2 or greater in similarity index magnitude) net conditioning effects, with antagonism almost as likely as cooperation. There is a positive correlation between the similarity index and the difference in FSI ($R=0.50 \pm 0.19$ s.e., $0.01<p<0.02$). Cooperative conditioning tends to increase the feature selectivity of the thalamic spikes that are propagated through cortex, and antagonistic conditioning tends to decrease it.

Thalamocortical contribution

With STRFs from distinct subsets of spikes we can estimate the strength of functional thalamic input to a particular cortical cell. Traditionally, one would use a measure called

contribution, the percentage of cortical spikes preceded by a thalamic cell's spikes, above that expected. This spike-based contribution ideally has no relation to the cells' stimulus-response properties, and thus simply estimates how many inputs it would take to make the cortical cell fire. In contrast, an STRF-based measure of contribution estimates what proportion of the cortical cell's receptive field can be attributed to a given thalamic cell (see Methods for details).

Overall the traditional and receptive-field-based contributions are similar in mean (traditional = 4.5%, STRF-based = 3.4%) but less so in median (traditional = 2.6%, STRF-based = 0.9%). They are not significantly correlated (correlation coefficient 0.28 $\pm$ 0.21 s.e, $p > 0.1$), so for each thalamocortical pair the traditional contribution may differ substantially from the STRF-based measure. In addition to revealing the amount of functional, as opposed to numerical, input a cortical cell receives, STRF-based contribution can be evaluated for excitatory and inhibitory stimulus-response features separately. In this way, we can isolate only those areas where the cortical peak and average cortical STRFs overlap and have the same sign. Excitatory subfields contribute twice as much as inhibitory subfields (mean 5.3% vs. 2.7%; paired t-test, $p=0.025$) to overlapping, sign-matched cortical STRF regions.

DISCUSSION

By evaluating spikes based on their fine temporal relationships, we demonstrate that potentially causal thalamic spikes may differ from average spikes in their selectivity for spectrotemporal stimulus features. We also illustrate for the first time how receptive field information passed from thalamic to cortical cells is modified by other inputs. The

spectrotemporal cooperativity or antagonism of these conditioning inputs partly accounts for the difference in feature selectivity between potentially causal and average thalamic spikes.

Previous work shows that thalamic activity can be more efficacious in causing cortical spikes when it occurs synchronously with other thalamic inputs (Alonso et al. 1996; Usrey et al., 2000; Roy & Alloway, 2001). Our report builds on those observations by quantifying whether potentially causal thalamic activity, time-locked to cortical spikes, transmits more or less information about the stimulus than average. We assess this difference for each thalamic cell by comparing the feature selectivity indices for potentially causal versus average spikes. While many cells show no difference in FSI and a few show a decrease, across all thalamic cells there is a greater mean feature selectivity for potentially causal spikes. That is, potentially causal thalamic spikes tend to carry more receptive field information than average. This is a significant conceptual extension of previous studies, which consider time-locked spikes for their efficacy rather than their role in transmitting information.

As described in the Introduction, differences in feature selectivity suggest that additional, stimulus-conditioned inputs influence whether a thalamic cell's spikes are propagated through cortex. Since feature selectivity depends on receptive field idiosyncrasies, these conditioning influences should differ spectrotemporally from the thalamic cell's preferences. We therefore develop a method to identify the spectrotemporal nature of these near-simultaneous conditioning inputs, based on receptive field shapes. Some have little in common with the response properties of the thalamic cell, some are cooperative, and some are antagonistic. One cannot predict solely

from the overlap between thalamic and cortical STRFs which sort of influence is present. Our results therefore provide a key complement to work within thalamus (Dan et al., 1998) and within cortex (Ghose et al., 1994; Reich et al., 2000) on the relationship between action potential timing and specific receptive field properties.

To demonstrate a relationship between conditioning influence and feature selectivity, we compared the cooperativity of the influence to the FSI difference between potentially causal and average spikes. They are significantly correlated: cooperative conditioning tends to increase the feature selectivity, and antagonistic conditioning tends to decrease it. We thus explain not only how much more or less information potentially causal spikes carry, but for exactly what stimulus-related purpose.

A topic closely related to conditioning influence is the degree of functional thalamocortical convergence. Traditional and STRF-based measures of contribution estimate the amount of a cortical cell's activity or receptive field, respectively, that can be attributed to a given input. Contribution thereby enables estimates of thalamocortical convergence, or how many thalamic cells might synapse strongly onto a cortical cell. A contribution of 5%, say, would lead one to estimate that 20 thalamic cells could fully activate a cortical cell. Traditional contribution (mean 4.5%, median 2.6%) would thus lead to an estimate of roughly 20-40 thalamic inputs per cortical cell, and STRF-based contribution (mean 3.4%, median 0.9%) would lead to an estimate of roughly 30-100. Since cooperation exists among inputs, however, both traditional and STRF-based methods tend to overestimate contribution and therefore underestimate the degree of convergence. Nevertheless, our estimates of traditional convergence based on spike numbers alone agree with those in the visual system, where approximately 30 thalamic

cells significantly affect a cortical cell's activity (Reid and Alonso, 1995). Our estimates based on STRF contribution, on the other hand, are considerably higher. The traditional and STRF-based measures, moreover, are uncorrelated. Since some spikes carry more information than others, one cannot determine from spike numbers alone how much receptive field energy a given input contributes. Unlike the traditional measure, STRF-based contribution can also compare excitatory and inhibitory receptive field inputs. Considering only areas where STRF overlaps have the same sign, a profound imbalance exists, as excitatory subfields contribute twice as much as inhibitory subfields. The typical thalamic inputs, therefore, need to be supplemented by additional inhibition to create a full cortical STRF. This additional inhibition would presumably be fast feed-forward and intracortical in origin (Swadlow and Gusev , 2000).

Several factors qualify the interpretation of our data. First, the STRF is a linear descriptor with respect to the spectrotemporal envelope of the stimulus. Therefore, the STRF-based measures we used, including FSI and similarity index, may be insensitive to certain stimulus-response nonlinearities. The strong and consistent relationship, however, between STRFs and functional thalamocortical connectivity suggests that if stimulus-response nonlinearities play a role, it is relatively minor (Miller et al., 2000). We would also emphasize that we recorded in the anesthetized animal. Thalamocortical interactions may differ in the awake animal, especially with regard to the brain's dynamic state and corticothalamic feedback (Fanselow and Nicolelis, 1999; Suga et al., 2000; Wörgötter and Eysel, 2000). Nevertheless, since the conditioning influence we report is virtually simultaneous with short-latency monosynaptic thalamic input, it is unlikely that multisynaptic feedback would have a large effect on our results.

Our observations point to a number of directions for further study. For instance, we only treated a composite of presumed causal spikes, expressed in the peak STRF. It would be illuminating to distinguish precisely which time-locked thalamic spikes caused cortical spikes. Also, our conditioning influences are net effects of unknown origin. Other methods could help identify the sources of conditioning influence, whether thalamic or intracortical, and perhaps discriminate how spike patterns among inputs or within a single input (Usrey et al., 2000; Swadlow and Gusev, 2001) affect receptive field construction. Finally, it would be interesting to reveal if and how behavioral state changes affect the degree or type of conditioning influence. The present report provides a basis for future work by introducing novel methods to quantify the detailed, functional transformation from one neuron to another.

ACKNOWLEDGMENTS

Supported by the National Institutes of Health (DC02260, NS34835), the National Science Foundation (NSF97203398), and the Whitaker Foundation.

REFERENCES

Aertsen AMHJ, Johannesma PIM (1980) Spectro-temporal receptive fields of auditory neurons in the grassfrog. Biol Cyber 38:223-234.

Alonso JM, Usrey WM, Reid RC (1996) Precisely correlated firing in cells of the lateral geniculate nucleus. Nature 383:815-9.

Creutzfeldt O, Hellweg FC, Schreiner CE (1980) Thalamocortical transformation of responses to complex auditory stimuli. Exp Br Res 39:87-104.

Cotillon N, Nafati M, Edeline JM (2000) Characteristics of reliable tone-evoked oscillations in the rat thalamo-cortical auditory system. Hear Res 142:113-30.

Dan Y, Alonso JM, Usrey WM, Reid RC (1998) Coding of visual information by precisely correlated spikes in the lateral geniculate nucleus. Nat Neurosci 1:501-7.

DeAngelis GC, Ghose GM, Ohzawa I, Freeman RD (1999) Functional micro-organization of primary visual cortex: receptive field analysis of nearby neurons. J Neurosci 19:4046-64.

Eggermont JJ (1992) Stimulus induced and spontaneous rhythmic firing of single units in cat primary auditory cortex. Hear Res 61:1-11.

Escabí MA, Schreiner CE, Miller LM (1998) Dynamic time-frequency processing in the cat auditory midbrain, thalamus, and auditory cortex: Spectrotemporal receptive fields obtained using dynamic ripple spectra. Soc Neurosci Abs 24:1879.

Escabí MA, Miller LM, Read HL, Osborne LC, Schreiner CE (2000) Response specificity to dynamic ripple and ripple noise stimuli: neuronal selectivity in the auditory midbrain, thalamus, and cortex. Soc Neurosci Abs 26:358.2.

Fanselow EE, Nicolelis MA (1999) Behavioral modulation of tactile responses in the rat somatosensory system. J Neurosci 19:7603-16.

Ghose GM, Ohzawa I, Freeman RD (1994) Receptive-field maps of correlated discharge between pairs of neurons in the cat's visual cortex. J Neurophysiol 71:330-46.

Klein DJ, Depireux DA, Simon JZ, Shamma SA (2000) Robust spectrotemporal reverse correlation for the auditory system: optimizing stimulus design. J Comp Neurosci 9:85-111.

Kowalski N, Depireux DA, Shamma SA (1996) Analysis of dynamic spectra in ferret primary auditory cortex. I. Characteristics of single-unit responses to moving ripple spectra. J Neurophysiol 76:3503-23.

Levick WR, Cleland BG, Dubin MW (1972) Lateral geniculate neurons of cat: retinal inputs and physiology. Investigative Ophthalmology 11:302-11.

Miller LM, Schreiner CE (2000) Stimulus-based state control in the thalamocortical system. J Neurosci 20:7011-6.

Miller LM, Escabí MA, Read HL, Schreiner CE (2000) Functional convergence and divergence in the auditory thalamocortical system. Soc Neurosci Abs 26:358.3.

Lewicki MS (1994) Bayesian modeling and classification of neural signals. J Neural Comp 6:1005-1030.

Perkel DH, Gerstein GL, Moore GP (1967) Neuronal spike trains and stochastic point processes. II. Simultaneous spike trains. Biophys J 7:419-40.

Reich DS, Mechler F, Purpura KP, Victor JD (2000) Interspike intervals, receptive fields, and information encoding in primary visual cortex. J Neurosci 20:1964-74.

Reid RC, Alonso J-M (1995) Specificity of monosynaptic connections from thalamus to visual cortex. Nature 378:281-4.

Roy SA, Alloway KD (2001) Coincidence detection or temporal integration? What the neurons in somatosensory cortex are doing. J Neurosci 21:2462-2473.

Schreiner CE, Calhoun BM (1994) Spectral envelope coding in cat primary auditory cortex: properties of ripple transfer functions. Aud Neurosci 1:39-61.

Suga N, Gao E, Zhang Y, Ma X, Olsen JF (2000) The corticofugal system for hearing: recent progress. PNAS 97:11807-14.

Swadlow HA, Gusev AG (2000) The influence of single VB thalamocortical impulses on barrel columns of rabbit somatosensory cortex. J Neurophysiol 83:2802-13.

Swadlow HA, Gusev AG (2001) The impact of 'bursting' thalamic impulses at a neocortical synapse. Nat Neurosci 4: 402-408.

Tanaka K (1983) Cross-correlation analysis of geniculostriate neuronal relationships in cats. J Neurophysiol 49:1303-18.

Usrey WM, Alonso JM, Reid RC (2000) Synaptic interactions between thalamic inputs to simple cells in cat visual cortex. J Neurosci 20:5461-7.

Wörgötter F, Eysel UT (2000) Context, state and the receptive fields of striatal cortex cells. TINS 23:497-503.

FIGURE LEGENDS

Fig. 1 A functionally connected thalamocortical pair. (**a**) The cross-correlogram is normalized to express thalamic firing rate relative to a cortical spike occurring at time lag zero. The brief, short-latency peak, with thalamic spikes leading cortical (2 ms), is indicative of a monosynaptic-like functional connection. The yellow box denotes the time-locked thalamic spikes that precede a cortical spike by 1-10 ms. The cyan line is the mean, and the green lines are the 99% confidence intervals, under an assumption of independent, Poisson spike trains. (**b**) Thalamic STRF. The abscissa represents time-preceding-a-spike, and the ordinate represents stimulus frequency. STRF color indicates a differential change in firing rate from the occurrence of stimulus energy in a particular spectrotemporal location. Warm colors mean that stimulus energy at that location tends to increase firing rate above the mean (4.85 spikes/sec), and cool colors indicate a decrease in firing rate. This cell, for instance, fires maximally 7.5 ms after stimulus energy occurs at 13-14 kHz. (**c**) Cortical STRF. Overlying the cortical STRF, for comparison, is a green contour circumscribing the high-energy peak of the thalamic STRF. If one would shift the green contour by the 2 ms lag seen in the correlogram, these STRFs would overlap very well.

Fig. 2 Potentially causal thalamic spikes are more selective for stimulus features than expected. The differences in FSI for all thalamic cells between time-locked spikes and average spikes are summarized in a histogram. Positive differences mean time-locked spikes have greater FSI than average. Many cells show very little difference; a few have negative difference, indicating that time-locked spikes are less selective than average; and

many show a positive difference, up to fourfold greater. The mean difference of 65% is significantly different from zero (paired t-test, p=.013). That is, time-locked thalamic spikes tend to be more selective than average for spectrotemporal stimulus features.

Fig. 3 Schematic of methods to identify the stimulus-dependent influence that conditions whether a thalamic cell's spikes are propagated by the target cortical cell. (**a**) The cross-correlogram can be conceptually divided into subsets of thalamic spikes. Time-locked spikes (yellow box) are those that precede a cortical spike by 1-10 ms. Of the time-locked spikes, the baseline spikes (blue) would have occurred even in the absence of a functional connection. Peak spikes (red) are those that actually caused the cortical cell to fire. The cyan line is the mean, and the red lines are the 99% confidence intervals, under an assumption of independent, Poisson spike trains. In this figure only, STRFs are simulated for clarity (**b-g**). The time-locked STRF (**b**) minus the baseline STRF (**c**) (see Methods) gives an estimate of the peak, causal STRF (**d**). The degree to which the peak STRF differs from the average thalamic STRF is the degree to which other influences condition whether the thalamic spikes are propagated by cortex. Therefore, the peak STRF (**e**) minus the average thalamic STRF (**f**) gives a spectrotemporal description of the conditioning influence (**g**). Positive regions in the conditioning influence mean that in order for this thalamic cell's spikes to be propagated through cortex, there must be more energy in that region than typically drives the thalamic cell. Negative regions require that in order for spikes to be propagated, there must be less energy in that region than usually drives the thalamic cell.

Fig. 4 Absence of conditioning influence. (**a**) In the thalamocortical correlogram, red bins are the peak thalamic spikes, those that presumably caused a cortical spike. (See Figure 2 legend for other correlogram details). (**b**) Thalamic STRF. (**c**) Cortical STRF. To aid interpretation, only the significant ($p < 0.002$) STRFs are plotted. In deriving the peak and conditioning STRFs, however, all operations were performed on the raw, non-thresholded signals. The STRFs in (**d**)-(**f**) are plotted with the same colorscale for comparison. (**d**) The peak STRF (spike-normalized) estimates the response properties of only the thalamic spikes that caused a cortical spike. (**e**) The thalamic STRF is replotted, but here spike-normalized for direct comparison with the peak STRF. In this case, the peak STRF is similar in location and magnitude to the average thalamic STRF. (**f**) Stimulus-related conditioning influence upon whether thalamic spikes are propagated through the cortical cell. For this thalamic neuron, when the average STRF is subtracted from the peak STRF only noise remains, so that no significant conditioning influence is observed; the presumed causal spikes are not unique in the way they represent stimuli. For visual reference in (c), (d), and (f), a green contour indicates the location of the high-energy peak of the thalamic STRF.

Fig. 5 Cooperative conditioning influence. (**a**) In the thalamocortical correlogram, red bins are the peak thalamic spikes, those that presumably caused a cortical spike. (See Figure 2 legend for other correlogram details). (**b**) Thalamic STRF. (**c**) Cortical STRF. To aid interpretation, only the significant ($p < 0.002$) STRFs are plotted. In deriving the peak and conditioning STRFs, however, all operations were performed on the raw, non-thresholded signals. The STRFs in (**d**)-(**f**) are plotted with the same colorscale for

comparison. (**d**) The peak STRF (spike-normalized) estimates the response properties of only the thalamic spikes that caused a cortical spike. (**e**) The thalamic STRF is replotted, but here spike-normalized for direct comparison with the peak STRF. In this case, the peak STRF has considerably greater magnitude than the average thalamic STRF. Its excitatory region, moreover, overlaps only the lower frequency portion of the average thalamic excitatory subfield. (**f**) Stimulus-related conditioning influence upon whether thalamic spikes are propagated through the cortical cell. For this thalamic neuron, the conditioning influence is cooperative. In order for thalamic spikes to cause a cortical spike, the stimulus must be of higher contrast and slightly different frequency content than typically causes the thalamic cell to fire. For visual reference in (c), (d), and (f), a green contour indicates the location of the high-energy peak of the thalamic STRF.

Fig. 6 Antagonistic conditioning influence. (**a**) In the thalamocortical correlogram, red bins are the peak thalamic spikes, those that presumably caused a cortical spike. (See Figure 2 legend for other correlogram details). (**b**) Thalamic STRF. (**c**) Cortical STRF. To aid interpretation, only the significant ($p < 0.002$) STRFs are plotted. In deriving the peak and conditioning STRFs, however, all operations were performed on the raw, non-thresholded signals. The STRFs in (**d**)-(**f**) are plotted with the same colorscale for comparison. (**d**) The peak STRF (spike-normalized) estimates the response properties of only the thalamic spikes that caused a cortical spike. (**e**) The thalamic STRF is replotted, but here spike-normalized for direct comparison with the peak STRF. In this case, the peak STRF is similar in magnitude but more limited in spectrotemporal extent than the average thalamic STRF. (**f**) Stimulus-related conditioning influence upon whether

thalamic spikes are propagated through the cortical cell. For this thalamic neuron, the conditioning influence is antagonistic. In order for thalamic spikes to cause a cortical spike, the stimulus must contain less energy in regions that typically excite the thalamic cell. For visual reference in (c), (d), and (f), a green contour indicates the location of the high-energy peak of the thalamic STRF.

Fig. 7 Relationship between the cooperativity of conditioning influence and the difference in feature selectivity for potentially causal spikes. The similarity index for the conditioning influence and the average thalamic STRF indicates the degree of cooperation (positive values) or antagonism (negative values). The FSI difference between time-locked, potentially causal spikes and average spikes quantifies how much more or less stimulus information the time-locked spikes carry. Similarity index and FSI difference are significantly and positively correlated ($R=0.50$, $0.01<p<0.02$). The dashed line is the best fit in a least-mean-squares sense. Cooperative conditioning influences tend to increase the feature selectivity of time-locked spikes, and antagonistic conditioning tends to decrease it.

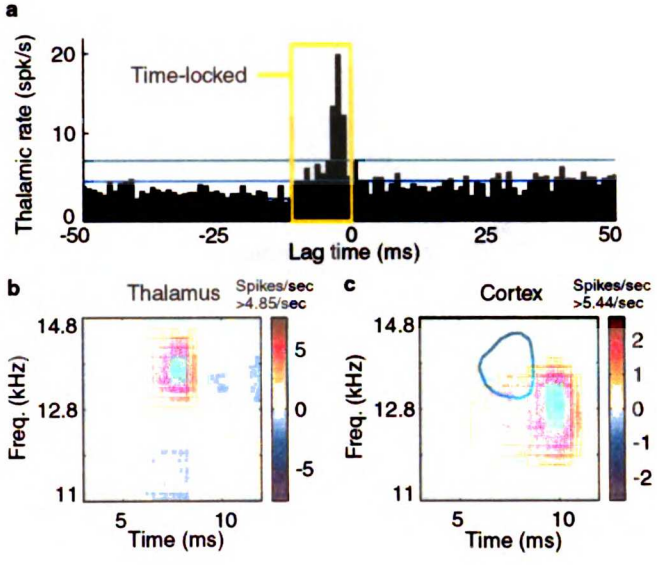
a
Thalamic rate (spk/s)
20
10
0
Time-locked
-50
-25
0
25
50
Lag time (ms)
b
Thalamus
Spikes/sec
>4.85/sec
14.8
12.8
11
Freq. (kHz)
5
0
-5
5
10
Time (ms)
c
Cortex
Spikes/sec
>5.44/sec
14.8
12.8
11
Freq. (kHz)
2
1
0
-1
-2
5
10
Time (ms)

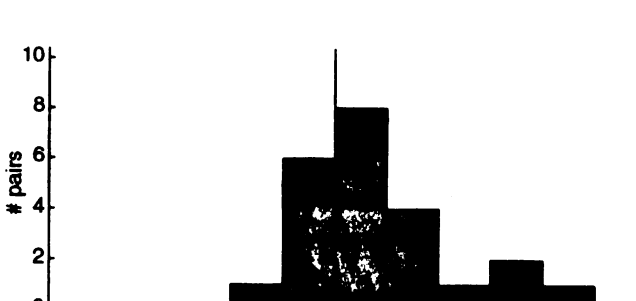
10
8
6
4
2
0
pairs
-400
-300
-200
-100
0
100
200
300
400
FSI difference (timelocked vs average, %)

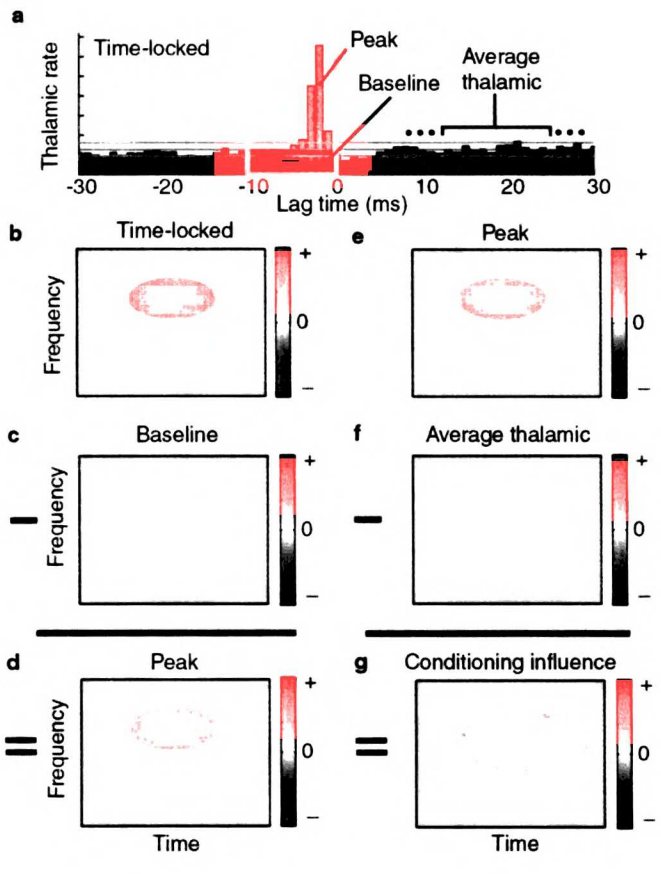
a
Thalamic rate
Time-locked
Peak
Baseline
Average thalamic
-30
-20
-10
0
10
20
30
Lag time (ms)
b
Time-locked
Frequency
+
0
–
e
Peak
c
Baseline
f
Average thalamic
d
Peak
Time
g
Conditioning influence

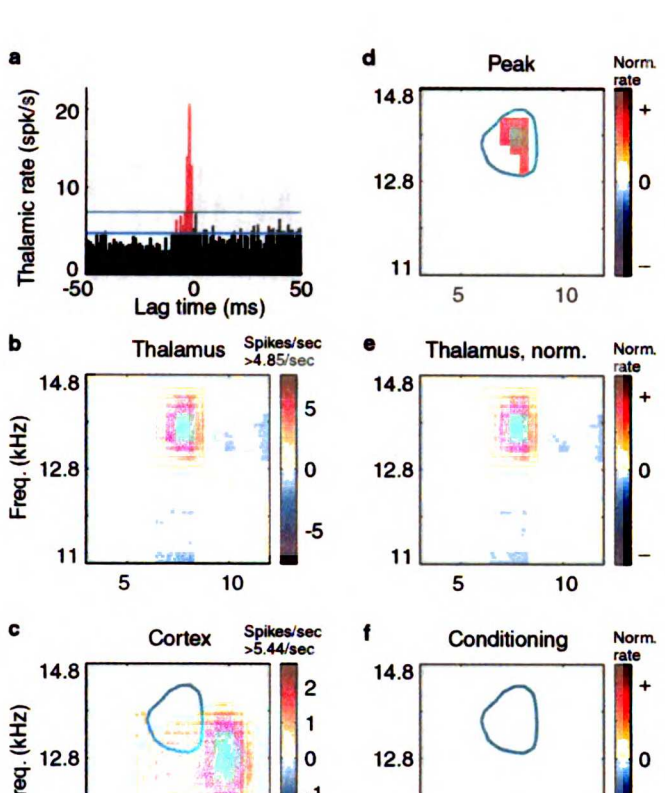
a
Thalamic rate (spk/s)
20
10
0
-50
0
50
Lag time (ms)
b
Thalamus
Spikes/sec
>4.85/sec
Freq. (kHz)
14.8
12.8
11
5
10
5
0
-5
c
Cortex
Spikes/sec
>5.44/sec
Freq. (kHz)
14.8
12.8
11
5
10
Time (ms)
2
1
0
-1
-2
d
Peak
Norm.
rate
14.8
12.8
11
5
10
+
0
–
e
Thalamus, norm.
Norm.
rate
14.8
12.8
11
5
10
+
0
–
f
Conditioning
Norm.
rate
14.8
12.8
11
5
10
Time (ms)
+
0
–

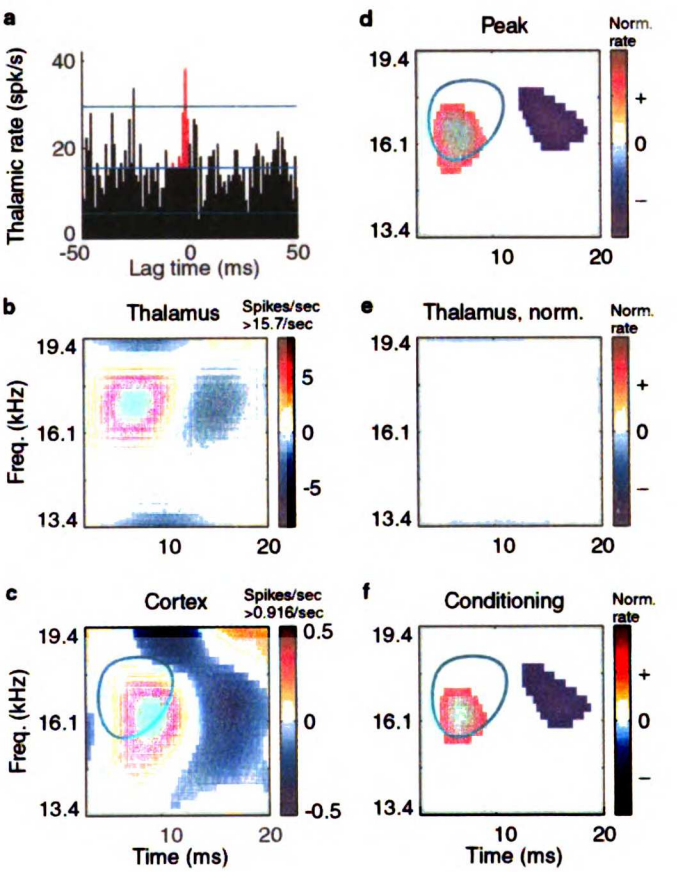
a
Thalamic rate (spk/s)
40
20
0
-50
0
50
Lag time (ms)
b
Thalamus
Spikes/sec
>15.7/sec
Freq. (kHz)
19.4
16.1
13.4
5
0
-5
10
20
c
Cortex
Spikes/sec
>0.916/sec
0.5
0
-0.5
Time (ms)
d
Peak
Norm.
rate
+
0
–
e
Thalamus, norm.
f
Conditioning

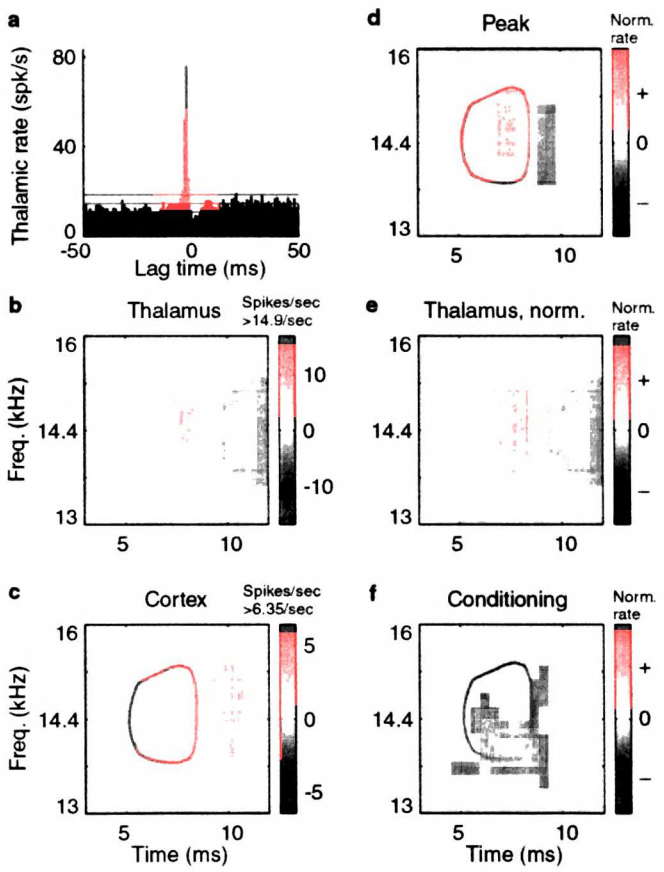
a
Thalamic rate (spk/s)
80
40
0
-50
0
50
Lag time (ms)
b
Thalamus
Spikes/sec
>14.9/sec
Freq. (kHz)
16
14.4
13
10
0
-10
5
10
c
Cortex
Spikes/sec
>6.35/sec
Freq. (kHz)
16
14.4
13
5
0
-5
5
10
Time (ms)
d
Peak
Norm.
rate
16
14.4
13
+
0
–
5
10
e
Thalamus, norm.
Norm.
rate
16
14.4
13
+
0
–
5
10
f
Conditioning
Norm.
rate
16
14.4
13
+
0
–
5
10
Time (ms)

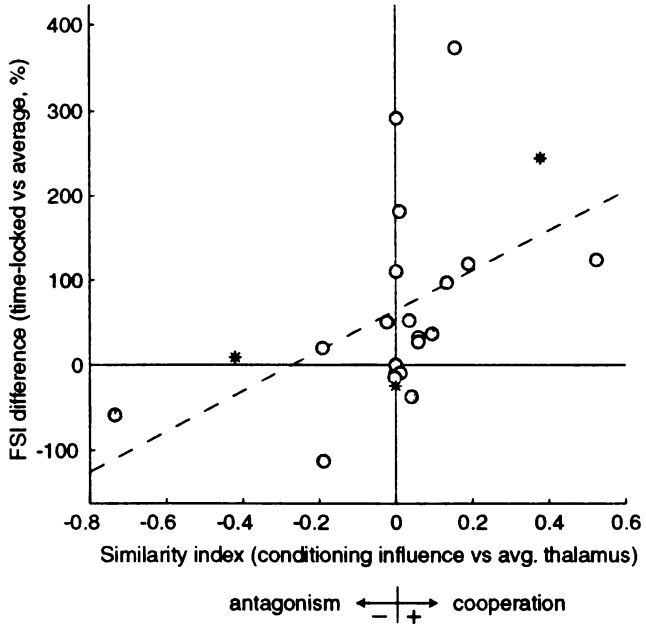
400
300
200
100
0
-100
FSI difference (time-locked vs average, %)
-0.8
-0.6
-0.4
-0.2
0
0.2
0.4
0.6
Similarity index (conditioning influence vs avg. thalamus)
antagonism
cooperation
–
+